Chemo-dynamical Simulations of the Milky Way

by

Chris Brook

A Dissertation
Presented in fulfillment of the requirements
for the degree of
Doctor of Philosophy
at Swinburne University Of Technology

March 2004

Abstract

Using a state of the art galaxy formation software package, GCD+, we model the formation and evolution of galaxies which resemble our own Galaxy, the Milky Way. The simulations include gravity, gas dynamics, radiative gas cooling, star formation and stellar evolution, tracing the production of several elements and the subsequent pollution of the interstellar medium. The simulations are compared with observations in order to unravel the details of the Milky Way's formation. Several unresolved issues regarding the Galaxy's evolution are specifically addressed. In our first study, limits are placed on the mass contribution of white dwarfs to the dark matter halo which envelopes the Milky Way. We obtain this result by comparing the abundances of carbon and nitrogen produced by a white dwarf-progenitor-dominated halo with the abundances observed in the present day halo. Our results are inconsistent with a white dwarf component in the halo $\gtrsim 5\,\%$ (by mass), however mass fractions of $\sim$1-2 % cannot be ruled out. In combination with other studies, this result suggests that the dark matter in the Milky Way is probably non-baryonic. The second component of this thesis probes the dynamical signatures of the formation of the stellar halo. By tracing the halo stars in our simulation, we identify a group of high-eccentricity stars that can be traced to now-disrupted satellites that were accreted by the host galaxy. By comparing the phase space distribution of these stars in our simulations to observed high-eccentricity stars in the solar neighbourhood, we find evidence that such a group of stars - a "stellar stream" - exists locally in our own Galaxy. Our next set of simulations demonstrate the importance of strong energy feedback from supernova explosions to the regulation of star formation. Strong feedback ensures that the building blocks of galaxy formation remain gas-rich at early epochs. We demonstrate that this process is necessary to reproduce the observed low mass and low metallicity of the stellar halo of the Milky Way. Our simulated galaxy is shown to have a thick disk component similar to that observed in the Milky Way through an abrupt discontinuity in the velocity dispersion-versus-age relation

for solar neighbourhood stars. This final study suggests that the thick disk forms in a chaotic merging period during the Galaxy's formation. Our thick disk formation scenario is shown to be consistent with observed properties of the thick disk of the Milky Way.

Acknowledgements

First and foremost, I thank my supervisors Brad Gibson and Daisuke Kawata.

Brad took me on as a PhD student through email correspondence alone. We both took a bit of a risk and from my point of view it could not have worked out better. Brad's enthusiasm and energy are legendary. The faith he shows in his students and postdocs provides confidence, and this has definitely been true in my case.

Daisuke has been invaluable in helping me attain my PhD. He is always helpful, as well as knowledgeable. I am very lucky to have worked with you Daisuke, and wish you a very successful future, which you no doubt have coming.

It has been great to make two such good freinds in Brad and Daisuke.

Thanks to Chris Flynn for his useful advice during my PhD candidacy. It is always a great pleasure to work with someone as positive as Chris and he remains a great inspiration to me. I thank Chris and his wonderful wife Lena for their hospitality in my stay in Tuorla, and appreciate the Tuorla Observatory for facilitating my visit.

I thank everyone at the Centre for Astrophysics and Supercomputing at Swinburne University. Matthew Bailes accepted me as a PhD student and I am proud to have been a part of the exciting Centre that he has built up. I further thank Matthew for the financial support that he provided on top of the APA.

Huge gratitude and salutations to Annie Hughes for getting me invovled at the centre, for her unsurpassed skills as an editor, but primarily for being a great freind over the past eight years.

Thanks to David Barnes, James Murray, Andrew Jamieson and Craig West for their assistance with all things computer-related.

Thanks to Paul Bourke for his help in creating fantastic animations of our galaxy formation simulations, as well as his assistance in creating posters for Research Week and conferences.

I am grateful to the Department of Education and Science for their financial assistance in the form of an Australian Postgraduate Award.

Thanks to Masashi Chiba and Tim Beers for providing the data for figure 4.10. Thank you to Andi Burkert and MPIA in Heidleberg, Gerhard Hensler and Kiel University for their hospitality and facilitating stays at their institutions.

Many people have made suggestions which have helped improve the studies found in this thesis, including Gerhard Hensler, Andi Burkert, Amina Helmi, Mike Beasley, Stuart Gill, Vincent Eke, Alice Quillen, Tim Connors and a couple of anonymous referees.

It has been a pleasure to work with the people at Swinburne, and to make freindships which will endure. Cheers to Stuart Gill and his wife Nikki, Mike and Amaya, Steve Ord, Chris T., Yeshe, Sarah and Dave, Ago, Craig and anyone I missed.

The support of Max and Sue Brook of my indulgences has been ever present, and unwavering.

Finally, thanks to Kim Kneipp for her encouragement, her support and her love.

Declaration

This thesis contains no material that has been accepted for the award of any other degree or diploma. To the best of my knowledge, this thesis contains no material previously published or written by another author, except where due reference is made in the text of the thesis. All work presented is primarily that of the author.

Science is a collaborative pursuit, and the studies presented in this thesis are very much part of a team effort. The collaborators listed below have great experience and knowledge, and were all integral in obtaining the presented results.

Chapter 3 was previously published as C. B. Brook, D. Kawata, B. K. Gibson, 2003, "Simulating a white dwarf dominated Galactic halo", *MNRAS* **343** 913.

Chapter 4 was previously published as C. B. Brook, D. Kawata, B. K. Gibson, & Flynn C. 2003, "Galactic Halo Stars in Phase Space: A Hint of Satellite Accretion?", *MNRAS* **585** L125.

Chapter 5 was previously published as C. B. Brook, D. Kawata, B. K. Gibson, & Flynn C. 2004, "Stellar Halo Constraints on Simulated Late Type Galaxies ", *MNRAS* **349** 52.
The results section has been expanded slightly to include two additional satellite disruptions events.

Chapter 6 has been submitted to *ApJ.* as C. B. Brook, D. Kawata, B. K. Gibson, & Freeman K. C. "The Emergence of a Thick Disk in a CDM Cosmology".

Minor alterations have been made to these studies in order to maintain consistency of style.

Chris Brook

16 March 2004

Contents

List of Figures

List of Tables

"Equipped with his five senses, man explores the Universe around him and calls this adventure science."

Edwin Hubble

"It is not worth an intelligent man's time to be in the majority. By definition, there are already enough people to do that."

Godfrey H. Hardy

Chapter 1

Background

1.1 Introduction

Galaxies are the major structural components of our Universe, yet their formation and evolution remain perhaps the outstanding mystery of contemporary astrophysics. The latest generation of telescopes, including KECK, VLT, Gemini and HST provide snapshots of galaxies at various redshifts, providing detail to a degree almost inconceivable little more than a decade ago (figure 1.1), yet the path taken for galaxies to evolve between these stages is not clear. At the same time, rapid development in computational power has allowed researchers to create increasingly detailed models of the processes of galaxy formation and evolution. Obviously, the galaxy for which we have the most information is our home galaxy, the Milky Way. We have unprecedented access to observational data for the stars of our Galaxy, including their distances, kinematics (3 dimensional in many cases), ages and exquisite chemical abundance determinations. This information is being matched with increasingly sophisticated galaxy formation models and simulations, the goal of which remains the reconstruction of the Milky Way's formation and subsequent evolution. It is hoped that this history will provide a blueprint for the evolution of other disk galaxies, and indeed the impetus for unraveling a general sequence for the formation of all galaxies. In this thesis, use is made of a state-of-the-art galaxy formation simulation code, *Galactic Chemo-dynamics Plus* -(`GCD+`)-, to simulate disk galaxies representative of our Milky Way. These simulations are then compared with observational data in a series of studies, in order to illuminate specific issues related to the formation of the Milky Way.

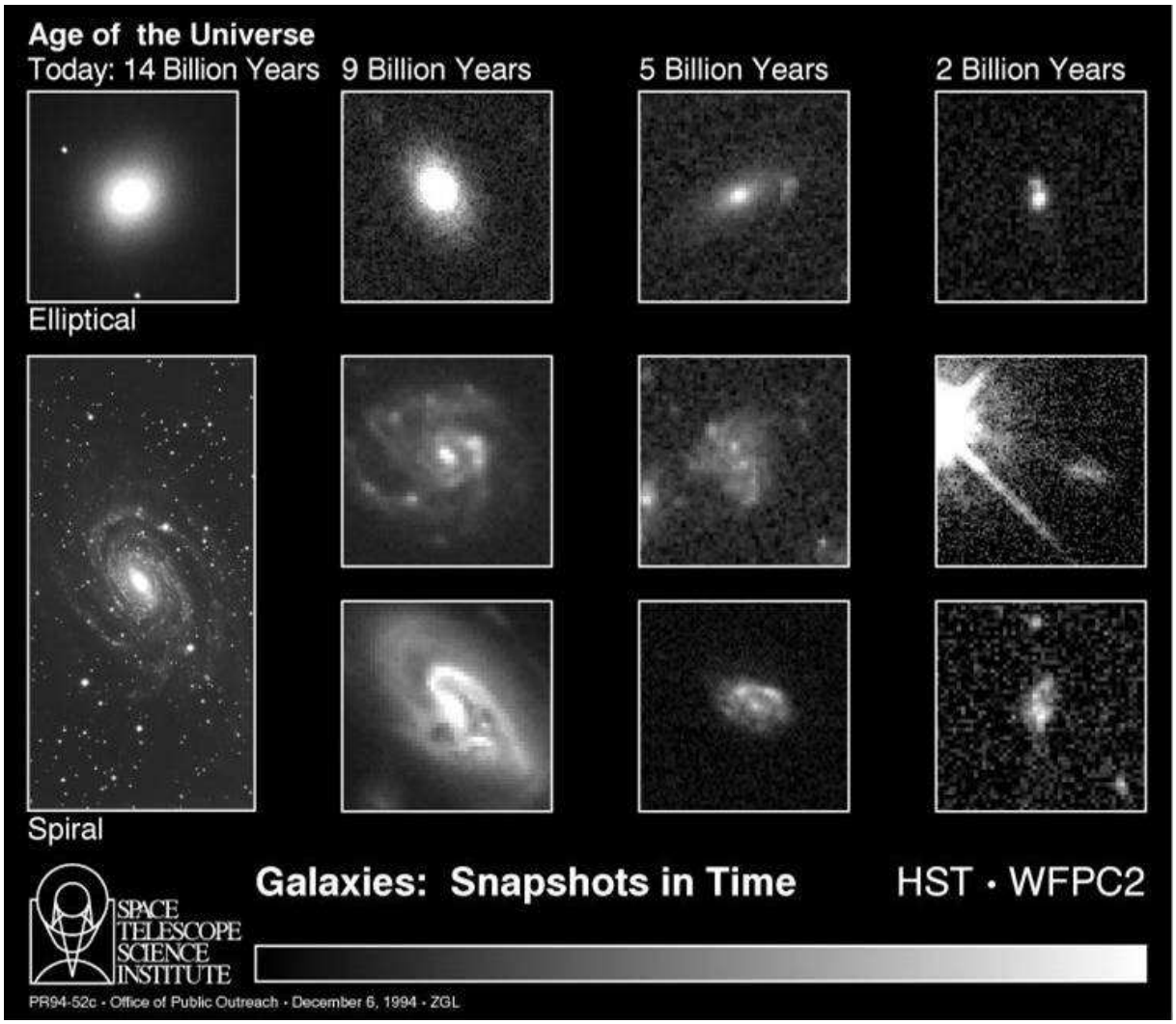

Figure 1.1: This sequence of NASA Hubble Space Telescope images of remote galaxies offers clues to their evolution. The galaxies on the far left are spiral and elliptical-shaped galaxies, the two major morphological classes seen today ($\sim$14 billion years after the birth of the Universe in the Big Bang). Elliptical galaxies contain primarily older stars, while spirals have ongoing star formation in their disks. Both galaxies in this column are nearby, only a few tens of millions of light-years away, and are representative of galaxies at the current stage of the Universe. The galaxies in the centre-left column existed when the universe was approximately two-thirds its present age. Elliptical galaxies (top) appear to resemble today's descendants, whereas the spiral population appears more disrupted. When the universe was nearly one-third its present age, spiral structure appears even more chaotic. However, even this far back in time, an elliptical galaxy (top) is still recognizable. The extremely remote, primeval objects in the far right column existed with the universe was only one-seventh of its current age. It is difficult to distinguish galaxy types at this epoch. Credit: A. Dressler (Carnegie Institutions of Washington), M. Dickinson (STScI), D. Macchetto (ESA/STScI), M. Giavalisco (STScI), and NASA

The remainder of this chapter is used to present a general background to these studies. A historical context and a cursory examination of the Milky Way's major structural components is provided in section 1.2. As theories of galaxy formation are made within a context of cosmological structure formation, it is necessary to outline the Big Bang paradigm in section 1.3. A broad picture of current theories of galaxy formation follows in section 1.4. In section 1.5 galaxy formation models are introduced, in particular those based upon N-body chemo-dynamical codes. Finally in section 1.6 we summarise the specific galaxy formation problems investigated in this thesis.

The chemo-dynamical galaxy evolution code (GCD+), employed here is described in chapter 2. Chapters 3-6 contain the primary outcomes of this thesis, with each chapter representing an original study relating to the formation and evolution of the Galaxy's dark halo, stellar halo, thin disk and thick disk. A brief note on potential future work is made in chapter 7.

1.2 Our Home Galaxy, The Milky Way

One of the great sights afforded to mankind is the view of the night sky, highlighted by the brilliant streak of the Milky Way. It was Galileo who first observed that the light of the Milky Way emanated from a vast array of stars, showing that the Milky Way was a stellar system. Subsequent work by, amongst others, Herschel, Kapteyn and Parsons, set out to discover the structure of the Milky Way, our place within it, and its relation to other structures such as spiral nebulae. The discovery of such nebulae, fuzzy objects in the sky that were not planets, comets or stars, is attributed to Messier in the late 1700s. Herschel (1792-1871) used a large reflecting telescope to produce a general catalog of these nebulae. By 1920, the two primary astronomical problems of the day were the size and scale of our Galaxy, and whether spiral nebulae were extragalactic systems. By 1927, these questions had been settled, primarily due to observations made by E. Hubble using Cepheid variable stars as standard candles, setting distance scales to show that spiral nebulae were a great distance from the Milky Way. In addition, analysis of the kinematics of stars done by J. H. Oort allowed an estimate of total mass and spatial extent of our Galaxy. Estimates of the scale of the Milky Way were subsequently improved once the nature of the absorbing medium in the Galactic Plane was appreciated, for example through

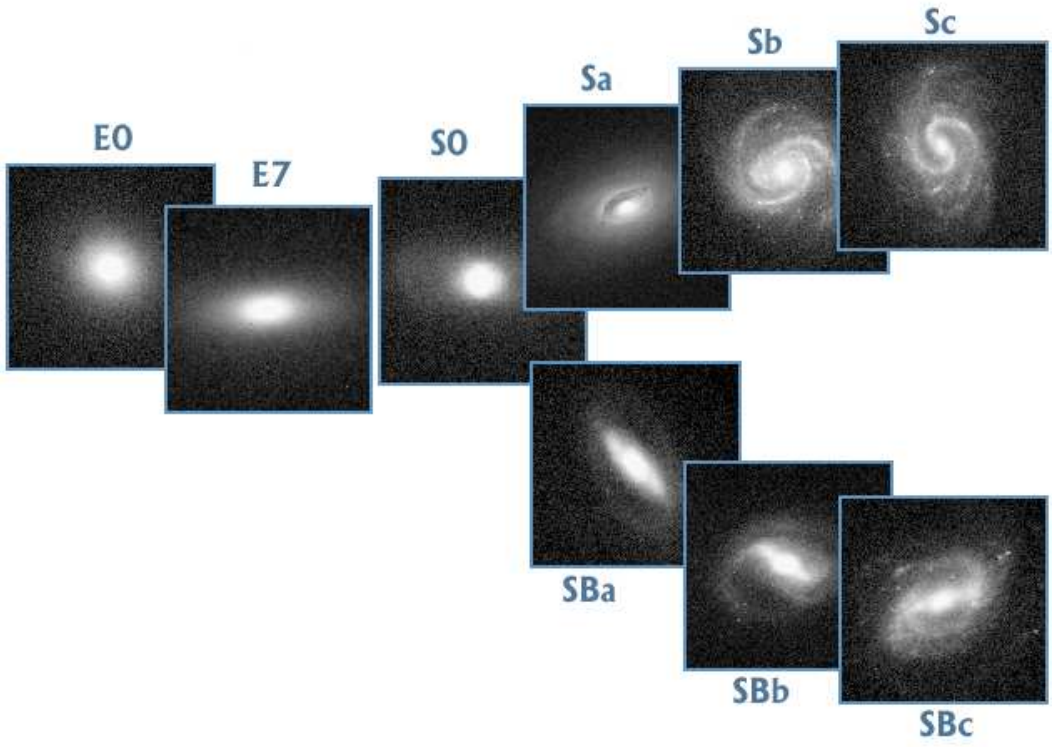

Figure 1.2: Illustration of the Hubble sequence using representative galaxies from the galaxy catalogue of Frei et al. 1996. On the left hand side of the sequence are the ellipticals which range from E0 up to E7 based on their ellipticity. E0s are spherical while an E7 is more cylindrical. At the vertex we have the S0s, which have disks, but no spiral pattern and also a dominant bulge. We then branch into the spirals, Sa, Sb and Sc and the barred spirals, SBa, SBb and SBc. Credit: Zsolt Frei and James E. Gunn

the work of C. Schalen and R. J. Trumpler.

By the end of the 1930s, astronomers had come to realise that the Milky Way was similar to countless other galaxies, and that galaxies as a whole were the dominant structural units of the Universe. Hubble spent many years surveying thousands of these galaxies and, noticing a trend, ordered them into a sequence based on their morphology, the so called Hubble Sequence (figure 1.2).

Further progress in our understanding of the Galaxy came with the realisation of W. Baade that the luminous blue supergiant stars within spiral arms (Population I stars), were different in nature to the red giant stars in spheroidal systems (Population II stars). Population II stars were found to be old and metal poor[1], relative to the Sun. By contrast, Population I stars are relatively young and typically have metal contents comparable to those found in the Sun. The implications were that

[1]Astronomers refer to all elements heavier than hydrogen and helium as *metals.*

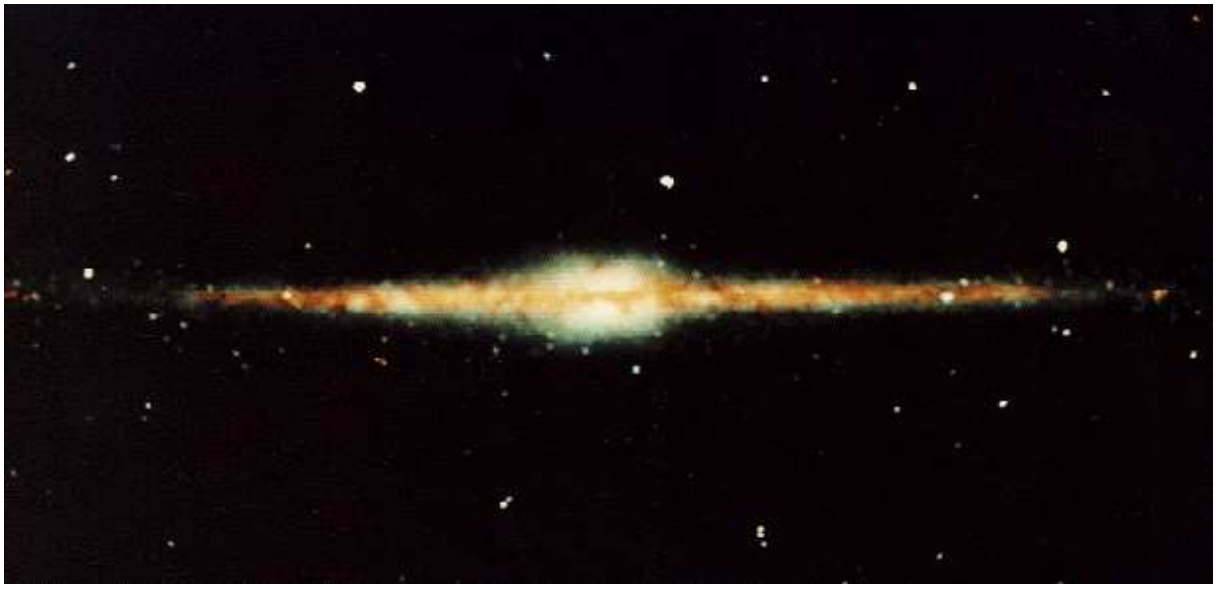

Figure 1.3: This picture was taken by the COBE satellite, and shows the plane of our Galaxy in infrared light. The thin disk is clearly apparent, with stars appearing white and interstellar dust appearing red. Credit: E. L. Wright (UCLA), The COBE Project, DIRBE, NASA

the chemical composition of the old stars were likely indicative of primordial material formed in the Big Bang, and that heavy elements were made by nucleosynthesis in the interiors of stars and then recycled into the interstellar medium (ISM). This work provided insights into stellar evolution, and led to rapid developments in the fields of stellar structure and evolution, from both a theoretical and observational perspective. This classification also naturally supported a scenario on which these two components of the Milky Way formed on different timescales: an old metal-weak spheroid, and a young, metal rich disk. The concept of characterising distinct stellar populations by their spatial distribution, kinematic structure, metal content and age became key in interpreting observations of the Milky Way and other galaxies.

Astronomical work has continued in recent times in establishing details of the Milky Way's structure, and characteristics of its constituent stars (figure 1.3). We know now that our Sun is one of the 200 billion stars in the Milky Way, which itself has a total mass of approximately 500 billion solar masses ($5\times10^{11}M_{\odot}$) and diameter 100,000 light years [2]. The Milky Way is classified as Hubble type Sb or Sc (Sbc) (e.g. Hodge 1983), with the possibility of the existence of a central bar (e.g. Kuijken 1996), which would make it an SBbc, and resides on the periphery of the great Virgo super cluster. It is widely accepted that our Galaxy has several

[2] 100,000 lyrs $\simeq$30 kpc, where 1 pc= 3.1×10^{13}km

distinct structural components, and that these components appeared at different stages in its evolution. The stellar components, the *thin disk*, the *thick disk*, and the *spheroid* (often broken down again to an inner *bulge* and outer *stellar halo*), have different stellar populations in terms of their kinematic and dynamic properties, ages, and chemical compositions. The final component of the Galaxy is the dark halo, presumed to be composed of non-stellar, non-baryonic, matter.

1.2.1 The Thin Disk

The defining stellar component of spiral galaxies, the *disk* contains stars, star clusters, gas and dust which are confined to the Galaxy's plane of rotation. The disk contains ∼90 % of the Milky Way's baryonic material, approximated by an exponential density distribution with a radial scale length of 4.5 kpc and a scale height of about 300 pc. The rotation velocity of stars in the disk is relatively constant with radial distance from the centre (a flat rotation curve, see figure 1.4), with the disk rotating at about 220 km/s. Thin disk stars are relatively young, with an average age around 6 Gyrs, with the oldest disk stars around 10 Gyrs old (e.g. Edvardsson et al. 1993). Age determinations come from the white dwarf cooling sequence, isochrone estimates for individual evolved stars and open clusters, and radioactive dating. Disk stars are also metal rich, with a narrow distribution peaking around solar metalicity, as shown in the middle panel of figure 1.5. The disk contains significant quantities of gas and dust, and is an active site of ongoing star formation, especially in the spiral arms. Star formation there is believed to be triggered both by density waves through the spiral arms (Lin & Shu 1964) and by self-sustained star formation (Talbot & Arnett 1975). Self-sustained star formation occurs when stellar winds and supernovae explosions from massive stars compress neighbouring clouds of gas, triggering further star formation. Young hot stars in the disk are often contained in *associations*, groups of 10-100 stars which formed recently from the same nebula, and are moving together through space. Larger, gravitationally bound *open clusters* of 100-10,000 stars, also reside in the disk.

1.2.2 The Thick Disk

Using star counts, Gilmore & Reid (1983) showed that the Galaxy has a second disk component, referred to as the thick disk due to its significantly greater (relative to the thin disk) vertical scale height, of around 1 kpc (e.g. Phelps et al. 1999). The

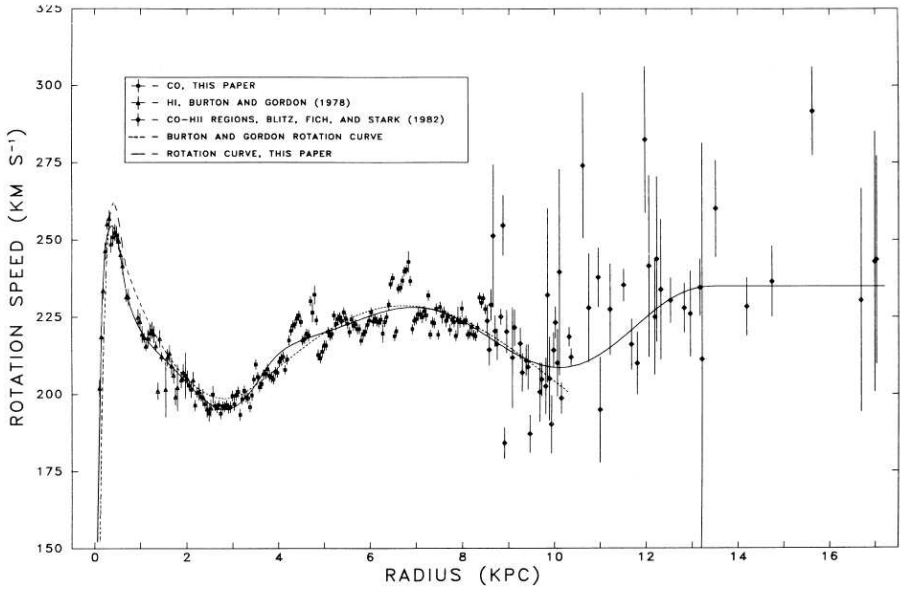

Figure 1.4: A rotation curve for the Milky Way is constructed from measurements of stars and gas in the galactic disk. Figure from Clemens (1985).

thick disk has a surface brightness about 10% that of the thin disk, and the stars therein are almost exclusively older than 12 Gyrs old (e.g. Gilmore & Wyse 1995). The bulk of the thick disk stars have metallicities[3] in the range $-1<$[Fe/H]<-0.2, with a peak near [Fe/H]~ -0.6 (fourth panel of figure 1.5), although there is evidence for the existence of both metal weak (Chiba & Beers 2000), and metal rich (Feltzing Bensby & Lundström 2003) tails to the metallicity distribution. The thick disk rotates, lagging the thin disk by about 40 km/s (Gilmore et al. 1989), and is hotter than the thin disk, with a vertical velocity dispersion of 40-45 km/s (e.g. Chiba & Beers 2000). The kinematics, age and chemical properties of the thick disk all support the hypothesis that it is truly a *distinct* component of the Milky Way, and not simply a sub-component of the thin disk. Thick disks were not believed to exist in all disk galaxies (Fry et al. 1999), until the study of 47 edge on disk galaxies by Dalcanton & Burnstein (2002) provided evidence that thick disks may be ubiquitous.

1.2.3 The Bulge

The central *bulge* of the Galaxy is a dense swarm of stars, containing approximately 10% of the Galaxy's mass in a slightly flattened spheroidal distribution with effective

[3] [Fe/H]$\equiv$log(Fe/H)$-$log(Fe$\odot$/H$\odot$), ie the abundance of iron relative to hydrogen of the star, compared to solar ratio, on a log-based ten scale

radius of ∼2.7 kpc. The bulge stars are generally assumed to be old, an assumption supported by the presence of RR Lyrae stars, as well as the field colour-magnitude diagram (Rich 2001). The advent of infrared cameras and adaptive optics techniques though, has also has revealed the presence of massive stars in the bulge, indicative of recent star formation. The ISOGAL consortium (van Loon et al. 2003) has confirmed that the bulge is dominated by old stars (>7 Gyr), but that intermediate age and young stars (<200 Myr) are also present. The presence of the later is consistent with the bulges of other spirals, such as M31 (e.g Davies et al. 1991), M33 (Mighell & Rich 1995), NGC 247 and NGC 2403 (Davidge & Couteau 2002). The metallicity distribution of the bulge shows significant spread, with a peak near [Fe/H]∼−0.25 (second panel of figure 1.5). The Milky Way's bulge appears to be typical of bulges in late type spirals (Frogel 1990).

1.2.4 The Stellar Halo

The Galactic stellar halo is an approximately $10^9\,M_\odot$ spherical population of stars and globular clusters, of which there are around 100, and contains little gas, dust or on-going star formation. The halo has a density distribution which is well approximated by a power law, $\rho \propto r^{-3.5}$. Only ∼1 % of the Milky Way's stellar component is found in the halo. The halo has almost no net rotation (Freeman 1987) and is supported almost entirely by its velocity dispersion. The most kinematically energetic halo stars have apogalacticons more than 100 kpc from the Galactic centre (Carney et al. 1990). Galactic halo stars are uniformly old, and were probably among the first galactic objects to form. Dating of halo globular clusters by their main-sequence turnoff points indicates that they may be as old as 14 Gyrs (e.g. Gratton et al. 2003). Halo stars are metal poor, with a distribution peak near [Fe/H]∼−1.5 (top panel of figure 1.5), although there does exist a significant range in the halo MDF. The most metal-poor object known in the Universe is a halo star with an iron abundance of [Fe/H]∼ −5.4 (Christlieb et al. 2002). The low luminosity of the stellar halo makes observations of similar extragalactic halos difficult, although a study by Zibetti et al. (2004) provides some evidence that stellar halos are common in disk galaxies.

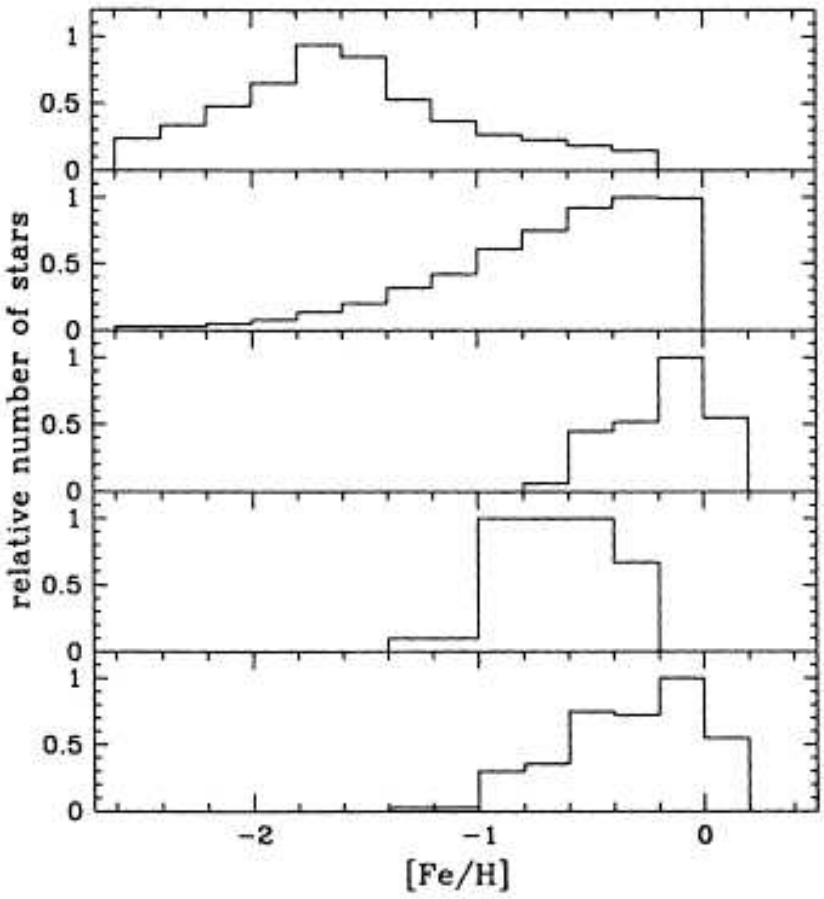

Figure 1.5: **This figure is taken from Wyse (1999), and shows abundance distributions of Milky Way components, normalised to unity. From top to bottom; the Solar neighbourhood halo (Carney et al. 1994); the outer Galactic bulge (Ibata & Gilmore 1995), truncated at solar metallicity due to calibration limitations; the volume complete local thin disk F/G stars (from the Gliese catalogue); the volume complete local thick disk stars; and the "solar cylinder", i.e. F/G stars integrated vertically from the disk plane to infinity.**

1.2.5 The Dark Halo

The observed rotation of the stars and gas clouds of the Galactic disk suggest that the visible matter of the Milky Way is surrounded by a *dark halo* which contains 90% of the Galaxy's mass, and extends to at least 100 kpc (e.g. Kochanek 1996). The nature of the dark matter is unknown, and is peraps the greatest contemporary question facing astrophysics. We will review the evidence for its existence below in the context of structure formation within current theories of cosmology. The dark halo of the Milky Way has a density distribution $\rho \sim r^{-2}$, and is believed to be spheroidal (Crézé et al. 1998; Ibata et al. 2001; c.f. Helmi 2004).

1.3 Cosmology and Structure Formation

Studying the Coma and Virgo clusters in 1933, Fritz Zwicky found that nearly 10 times as much mass as observed in the form of visible light was needed to keep the individual galaxies within the cluster gravitationally bound. Zwicky reasoned that luminous matter made up only a fraction of the matter in the Universe. Scientists began to explore this discrepancy comprehensively in the 1970's, and the existence of *dark matter* began to be taken seriously. At this time Rubin, Freeman and Peebles, amongst others, started measuring rotation curves for galaxies, and found that their orbital speeds remained remarkably constant as radius increased (recall figure 1.4). The implication was that the there was a significant component of the Galaxy that we were unable to see. Peebles & Ostriker (1973) found that numerical simulations of spiral galaxies were unstable when constructed using only the observed matter distributions; the presence of a dark matter halo enveloping the visible matter was required. Dark matter has since been invoked to explain a wide range of observational data, including the motions of stars within dwarf galaxies (e.g. Aaronson 1987), the motion of globular clusters within elliptical galaxies (e.g. Huchra & Brodie 1987), X-ray emmisions from clusters (e.g. Mulchaey et al. 1993) and elliptical galaxies (e.g. Mushotzky et al. 1994; Loewenstein & Mushotzky 2001), the gravitational lensing of very distant galaxies by foreground clusters (e.g. Tyson et al 1990), and Big Bang nucleosynthesis (Walker et al. 1991).

Independent of the quest for dark matter, the favoured cosmological framework for the Universe emerged in the form of the Big Bang model. Edwin Hubble had shown in 1929 that the more distant a galaxy, the more rapidly it appears to be

receding, suggesting that the space between galaxies was expanding. George Gamow argued that this implied that the Universe had emerged from an incredibly dense and hot state in a cataclysmic event, the so-called "Big Bang". This hypohesis was confirmed with the discovery of the predicted *cosmic microwave background* (CMB) in 1965 by A. A. Penzias and R. W. Wilson. The Wilkinson Microwave Anisotropy Probe (WMAP, Spergel et al. 2003) satellite has recently added unprecedented precision to earlier experiments, such as the Balloon Observations of Millimetric Extragalactic Radiation and Geophysics (BOOMERANG, de Bernardis et al. 2000) and the Millimeter Anisotropy Experiment Imaging Array (MAXIMA, Stompor et al. 2001), in measuring the temperature fluctuations of the CMB imprinted from the last scattering surface when radiation and matter decoupled.

The accuracy of the current CMB data has resulted in the establishment of what has been called a "concordance model" of cosmology. We live in a flat Universe, with total energy density close to the critical density, ρ_c, or $\Omega = \rho/\rho_c \simeq 1$. About 1/3 of the density is attributed to matter ($\Omega_M = 0.29 \pm 0.07$, Spergel el al. 2003), of which dark matter dominates ($\Omega_{DM} = 0.243 \pm 0.06$), with baryons contributing less than 5 % ($\Omega_B = 0.047 \pm 0.006$). The remainder of the critical density is contributed by a smoothly distributed vacuum energy ($\Omega_\Lambda = 0.73 \pm 0.04$), which acts to accelerate the expansion of the Universe. The existence of this "dark energy" was already suggested by observations of distant supernovae (Schmidt et al. 1998). The value obtained from WMAP for the expansion rate of the Universe, the Hubble constant H_0, is consistent with that obtained from earlier HST measurements ($H_0 = 71.4$km/s/kpc; Gibson et al. 2000).

Most cosmologists favour the cold dark matter (CDM) theory as a description of how the temperature (i.e. density) perturbations apparent in the CMB become the seeds for the collapse of matter into overdense regions, and the formation of structure. The assumption that dark matter is "cold", or non relativistic, is supported by the WMAP CMB observations. Warm dark matter may also exist, but its contribution to the energy density of the Universe is marginal, limited to a few percent at most (Spergel et al. 2003). In CDM cosmologies, the amplitudes of density perturbations increase with decreasing scale, with small-scale perturbations collapsing first. These then merge into larger structures in a process of hierarchical, or "bottom-up", structure formation. In order to study how strucure evolves and forms through these processes, from small fluctuations when the universe was around 300,000 years old to the present day, the non-linear nature of gravity has meant that

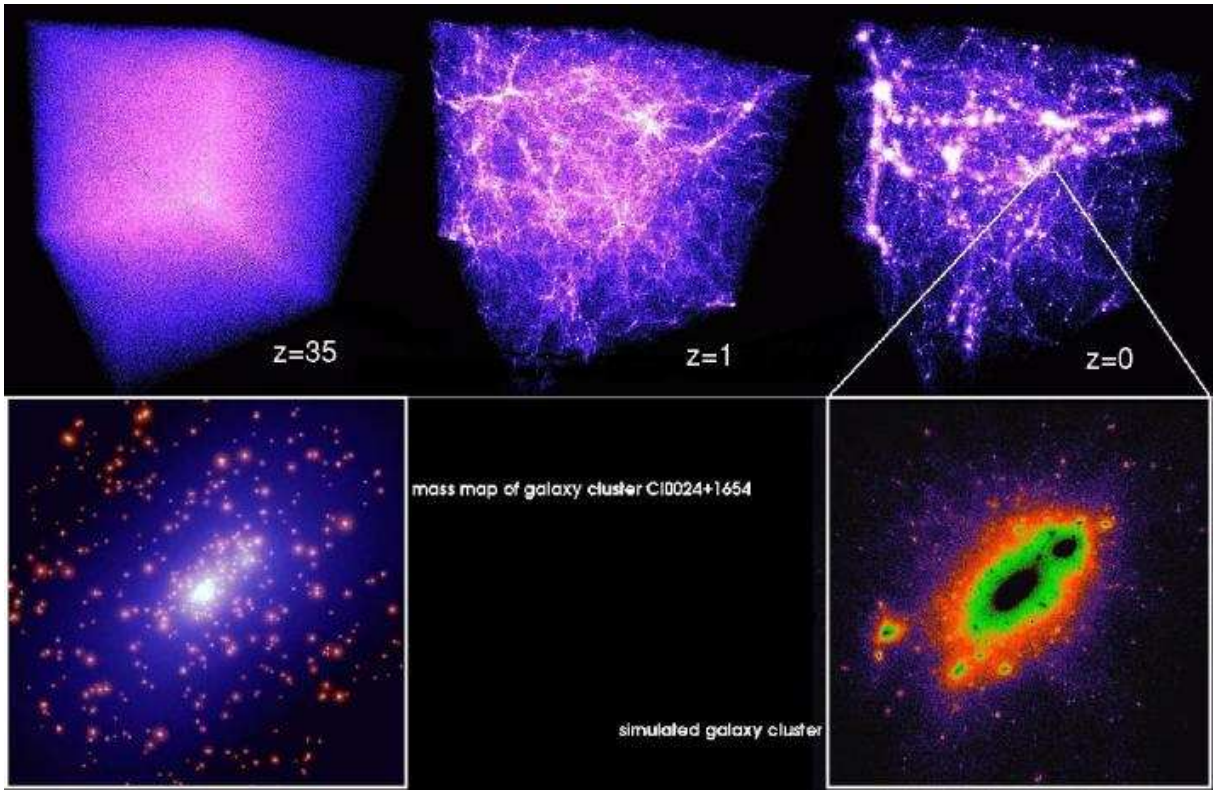

Figure 1.6: A numerical simulation of a ΛCDM Universe. In the top row, we see the formation of large scale structure from the early Universe to the present. The boxes shown are 100 Mpc in size. The statistical properties of the derived distribution at redshift zero provide a close match to those derived from large galaxy surveys. By zooming in on a 1 Mpc region, we see a cluster of galaxies (bottom left), which is seen to resemble the observed cluster C10024+1654 (bottom right). Credit: Alexander Knebe

numerical simulations become crucial. Such simulations have been highly successful in reproducing many observed structural features of the Universe (see figure 1.6).

The CDM model is consistent with an impressive array of observations, including the age of the oldest stars (e.g. Chaboyer et al. 1998), the extragalactic distance scale, as measured by distant Cepheids (e.g. Gibson et al. 2000), the baryonic mass fraction of galaxy clusters (e.g. White et al. 1993), the abundance of massive galaxy clusters (e.g. Eke, Cole & Frenk 1996), the shape and amplitude of galaxy clustering patterns (e.g. Wu, Lahav & Rees 1999), and the magnitude of large-scale coherent motions of galaxy systems (e.g. Strauss & Willick 1995; Zaroubi et al. 1997). However, at least two important discrepancies between the predictions of the CDM paradigm and the observations of galaxies have arisen. First the inner density profile of virialized CDM halos (Navarro, Frenk & White 1997) is too steep with respect

to what is inferred from rotation curves of dwarf spiral and low surface brightness galaxies (e.g. McGaugh & De Block 1998). Second, CDM predicts significantly greater numbers of dwarf galaxies than are observed in systems such as the Local Group (Moore et al. 1999; Klypin et al. 1999).

1.4 A Framework for Disk Galaxy Formation

A detailed prescription for the formation of disk galaxies was outlined in Fall & Efstathiou (1980). In their model, a uniformly rotating, homogeneous protogalactic cloud of gas begins to collapse when a galaxy de-couples from the Hubble flow and begins to collapse. This protogalaxy is endowed with angular momentum from tidal torques driven by surrounding structure (Peebles 1969). It is assumed in their model that the baryons destined to become the disk receive the same tidal torques as the dark matter before much disspiation occurs, and thus the two components initially have the same specific angular momentum. If the collapse is smooth, then specific angular momentum is conserved and the gas forms a thin, rapidly rotating disk. This type of model has been successful in explaining several properties of disk galaxies, including the slope and scatter of the Tully-Fisher relation (Mo, Mao & White 1998), and the distribution of disk surface brightness profiles (Dalcanton, Spergel & Summers 1997).

Admittedly a model predicated upon a homogeneous, uniformly rotating protogalaxy is at odds with the CDM hierarchical structure formation outlined above, in which a galaxy is formed through the merger of smaller "building blocks". The general scenario of galaxy formation within the cosmological context, as envisioned by White & Rees (1978), involves extended dark halos of galaxies forming hierarchically by gravitational clustering of non-dissipative dark matter. The luminous components form by a combination of the gravitational clustering and dissipative collapse. As the baryons cluster and collapse due to gravity, they are shoch-heated to the virial temperature of the halo, at which point the gas can be fully ionised and dissipate energy efficiently by means of bremsstrahlung radiation. With hierarchical structure formation, dark matter "building blocks" form first. The gas then collapses into these building blocks, rather than forming a homogeneous cloud. Problems with this model are encountered when gas falls to the centre of these building blocks. When the building blocks subsequently merge, the gas component

transfers angular momentum to the dark matter. This results in the so called "angular momentum catastrophe" in which simulated spiral galaxies are deficient in specific anglar momentum when compared with observation (e.g. Navarro, Frenk & White 1995). In order to reconcile the two models of formation -i.e. (i) creating a disk galaxy by a collapsing gaseous sphere, and (ii) the general mode of hierarchical clustyering- White & Rees (1978) suggested it was necessary to include energy feedback from star formation, preventing gas from collapsing into "building blocks". Thus it becomes imperative to include processes such as star formation, energy release by stellar winds and supernova explosions, and metal enrichment in modeling the baryonic components of galaxies.

1.5 Simulating Galaxy Formation

One approach which has been used to gain valuable insight into galactic evolution are semi-analytic galactic chemical evolution codes (Talbot & Arnett 1971; Tinsley 1980). These codes take advantage of the fact that the evolution of individual stars is reasonably well understood. The basic picture of chemical evolution is to start with gas of primordial composition and add in an empirical treatment of star formation (with the mass distribution of newly formed stars -the initial mass function (IMF)- specified), with chemical enrichment of the ISM traced self-consistently with each subsequent generation of star birth and death. In addition, these models may consider input and output of gas from any particular region, with either primordial or modified composition. Such semi-analytical models have become increasingly sophisticated, incorporating processes such as enrichment of the ISM, multiple epochs of infall, differential loss of various elements by galactic winds, multi-zone models, and time-dependent IMFs (e.g. Matteucci & François 1989; Pagel & Tautaišiene 1995; Timmes, Woosely & Weaver 1995; Fenner & Gibson 2003). By tracing the evolution of chemical abundances as they cycle through gas and stars, these models have been succesful in explaining mean trends in the chemical properties of galactic systems.

Semi-analytical models (SAMs) of galaxy formation attempt to tie galactic chemical evolution to structure formation. The merger history of a given halo is constructed, most commonly by Monte Carlo realisations of the Press-Schechter formalism. The gas processes involved in galaxy formation, namely the shock heating

and radiative cooling of gas, star formation and feedback are followed using a set of physical laws or, where the physics is poorly understood, phenomenological formalisms. The ease of calculations of these models allows large tracts of parameter space to be explored. White & Frenk (1991) used such models to recover observed properties of galaxies, including their luminosity functions and Tully-Fisher relation. Since that pioneering study, SAMs have also become increasingly sophisticated (e.g. Cole et al. 1994; Cole et al. 2000; Kauffmann 1996; Somerville & Primack 1999).

Numerical models of galaxy formation have one significant advantage over semi-analytical models by providing a self consistent treatment of kinematics and structural evolution. Early models incorporating gas dissipative processes can be traced to Larson (1969), whose axisymmetric models, with self-consistent chemical evolution included, reproduced several essential properties of elliptical (Larson 1974a,b, 1975) and disk (Larson 1976) galaxies. Carlberg (1984a,b) and Carlberg, Lake & Norman (1986) improved upon these models, treating gas and star formation processes in a phenomenological manner. Various parameters introduced include the collision rate of gas clouds, the rates of dissipation, star formation efficiency, and the strength of supernova energy feedback.

Advances in both hardware and software algorithms in the past decade have dramatically improved the quality of such numerical simulations, increasing the dynamical range of the models, as well as the sophistication of physical modeling. The simulations used in this thesis are predicated on the algorithm developed by Katz & Gunn (1991), whose code evolves self-gravitating fluids in three dimensions. Their code -TreeSPH (Hernquist & Katz 1989; Katz, Weinberg & Hernquist 1996)- is a Lagrangian code which combines smoothed particle hydrodynamics (SPH; Lucy 1977; Gingold & Monaghan 1977) with a hierarchical tree algorithm for computing gravitational forces (Barnes & Hut 1986). The explicit calculation of the thermodynamic state of the gas within the TreeSPH algorithm allows radiative cooling to be included via the use of standard cooling curves, resulting in more realistic modelling of gas dissipation. Further, TreeSPH allows for the natural inclusion of a treatment for star formation (Katz 1992) and the subsequent effects of chemical enrichment (Steinmetz & Müller 1994, 1995).

These early simulations were made within a "semi-cosmological" framework, by investigating the collapse of an isolated "top-hat" sphere of dark and baryonic matter which initially follows the Hubble flow. Large scale tidal fields, missing in the semi-cosmological treatment, are instead incorporated by providing the sphere with

an initial degree of solid-body rotation, characterised by a dimensionless spin parameter, λ (Peebles 1971). Small scale density perturbations were then superimposed on the sphere, consistent with the CMB and present day structure of the Universe. Semi-cosmological galaxy evolution models now trace information such as gas temperature and density, stellar age, and various chemical abundances in stars as well as the ISM. By use of stellar poplulation synthesis models, the photomeric properties of the simulated galaxies can be investigated and compared with observation (e.g. Bekki & Shioya 1998; 1999; Steinmetz & Navarro 1999; Mori, Yoshii & Nomoto 1999; Kawata 1999; Koda et al. 2000).

Full cosmological simulations are the most recent development in galaxy formation codes (e.g. Steinmetz & Navarro 1999; Navarro & Steinmetz 2000; Abadi et al. 2003; Kawata & Gibson 2003b). Here, galaxy sized regions of interest within larger scale, lower resolution, cosmological simulations are resimulated at higher resolution, with hydrodynamical gas processes and star formation treatments included. The background cosmological setting remains at low resolution, but still provides a realistic halo mass, merging history and tidal forces which ultimately provide angular momentum and set the collapse redshift. The downside to such simulations is the extra computational resources required when compared against semi-cosmological simulations. Semi-cosmological simulations have a further advantage in being readily suited to arbitrary user specified initial conditions. While computational power has partially eroded the advantages enjoyed by semi-cosmological codes, thier still superior parameter space coverage abilities made them the method of choice for this thesis.

1.6 Studies in this Thesis

Each of the components of this thesis is based upon a comparison of the predictions of our chemo-dynamical semi-cosmological simulations with specific observational data sets of the Milky Way. The overarching goal of this work is to shed light on unanswered questions concerning the formation and evolution of our Galaxy.

1.6.1 Simulating a White Dwarf-dominated Halo

Observational evidence has suggested the possibility of a Galactic halo which is dominated by white dwarfs (WDs). While debate continues concerning the in-

terpretation of this evidence, it is clear that an IMF biased heavily toward WD precursors ($1 \lesssim m/M_{\odot} \lesssim 8$), at least in the early Universe, would be necessary in generating such a halo. Within the framework of homogeneous, closed-box models of Galaxy formation, such biased IMFs lead to an unavoidable overproduction of carbon and nitrogen relative to oxygen (as measured against the abundance patterns in the oldest stars of the Milky Way). Using our three-dimensional Tree N-body smoothed particle hydrodynamics code, we study the dynamics and chemical evolution of a galaxy with different IMFs. Both invariant and metallicity-dependent IMFs are considered. Our variable IMF model invokes a WD-precursor-dominated IMF for metallicities less than 5% solar (primarily the Galactic halo), and the canonical Salpeter IMF otherwise (primarily the disk). Halo WD density distributions and C,N/O abundance patterns are presented. While Galactic haloes comprised of $\gtrsim 5\%$ (by mass) of WDs are not supported by our simulations, mass fractions of $\sim$1-2% cannot be ruled out. This conclusion is consistent with the present-day observational constraints.

1.6.2 High-eccentricity Halo Stars

The present day chemical and dynamical properties of the Milky Way bear the imprint of the Galaxy's formation and evolutionary history. One of the most enduring and critical debates surrounding Galactic evolution is that regarding the competition between "satellite accretion" and "monolithic collapse"; the apparent strong correlation between orbital eccentricity and metallicity of halo stars was originally used as supporting evidence for the latter. While modern-day unbiased samples no longer support the claims for a significant correlation, recent evidence has been presented by Chiba & Beers (2000) for the existence of a minor population of high-eccentricity metal-deficient halo stars. It has been suggested that these stars represent the signature of a rapid (if minor) collapse phase in the Galaxy's history. Employing velocity- and integrals of motion-phase space projections of these stars, coupled with a series of N-body/SPH chemo-dynamical simulations, we suggest an alternative mechanism for creating such stars may be the recent accretion of a polar orbit dwarf galaxy.

1.6.3 Halo Constraints on Simulated Late-type Galaxies

How do late type spiral galaxies form within the context of a CDM cosmology? The reconciliation of the models of hierarchical build up of galaxies proposed by White &

Rees (1978), with the disk galaxy formation model of Fall & Efstathiou (1980), is a central problem of galaxy formation modeling. It has long been assumed that such a reconciliation lies with the processes of energy feedback, primarily due to supernova explosions. Unfortunately these processes have been notoriously difficult to model. We contrast N-body, smoothed particle hydrodynamical simulations of galaxy formation which employ two different supernova feedback mechanisms. Observed mass and metallicity distributions of the stellar halos of the Milky Way and M31 provide constraints on these models. A strong feedback model, incorporating an adiabatic phase in star burst regions, better reproduces these observational properties than our comparative thermal feedback model. This demonstrates the importance of energy feedback in regulating star formation in small systems, which collapse at early epochs, in the evolution of late-type disk galaxies.

1.6.4 The Emergence of the Thick Disk in a CDM Universe

We simulate a Milky Way like disk galaxy using our chemo-dynamical code, `GCD+`; we demonstrate that this disk galaxy has a significant thick disk component. This is evidenced by the velocity dispersion versus age relation for solar neighbourhood stars, which clearly shows an abrupt increase in velocity dispersion at a lookback time of approximately 8 Gyrs, and is in excellent agreement with observation. These thick disk stars are formed from gas which is accreted onto the Galaxy during a chaotic period of hierarchical clustering at high redshift. This formation scenario is shown to be consistent with observations of both the Milky Way and extragalactic thick disks.

Chapter 2

GCD+

2.1 Introduction

Our Galactic chemo-dynamics software package GCD+ was originally developed by Kawata (1999). Work on this package is ongoing, as new techniques are developed in order to better simulate galaxy evolution. Studies employing this software package form the bulk of the work in this thesis, thus it is necessary to provide the reader with sufficient background to appreciate its inner workings and capabilities. A number of enhancements have been made to Kawata's (1999) original version of GCD+ during the course of this thesis. These enhancements, as well as the underlying structure of GCD+ are outlined below.

In GCD+, the dynamics of dark matter and stars are calculated using an N-body scheme, whilst gas dynamics are modeled using smoothed particle hydrodynamics (SPH). The code is based on earlier numerical models of galaxy formation which combine N-body techniques with the SPH method, including Hernquist & Katz (1989), Navarro & White (1993), Katz et al. (1996) and Steinmetz (1996).

GCD+ is vectorised and parallelized. Parallelization is achieved by use of the MPI library, so that the code can run efficiently on most platforms from clusters to PCs to large shared-memory supercomputers. Further details concerning GCD+ can be found in Kawata (1999, 2000, 2001, hereafter K99, K00, K01) and in Kawata & Gibson (2003a,b).

2.2 Modeling Dark Matter and Stellar Dynamics: The *N*-Body Method

Physical entities in GCD+ are represented by a large number, N, of point-like particles which represent the gas, stars and dark matter of the Universe. These particles are then "tagged" with characteristics corresponding to their physical properties. The cosmological framework in which GCD+ operates is a standard Cold Dark Matter (CDM) Universe. Incorporating the gravitational effects of dark matter is perhaps the most fundamental aspect of structure formation theory. Dark matter is typically represented within the theory as massive particles that interact with each other and with baryonic matter particles only through the gravitational force. Computationally this is done via the application of a gravitational N-body algorithm. In addition to such gravitational forces, gas particles interact with each other via hydrodynamical forces, which are dealt with in the next section.

We employ a gravitational force calculation based upon the hierarchical tree formalism (Barnes & Hut 1986; Pealzner & Gibbon 1996). The tree algorithm is computationally efficient, though at the expense of several approximations being required to describe the gravitational potential. One calculates the multipole moments of a nested hierarchy of particles in which each particle then interacts with other elements of the hierarchy, subject to accuracy conditions, in order to calculate gravitational forces. "Clustered" particles well away from from a given single particle are treated as a single entity with a given multipole expansion of sufficient accuracy. The ratio of the size of a "cluster" to its distance from the given particle is compared to a tolerance parameter to determine whether treating that cluster as a point mass is sufficient, or whether it is necessary to proceed further down the tree to smaller clusters. As the number of terms in the multipole expansion is typically small compared with the number of particles in the cluster, a significant gain in efficiency is realised. Conceptually, the detailed distribution of particles is neglected when calculating their collective gravitational effect on a given particle, up to a given level of accuracy, determined by a tolerance parameter. In GCD+, expansion is made to the quadrupole order with a tolerance parameter θ=0.8.

In order to minimise the effects of two body relaxation, a gravitational softening length is employed. Specifically, the gravitational force term of the i-th particle is

the sum of the contributions from dark matter, star and gas particles

$$\nabla_i \Phi = -G \sum_j \frac{m_j \mathbf{x}_{ij}}{(r_{ij}^2 + \epsilon_{ij}^2)^{3/2}} \tag{2.1}$$

where $r_{ij} \equiv |\mathbf{x}_{ij}|$, $\mathbf{x}_{ij} \equiv \mathbf{x}_i - \mathbf{x}_j$ and $\epsilon_{ij} \equiv (\epsilon_i + \epsilon_j)/2$ is the mean softening length of the i-th and j-th particles.

2.3 Modeling Gas Dynamics: The SPH Method

Gas dynamics in GCD+ is treated by modeling a collection of particles, using the smoothed particle hydrodynamics (SPH) method (Lucy 1977; Gingold & Monaghan 1977). These gas particles experience local forces from pressure gradients in addition to gravitational forces. In SPH the Lagrangian form of the hydrodynamical equations is used to determine the dynamics of the particles. Local physical conditions are described by a finite number of neighbour particles in order to mimic a fluid. It is assumed that the mass density of the fluid is roughly proportional to the particle mass density. A consequence of this is that susceptibility to local statistical fluctuations in particle numbers must be minimised, which is achieved by introducing the concept of a "kernel". GCD+ employs a spherically symmetric spline kernel of the form

$$W(r,h) = \frac{8}{\pi h^3} \begin{cases} 1 - 6(r/h)^2 + 6(r/h)^3 & \text{if } 0 \le r/h \le 1/2, \\ 2[1-(r/h)]^3 & \text{if } 1/2 \le r/h \le 1, \\ 0 & \text{otherwise,} \end{cases} \tag{2.2}$$

where r is the distance from the particle and h is a particle's individual smoothing length, chosen to keep the number of particles within its smoothing length roughly constant.

We use a smoothing length algorithm based upon that of Thacker et al. (2000), an improvement upon the original technique used by K99 and K00 (which was derived from Steinmetz 1996). This variable smoothing length ensures that all points in the fluid have smoothed quantities computed to the same level of mass resolution. First, neighbour particles are counted for the i-th particle using the smoothing kernel,

$$W_{nn}(r,h_i) = \begin{cases} 1 & \text{if } 0 \le r/h_i \le 3/4, \\ \frac{\pi h_i^3}{8} W(4(r/h_i - 3/4)) & \text{if } 3/4 \le r/h_i \le 1, \end{cases} \tag{2.3}$$

where r is the distance between the i-th particle and its neighbour, and W(x) is the spline kernel (equation 2.2). The number of neighbours, $N_{nb,i}$ is a real number rather than an integer, alleviating discontinuity in the number of neighbours. Then the smoothing length, h_i^{n+1}, at the time-step $n+1$ is determined by the smoothing length, h_i^n, and the number of neighbours, $N_{nb,i}^n$, at the previous time-step n:

$$h_i^{n+1} = h_i^n \left[1 - a + a \left(\frac{N_s}{N_{nb,i}^n} \right)^{1/3} \right], \tag{2.4}$$

where $N_s = 40$ is the desired number of neighbours. This adopted value for N_s provides acceptable accuracy as demonstrated by one-dimensional shock tube tests. The variable a changes as a function of the parameter $s = (N_s/N_{nb,i}^n)^{1/3}$, as

$$a = \begin{cases} 0.2(1+s^2) & \text{if } s < 1 \\ 0.2(1+1/s^3) & \text{if } s \ge 1 \end{cases} \tag{2.5}$$

Physical parameters pertaining to each particle, such as density, ρ, are then calculated by

$$\rho_i = \sum_j m_j W(r_{ij}, h_{ij}), \tag{2.6}$$

where $h_{ij} = (h_i + h_j)/2$ is the pair averaged smoothing length. Euler's equation is employed to trace the kinematics of particle i, and takes the form

$$\frac{d\mathbf{v}_i}{dt} = -\frac{1}{\rho_i} \nabla_i (P + P_{visc}) - \nabla_i \Phi_i \tag{2.7}$$

where Φ, P and P_{visc} are the gravitational potential, pressure, and the artificial viscous pressure, respectively. The gravitational force, $\nabla_i \Phi_i$, is computed as in equation (2.1). GCD+ uses the following smoothed estimate of the pressure-gradient term

$$\frac{1}{\rho_i} \nabla_i (P + P_{visc}) = \sum_j \left(\frac{P_i}{\rho_i^2} + \frac{P_j}{\rho_j^2} + Q_{ij} \right) \nabla_i W(\mathbf{x}_{ij}, h_{ij}), \tag{2.8}$$

where Q_{ij} is the artificial viscosity. The artificial viscous pressure term allows for the presence of shock waves in the flows to be included computationally. Shock fronts generate energy and transform kinetic energy into internal energy, preferably with minimum post-shock oscillations to the hydrodynamical variables. The form taken for the artificial viscosity follows Navarro & Steinmetz (1997),

$$Q_{ij} = \begin{cases} \dfrac{-\alpha v_{\mathrm{s},ij}\mu_{ij} + \beta\mu_{ij}^2}{\rho_{ij}} & \text{if } \mathbf{x}_{ij}\cdot\mathbf{v}_{ij} < 0, \\ 0 & \text{otherwise,} \end{cases} \tag{2.9}$$

with

$$\frac{\mu_{ij} = 0.5 h_{ij}\mathbf{v}_{ij}\cdot\mathbf{x}_{ij}}{r_{ij}^2 + \eta^2}, \tag{2.10}$$

where $\mathbf{v}_{ij} \equiv \mathbf{v}_i - \mathbf{v}_j$. The parameters $\alpha = 0.5$, $\beta = 1.0$, controlling the amplitude of post-shock oscillations, are set to reproduce features of the one-dimensional shock tube experiment. The parameter $\eta = 0.05 h_{ij}$ is introduced to prevent numerical divergences. A correction is then made in order to reduce the shear component of the artificial viscosity (see Balsara 1995; Navarro & Steinmetz 1997)

$$\tilde{Q}_{ij} = Q_{ij}\frac{f_i + f_j}{2}, \tag{2.11}$$

$$f_i = \frac{|\langle\nabla\cdot\mathbf{v}\rangle_i|}{|\langle\nabla\cdot\mathbf{v}\rangle_i| + |\langle\nabla\times\mathbf{v}\rangle_i| + 0.0002 v_{s,i}/h_i} \tag{2.12}$$

where v_s is the sound velocity. The velocity divergence and rotation are calculated by

$$\langle\nabla\cdot\mathbf{v}\rangle_i = -\frac{1}{\rho_i}\sum_j m_j \mathbf{v}_{ij}\cdot\nabla_i W(\mathbf{x}_{ij}, h_{ij}), \tag{2.13}$$

$$\langle\nabla\times\mathbf{v}\rangle_i = -\frac{1}{\rho_i}\sum_j m_j [v_{ij,z}\nabla_{i,y}W(\mathbf{x}_{ij}, h_{ij}) - v_{ij,y}\nabla_{i,z}W(\mathbf{x}_{ij}, h_{ij})], \tag{2.14}$$

where $v_{ij,x} \equiv v_{i,x} - v_{j,x}$. If the flow is shear-free and compressive, the corrected viscosity term is identical to the uncorrected term. In the presence of shear flows, the effect of the correction is to reduce the importance of the viscous term.

The velocity and position of each particle is updated by integrating equation (2.7) using a leap-frog algorithm with individual time-steps, following Hernquist & Katz

(1989) and Makino (1991). The time-step of the i-th particle is chosen to be $\Delta t_i = \min(0.3\Delta t_{CFL,i}, 0.1\Delta t_{f,i})$, where Δt_{CFL} is determined by the Courant-Friedrichs-Lewy condition

$$\Delta t_{CFL,i} = \frac{0.5 h_i}{v_{s,i} + 1.2(\alpha v_{s,i} + \beta max_j |\mu_{ij}|)}, \tag{2.15}$$

and Δt_i is determined by the requirement that the force should not change significantly from one time-step to the next. This is achieved by

$$\Delta t_{f,i} = \sqrt{\frac{h_i}{2} \left| \frac{d\mathbf{v}_i}{dt} \right|^{-1}}. \tag{2.16}$$

A lower limit for the smoothing length is set to be $h_{min} = \epsilon/2$. For collisionless dark matter and star particles, the time-step is determined by

$$\Delta t = min[0.16(\epsilon/v), 0.4(\epsilon/|dv/dt|^{1/2}]. \tag{2.17}$$

The leap-frog method then involves integrating the position and velocity in the following manner:

$$\mathbf{v}^{n+1/2} = \mathbf{v}^n + 0.5 \left(\frac{d\mathbf{v}}{dt}(\mathbf{x}^n, \tilde{\mathbf{v}}^n, ...) \right)^n \Delta t^{n \to n+1}, \tag{2.18}$$

$$\mathbf{x}^{n+1} = \mathbf{x}^n + \mathbf{v}^{n+1/2} \Delta t^{n \to n+1}, \tag{2.19}$$

$$\tilde{\mathbf{v}}^{n+1} = \mathbf{v}^{n+1/2} + 0.5 \left(\frac{d\mathbf{v}}{dt}(\mathbf{x}^n, \tilde{\mathbf{v}}^n, ...) \right)^n \Delta t^{n \to n+1}, \tag{2.20}$$

$$\mathbf{v}^{n+1} = \mathbf{v}^{n+1/2} + 0.5 \left(\frac{d\mathbf{v}}{dt}(\mathbf{x}^{n+1}, \tilde{\mathbf{v}}^{n+1}, ...) \right)^{n+1} \Delta t^{n \to n+1}, \tag{2.21}$$

where $\Delta t^{n \to n+1}$ represents a time interval between n and $n+1$ steps.

The smoothed form of the thermal energy equation used in GCD+ to determine the evolution of the internal energy, u_i is

$$\frac{du_i}{dt} = \frac{P_i}{\rho_i} \sum_j m_j \mathbf{v}_{ij} \cdot \nabla_i W(\mathbf{x}_{ij}, h_{ij}) + \frac{1}{2} \sum_j m_j Q_{ij} \mathbf{v}_{ij} \cdot \nabla_i W(\mathbf{x}_{ij}, h_{ij}) - \frac{\Lambda_i}{\rho_i} + H_i, \tag{2.22}$$

where $\Lambda\rho$ and H are the cooling rate and heating rate per unit mass. We consider cooling due to metallicity dependent radiative gas processes using cooling curves derived from the literature (see below). Heating in the form of supernovae (SNe) feedback also is taken into account.

The minimum time-step between the particles is employed when calculating the time evolution of internal energy for each particle. The energy equation is then integrated semi-implicitly using the trapezoidal rule,

$$u^{n+1} = u^n + 0.5 \left[\left(\frac{du}{dt} \right)^n + \left(\frac{du}{dt} \right)^{n+1} \right] \Delta t^{n \rightarrow n+1}. \tag{2.23}$$

This equation must be solved iteratively, since $(du/dt)^{n+1}$ depends on u^{n+1}. First, a prediction for the thermal energy $\tilde{u}^{n+1}$ is found by assuming that $(du/dt)^{n+1} = (du/dt)^n$. The predicted value $\tilde{u}^{n+1}$ is then used along with the predicted velocity $\tilde{\mathbf{v}}^{n+1}$ from equation (2.20), to estimate the adiabatic term, including the artificial viscosity and the heating in equation (2.22). Only the cooling term Λ^{n+1} is estimated iteratively using the corrected internal energy, once the adiabatic term is obtained. A convergence solution is found using the bisection technique. In order to ensure numerical stability, the radiative cooling is damped according to,

$$\left(\frac{du}{dt}_{rad}^{damped} = \right) \frac{a(du/dt)_{rad}}{\sqrt{a^2 + [(du/dt)_{rad}]^2}}, \tag{2.24}$$

$$a = 0.5 \frac{u}{\delta t} + \left(\frac{du}{dt} \right)_{rad}. \tag{2.25}$$

Here, $(\frac{du}{dt})_{rad}$ is the change in the thermal energy excluding the contribution from the undamped radiative cooling, $(\frac{du}{dt})_{rad} = \lambda\rho_g$ in equation (2.22).

An equation of state closes the system of equations describing the evolution of the fluid, as well as determines the pressure of each particle. The ideal gas law is used

$$P = (\gamma - 1)\rho u, \tag{2.26}$$

where u is the specific internal energy, and $\gamma = 5/3$ for a mono-atomic gas.

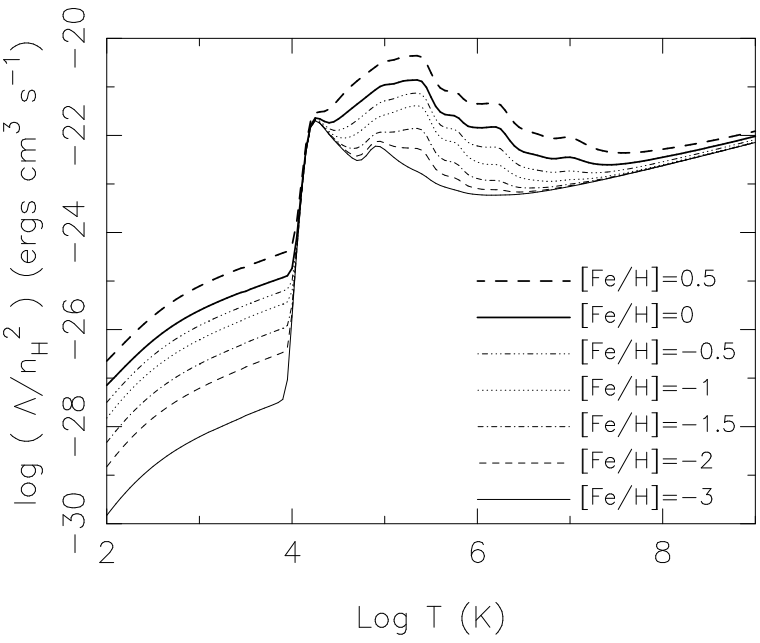

Figure 2.1: Cooling rates, plotted as a function of temperature, for the metallicities indicated. Linear interpolation of these curves is used to calculate cooling rates as a function of temperature and metallicity.

2.4 Radiative Gas Cooling

The temperature of gas particles in GCD+ is derived by $T_i = P_i \mu m_p/(k_B \rho_i)$, where P_i and ρ_i are the pressure and density of the i-th particle, μ is the mean molecular weight, k_B is Boltzmann's constant and m_p is the proton mass. For simplicity, the mean molecular weight is set to μ=0.6, independent of metallicity. The lower limit to the calculated temperature is T_{lim}=100 K, unless otherwise stated. Radiative cooling of gas is modeled using the cooling curves of MAPPINGS III (Sutherland & Dopita, 1993). It is important to use metallicity-dependent models due to the strong role played by metals in radiatively cooling gas (Käellander & Hultman 1998; Kay et al. 2000) . The models adopted in GCD+ are shown in figure 2.1. It is assumed that gas with metallicity below [Fe/H]$= -3$ cools at the same rate as gas with [Fe/H]$= -3$, and that the cooling rate for gas with [Fe/H]> 0.5 is the same as that for [Fe/H]$= 0.5$. The cooling rates for $-3 <$[Fe/H]< 0.5 are calculated, as a function of the temperature and metallicity of each gas particle, by linear interpolation of the cooling curves.

2.5 Star Formation

Star formation prescriptions similar to those of Katz (1992) and Katz, Weinberg & Hernquist (1996) were employed. Star formation occurs whenever

1. the gas density is greater than a critical density:
   $\rho_{crit} = 2 \times 10^{-25}$ g cm^{-3} (Katz et al. 1996),

2. the gas velocity field is convergent: $\nabla \cdot v_i < 0$, and

3. the gas is Jeans unstable, i.e. $h/v_s > \tau_g$, where h is the smoothing length, v_s the speed of sound, and $\tau_g = \sqrt{3\pi/16G\rho_g}$ is the dynamical time of the gas.

The adopted star formation law is written

$$\frac{d\rho_*}{dt} = -\frac{d\rho_g}{dt} = \frac{c_*\rho_g}{\tau_g} \tag{2.27}$$

where $\frac{d\rho_*}{dt}$ is the star formation rate (SFR). Equation (2.27) corresponds to a Schmidt law in which the SFR is proportional to $\rho_g^{1.5}$. The star formation timescale is assumed to be the local dynamical timescale, $\tau_g = \sqrt{(3\pi/16G\rho_g)}$ because in regions eligible for star formation, the dynamical timescale is generally longer than the cooling timescale. Star formation efficiency is parameterised by the dimensionless parameter c_*.

Equation (2.27) implies that the probability, p_*, with which one gas particle entirely transforms into a star particle during a discrete time step, Δt, is $p_* = 1 - exp(-c_*\Delta t/t_g)$. Entirely transforming gas particles into star particles, using such a probabilistic approach, avoids the creation of an intolerably large number of star particles of different masses being formed. The newly created star particle behaves as a collisionless particle, as described in section 2.2.

2.6 Initial Mass Function

In GCD+ simulations, "stars" are represented as particles, which for the simulations described here have a typical mass of $10^5 - 10^6$ M$_\odot$. The relative number distribution of stellar masses within a star particle at its birth is governed by the assumed initial mass function (IMF). Variation of this IMF, in particular with respect to low metallicity stars, is central to our feasibility study concerning white dwarfs being a

significant component of the dark matter of the halo of Milky Way (chapter 3). In other studies presented in this thesis, the IMF is considered to be universal, with the canonical Salpeter (1955) form adopted. The Salpter IMF is written (by number)

$$\Phi(m)\mathrm{d}m = dn/dm = Am^{-(1+x)}\,\mathrm{d}m, \tag{2.28}$$

with x=1.35. The coefficient A in equation (3.3) is determined by normalising the IMF to unity over the specified range of stellar masses.

2.7 Feedback

GCD+ takes into account metal enrichment and energy released by both Type II (SNe II) and Type Ia (SNe Ia) supernovae, as well as the metal enrichment from intermediate mass stars. The event rates and yields of SNe II and SNe Ia, and the yields of intermediate mass stars, are calculated for each particle at each time-step, by taking into account the IMF and stellar lifetimes.

The amount of mass, energy, and heavy elements released by SNe is smoothed over neighbouring gas particles using the SPH kernel (Katz 1992). For example, in the time-step in which mass $M_{ej,i}$ is ejected from the i-th star particle, the increment of the mass of the j-th neighbour particle is

$$\Delta M_{ej,j} = \frac{m_j}{\rho_{g,i}} M_{ej,i} W(r_{ij}, h_{ij}) \tag{2.29}$$

where

$$\rho_{g,i} = \langle \rho_g(x_i) \rangle = \sum_{j \neq i} m_j W(r_{ij}, h_{ij}) \tag{2.30}$$

and $W(r_{ij}, h_{ij})$ is the SPH kernel (equation 2.2).

2.7.1 Supernovae

It is assumed that each massive star ($\geq$8 $\mathrm{M}_\odot$) explodes as a SNe II. Rates for SNe Ia are calculated following the model proposed by Kobayashi, Tsujimoto & Nomoto (2000, KTN00 hereafter). This model assumes that SNe Ia occur in binary systems which consist of primary and companion stars with appropriate masses. The model also assumes that SNe Ia do not occur in low metallicity stars with [Fe/H]< -1.1

(although this is implemented in GCD+ by using total metallicity rather than iron abundance, $\log Z/Z_{\odot} < -1.1$).

In this formalism, primary stars have main-sequence masses in the range of $\mathrm{m}_{p,l} = 3\,\mathrm{M}_{\odot}$ and $\mathrm{m}_{p,u} = 8\,\mathrm{M}_{\odot}$, and evolve into C+O white dwarfs (WDs). The mass range of companion stars are restricted to being between $\mathrm{m}_{d,RG,l} = 0.9\,\mathrm{M}_{\odot}$ and $\mathrm{m}_{d,RG,u} = 1.5\,\mathrm{M}_{\odot}$ for low-mass red giants, with the system designated a 'RG+WD system' and between $\mathrm{m}_{d,MS,l} = 1.8\,\mathrm{M}_{\odot}$ $\mathrm{m}_{d,MS,u} = 2.6\,\mathrm{M}_{\odot}$ for slightly evolved main sequence companions, designated a 'MS+WD system'. The total number of SNe Ia is then obtained as a function of age, t, of a star particle with the mass of $\mathrm{m}_s\,\mathrm{M}_{\odot}$, via

$$\begin{aligned} N_{\mathrm{SNeIa}}(t) &= m_s \int_{m_{p,l}}^{m_{p,u}} m^{-(1+x)} dm \left\{ \int_{M_l}^{M_u} m^{-x} dm \right\}^{-1} \\ &\times \left[b_{\mathrm{MS}} \frac{\int_{\max(m_{d,MS,l}, m_t)}^{m_{d,MS,u}} \Phi_d(m) dm}{\int_{m_{d,MS,l}}^{m_{d,MS,u}} \Phi_d(m) dm} \right. \\ &\left. + b_{\mathrm{RG}} \frac{\int_{\max(m_{d,RG,l}, m_t)}^{m_{d,RG,u}} \Phi_d(m) dm}{\int_{m_{d,RG,l}}^{m_{d,RG,u}} \Phi_d(m) dm} \right], \end{aligned} \tag{2.31}$$

where m_t is the mass of a star whose lifetime is equal to t, and the mass function of the companion stars is assumed to be $\Phi_d(m) \propto m^{-0.35}$, following KTN00. The term before the square bracket indicates the number of C+O WDs, i.e. primary stars. The first term within the square bracket determines the fraction of C+O WDs which evolve into SNe Ia from MS+WD systems, and the second term determines the fraction of C+O WDs which evolve into SNe Ia from RG+WD systems. Following KTN00, we set $b_{MS} = 0.05$ and $b_{RG} = 0.02$. The nucleosynthesis prescriptions for SNe Ia are taken from the W7 model of Iwamoto et al. (1999).

2.7.2 Heavy Elements

The evolution of several chemical elements are followed in GCD+; ^{1}H, ^{4}He, ^{12}C, ^{14}N, ^{16}O, ^{20}Ne, ^{24}Mg, ^{28}Si, ^{56}Fe and total metallicity, Z. The stellar yields of Woosley & Weaver (1995, hereafter WW95) are used to provide the mass of gas and metals ejected by SNe II. These provide yields for stars between the mass range $11\,\mathrm{M}_{\odot}$ and $40\,\mathrm{M}_{\odot}$ (using their 'B' Model for stars greater than $30\,\mathrm{M}_{\odot}$). For masses above

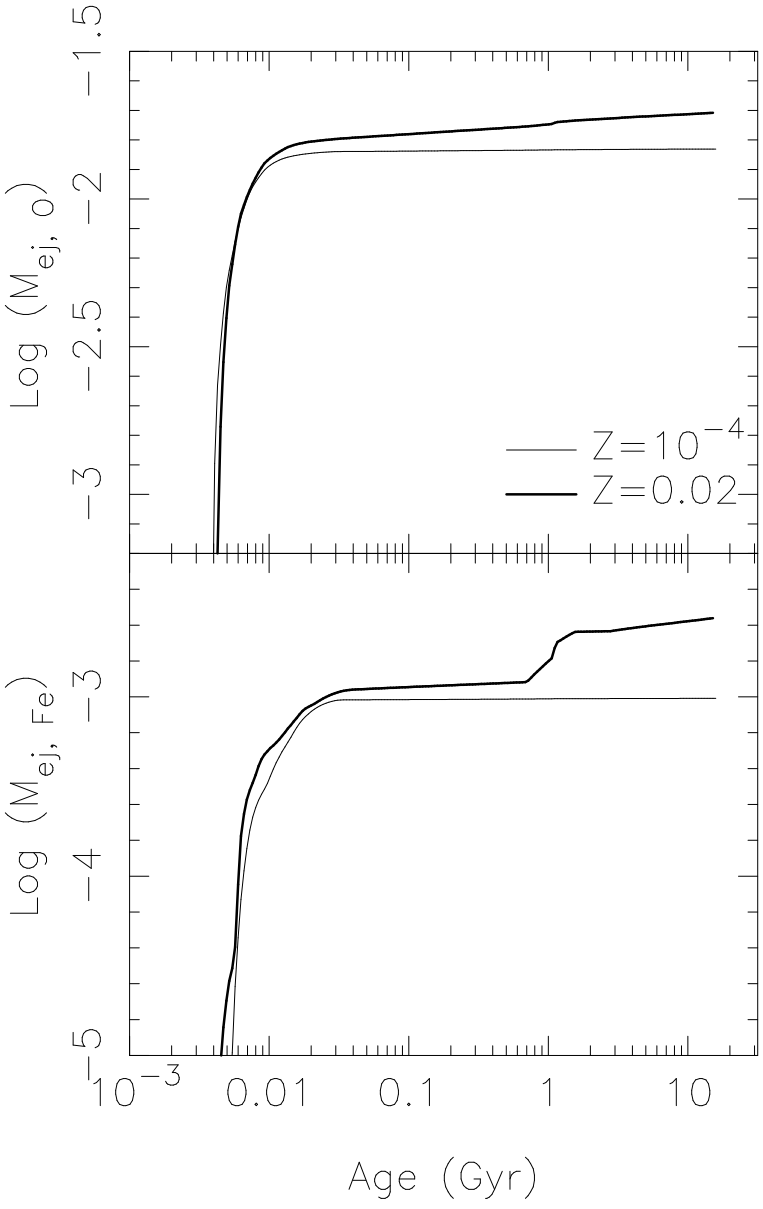

Figure 2.2: Chemical yields of a burst of star formation of mass 1 $M_\odot$ as a function of time. The upper (lower) panel shows the total ejected oxygen (iron) mass. The history of a star particle are shown for two metallicities, Z=0.02 (thick line) and Z=10^{-4} (thin line).

$40\,M_\odot$ the same abundance ratios for stars of mass $40\,M_\odot$ are assumed. The yields of WW95 are metallicity dependent, and the code makes linear interpolations between grids of different metallicity to calculate the yields.

For intermediate mass stars ($\leq 8\,M_\odot$) yields and remnant masses are taken from van den Hoek & Groenwegen (1997), which provide metallicity dependent yields of ^{1}H, ^{4}He, ^{12}C, ^{14}N and ^{16}O for stars in the mass range $0.8\,M_\odot$-$8\,M_\odot$. Abundances for ^{20}Ne, ^{24}Mg, ^{28}Si, and ^{56}Fe are scaled to the solar abundance set. Yields for stars in the mass range $8\,M_\odot$-$11\,M_\odot$ remain uncertain, so linear interpolation is used between yields of the most massive stars in the van den Hoek & Groenwegen (1997) tables and the lowest mass stars in the tables of WW95.

A further uncertainty is in the yields from zero metallicity stars. We simply use the yields from the lowest metallicity stars in the vdHG tables, i.e. Z= 0.001, for all stars with lower metallicity. Recent yields of Limongi & Chieffi (2003) indicate that this simplification will not have a dramatic effect. It is important though to acknowledge those particular studies for which such an assumption could be problematic. This is the case for our study of a putative white dwarf dominated Galactic halo (chapter 3).

A look-up table of all yields, remnant masses and number of SNe as a function of a star particle's age and metallicity is used for each star particle at each time-step. Here, we use the stellar lifetimes adopted by Kodama (1997) and Kodama & Arimoto (1997). Figure 2.2 shows the total amount of oxygen and iron ejected from a $1\,M\odot$ burst of star formation as a function of time. Metals are initially ejected by SNe II, which produce most of the oxygen. After SNe II cease, at the time of death of an $8\,M\odot$ star, any additional oxygen ejection is due to intermediate-mass stars. The timescale for iron production is set by the lifetime of the secondary in the binary systems which lead to SNe Ia.

2.7.3 Energy Feedback

Structure formation in our models is driven by dark matter, initially expanding with the Hubble flow, then collapsing due to local overdensities. Gas initially traces this dark matter, with star formation triggered within the most dense regions. When the most massive of these stars end their lives they "feedback" energy into the surrounding ISM, affecting galaxy evolution on a global scale. These effects are seen on scales ranging from the inter galactic medium and galaxy clusters, to globular

cluster and dwarf galaxies.

The implementation of energy feedback into galaxy formation codes remains a challenge. In a simulation by Katz (1992), energy feedback was implemented by depositing thermal energy into the surrounding gas, using the SPH kernel. This form of energy feedback was found to be inefficient, as the regions in which star formation is occurring are, by design, high density regions, and hence have short cooling timescales. Thus the thermal energy is radiated away rapidly, without regulating star formation. The model assumes that SNe energy affects the temperature of the surrounding gas, thereby increasing the internal energy of neighbour particles. Hence, when the i-th particle ejects SNe energy of $E_{SN,i}$, it deposits energy $\Delta E_{SN,j}$ in the j-th neighbour gas particle, using the smoothing kernel

$$\Delta E_{SN,j} = E_{SN,i} \frac{m_j}{\rho_{g,i}} W(r_{i,j}, h_{i,j}). \tag{2.32}$$

In GCD+ it is assumed that each SNe yields an energy of $\epsilon_{SN} \times 10^{51}$ ergs.

The difficulties in implementing feedback in galaxy evolution codes and the problems that result in terms of simulating galaxy formation are examined in some detail in our study of disk galaxy formation in chapter 5. It is important in our studies to be aware of these problems and to be aware of their potential effects on the particular aspect of galaxy formation which is being probed.

Chapter 3

Simulating a White Dwarf dominated Halo

3.1 Introduction

Evidence gathered by microlensing surveys toward the Large Magellanic Cloud suggest that a substantial fraction of the Milky Way's dark matter halo is comprised of $\sim$0.5 $M_{\odot}$ objects: the MACHO Team claim 20% of the halo's dynamical mass may be tied up in these half-solar mass constituents (Alcock et al. 2000), while the EROS Team favour an upper limit of 30% (Lasserre et al. 2000). Constraints set by Hubble Space Telescope red star counts (Flynn et al. 1996) rule out large numbers of low-mass hydrogen burning stars in the halo. By process of elimination, white dwarfs represent one potential baryonic candidate for these microlensing events. This would correspond to of order 2×10^{11} white dwarfs out to a distance of 60 kpc in the Galactic halo (see Zritsky 1999).

The apparent identification of 2-5 high proper motion white dwarfs in the Hubble Deep Field-North supported the white dwarf-dominated halo hypothesis (Ibata et al. 1999), as did the colour analysis of the Hubble Deep Field-South (Mendez et al. 2000). The Ibata et al. claim has since been retracted (Richer 2001). Ground-based searches for nearby high-proper motion white dwarfs initially suggested a white dwarf halo mass fraction of 10% (Ibata et al. 2000), although Flynn et al. (2001) favoured $\lesssim$ 2%. Based upon dynamical arguments and Galactic winds driven by a putative population of white dwarf progenitors, Zhao (2002) suggest a fraction <4%. Regardless, Oppenheimer et al. (2001, hereafter OHDHS) have recently revived the

white dwarf-dominated halo picture with their claim that >2% of the halo is made up of white dwarfs. While criticism of the OHDHS analysis is appreciable (Gibson & Flynn 2001; Reid et al. 2001; Reylé et al. 2001; Flynn et al. 2003; Torres et al. 2002), their result (if confirmed) may yet be made consistent with the MACHO and EROS Team results[1]

White dwarfs represent the end point in the life cycle of stars with initial masses in the approximate range $1 - 8\,M_\odot$. Populating a white dwarf-dominated Galactic halo, in conjunction with a standard stellar initial mass function (IMF), would lead to a corresponding increase in the production of Type II supernovae (SNeII) and the rapid overproduction of heavy elements (Gibson & Mould 1997, hereafter GM97). In addition, the expected number of low-mass red dwarfs would violate the deep halo star counts of Flynn et. al. (1996). These high- and low-mass constraints imply that a standard IMF cannot be employed to populate a putative white dwarf-dominated Galactic halo. Instead, the IMF would have had to have been comprised almost exclusively of stars in the range $1 \lesssim m/M_\odot \lesssim 8$; such white dwarf-heavy IMFs have been discussed in the literature by Chabrier et al. (1996, hereafter C96) and Adams & Laughlin (1996).

Besides the requirement that any white dwarf-heavy IMF be restricted to $1 \lesssim m/M_\odot \lesssim 8$, there is an additional constraint provided by the observed abundance patterns in Population II halo stars. GM97 found that a white dwarf-dominated IMF (wdIMF) inevitably leads to the overproduction of carbon and nitrogen relative to oxygen - *by more than an order of magnitude* - in comparison with that seen in the oldest stars of the Milky Way's halo. This result is a natural consequence of the life cycle of low- and intermediate-mass stars, the stars which are responsible for synthesising the majority of the carbon and nitrogen in the Universe. Fields et al. (2000) confirmed the analysis of GM97, concluding that the carbon and nitrogen content of the halo provides the strictest constraint to any white dwarf-dominated halo scenario.

While there is no compelling direct evidence for variable IMFs, *at the present time* (e.g. Gilmore 2001), several theoretical studies suggest that the IMF of the first

[1]Note that Nelson et al. (2002) claim a 7% white dwarf dark halo based upon 24 candidate high-proper motion objects in the Groth Strip. Likewise Mendez (2002) argues that most of the dark matter in the solar vincinity can be accounted for by halo and thick-disk white dwarfs (albeit based upon one apparent high-proper motion white dwarf seen towards NGC 6397). The EROS-2 white dwarf proper motion survey find that the halo white dwarf fraction cannot exceed 5% (95% c.l.).

generation of stars (so-called Population III) might be quite different from that of the canonical Salpeter IMF (sIMF). Direct attempts to form Pop III stars in numerical simulations indicate an IMF biased toward super massive stars ($M > 100\,M_{\odot}$) rather than white dwarf progenitors (Abel, Bryan & Norman 1999, 2002). It is the lack of metals, which cause cloud fragmentation of gas in star forming regions, that results in such a top heavy IMF (see also Bromm et. al 2001). Other studies also indicate a different IMF for Pop III stars, e.g. Yoshii & Saio (1987) and Nakamura & Umemura (2001), the latter study proposing a bimodal IMF that produces large numbers of super massive stars around $100\,M_{\odot}$ and a futher peak in the intermediate, white dwarf progenitor mass range. It is possible that the stars from the high mass peak of such an IMF would not contribute to chemical enrichment due to the formation of black holes, thus making such an IMF effectively favour white dwarf progenitors. This Pop III IMF is expected to apply to the first generation of halo stars - the generation which would manifest itself *now* in the population of putative high-proper motion stellar halo white dwarfs. Such studies remain, however, highly uncertain. Our motivation for invoking the wdIMF remains the MACHO observations and the necessity for invoking such an IMF in order for these observations to be explained by a large population of white dwarf stars populating the halo. In addition to the wdIMF and sIMF possibilities, in what follows we will also consider a variable IMF in which stars formed from the low (high) metallicity gas are distributed following the adoption of the wdIMF (sIMF). One can anticipate that while the wdIMF phase will invariably lead to high C/O and N/O ratios (as discussed by GM97), the subsequent sIMF phase can ameliorate this effect. A variable IMF scenario was not considered by GM97.

The currently favoured hierarchical clustering scenario of galaxy formation postulates that star formation progresses through the on-going accretion of galactic building blocks. Within this framework, highly inhomogeneous chemical evolution occurs; homogeneous closed-box models for the Milky Way's evolution (as were adopted by GM97) are no longer suitable. The early phases of galaxy formation demand a chemo-dynamical approach, one which we adopt here explicitly within the context of the white dwarf-dominated IMF hypothesis. In what follows, we examine the ability of metallicity-dependent variable IMFs to resolve the apparent contradiction between a significantly white dwarf-heavy Galactic halo and the C/O and N/O abundance patterns of halo stars. To achieve this, we perform numerical simulations that calculate the chemical and dynamical evolution of a Milky Way-like

galaxy in a self-consistent manner.

In section 3.2, we describe our numerical methods, concentrating upon the code itself and our treatments of star formation, IMFs, and energy feedback to the interstellar medium (ISM). Section 3.3 presents the results of our simulations in terms of resulting white dwarf halo densities, and Galactic chemical evolution of carbon, nitrogen, and oxygen. The implications for a white dwarf-dominated Galactic dark matter halo are described in section 3.4.

3.2 Method

3.2.1 The Code

Our simulations were performed using a modified version of the software package described by Kawata (1999, 2001). An overview of the code is provided here along with the relevant modifications made for the current study - the reader is referred to Kawata (1999, 2001) for all other details. Our code is based upon the Hernquist & Katz 1989 and Katz, Weinberg & Hernquist 1996 `TreeSPH`, combining a tree algorithm (Barnes & Hut 1986) with smoothed particle hydrodynamics (SPH) (Lucy 1977; Gingold & Monaghan 1977) for the computation of gravitational forces and numerical hydrodynamics respectively. This three-dimensional code is fully Lagrangian, with individual smoothing lengths and time-steps making it highly adaptive in space and time. It includes a self-consistent treatment of physical processes governing galaxy formation, including self-gravity, hydrodynamics, radiative cooling, star formation, supernovae feedback, and metal enrichment. We employ metallicity-dependent gas cooling rates derived from MAPPINGS III (Sutherland & Dopita 1993); their implementation is described by Kawata & Gibson (2003a).

Star Formation

Star formation prescriptions similar to those of Katz (1992) and Katz, Weinberg & Hernquist (1996) were employed. Star formation occurs whenever

1. the gas density is greater than a critical density:
   $\rho_{crit} = 2 \times 10^{-25}$ g cm^{-3} (Katz et al. 1996), and

2. the gas velocity field is convergent: $\nabla \cdot v_i < 0$.

Our adopted star formation law is written

$$\frac{d\rho_*}{dt} = -\frac{d\rho_g}{dt} = \frac{c_*\rho_g}{\tau_g} \tag{3.1}$$

where $\frac{d\rho_*}{dt}$ is the star formation rate (SFR). Equation 3.1 corresponds to a Schmidt law in which the SFR is proportional to $\rho_g^{1.5}$. The dynamical timescale of the gas is given by $\tau_g = \sqrt{(3\pi/16G\rho_g)}$; in regions eligible for star formation, this dynamical timescale is generally longer than the cooling timescale. Star formation efficiency is parameterised by the dimensionless parameter c_*, which, after Kawata (1999, 2001), is set to $c_* = 0.5$.

Equation 3.1 implies that the probability, p_*, with which one gas particle entirely transforms into a star particle during a discrete time step, Δt, is $\mathrm{p}_* = 1 - exp(-c_*\Delta t/t_g)$. This avoids an intolerably large number of star particles of different masses being formed. The newly created star particle behaves as a collisionless particle.

Initial Mass Functions

In our `TreeSPH` simulations, stars are represented as particles with a typical mass of order $10^5\,\mathrm{M}_\odot$; the relative number distribution of stellar masses within a "particle" is governed by the assumed initial mass function (IMF). Fundamental to our modeling is the adoption of the Chabrier et al. (1996) white dwarf progenitor-dominated IMF (wdIMF). We represent this IMF by a truncated power-law of the form

$$\Phi(m)\,\mathrm{d}m = dn/dm = Ae^{-(\bar{m}/m)^\beta} \times m^{-\alpha}\,\mathrm{d}m \tag{3.2}$$

for which we use $\bar{m} = 2.7$, $\beta = 2.2$, and $\alpha = 5.75$. The peak of this wdIMF occurs at $m \approx 2\,\mathrm{M}_\odot$, favouring the production of white dwarf progenitors.

The canonical Salpeter (1955) IMF (sIMF) is used to describe the local stellar mass function (by number) and is written

$$\Phi(m)\mathrm{d}m = dn/dm = Am^{-(1+x)}\,\mathrm{d}m, \tag{3.3}$$

with x=1.35. The sIMF (red line) and wdIMF (green line) are shown in figure 3.1.

The coefficient A in equations 3.2 and 3.3 is determined by normalising the respective IMFs over the mass range $0.1 \leq m/\mathrm{M}_\odot \leq 40.0$. We explore simulations in

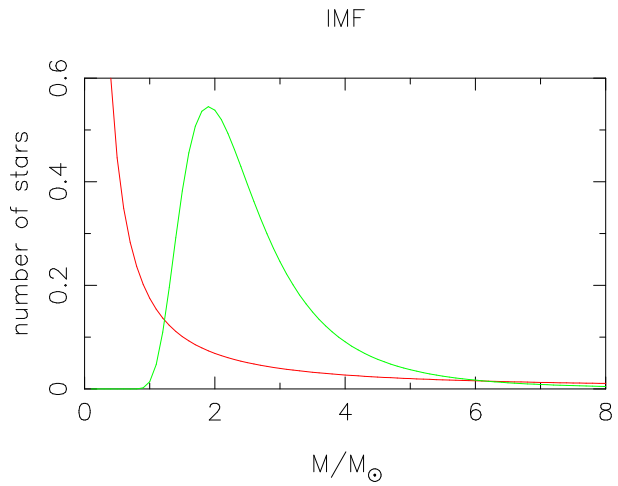

Figure 3.1: Comparison of the Salpeter (1955) (red line) and Chabrier et al. (1996) (green line) IMFs; the latter is dominated by white dwarf progenitors. Both IMFs have been normalised to unity over the mass range $0.1 \leq m/M_{\odot} \leq 40.0$.

which the adopted IMF is invariant in space and time (and governed by either the wdIMF or sIMF functions), as well as metallicity-dependent models (in which star formation in regions where the gas metallicity is less than 5% solar is governed by the wdIMF form, with the sIMF form applying otherwise).

We compare the results of our simulations using these very different IMF assumptions in terms of their chemical evolution properties, and contrast their inherent inhomogeneous nature with the original homogeneous models of GM97. Each IMF assumption also leads to very different outcomes for the halo and disk white dwarf densities, an issue we return to in section 3.3.

Feedback

Type II supernovae (SNeII) are assumed to be the end result for all stars of mass $m \geq 10\,M_{\odot}$. These massive stars explode within the simulation time-step in which they are born, and so the instantaneous recycling approximation (for the nucleosynthetic products associated with these stars) applies. SNeII release thermal and mechanical energy to the surrounding interstellar medium, in addition to their stellar yields; we assume that each supernova releases 10^{50} erg of thermal energy. For SNeII, the metallicity-dependant stellar yields of Woosley & Weaver (1995) are adopted.

For low- and intermediate-mass stars, we use the stellar yields of van den Hoek & Groenwegen (1997). The lifetimes of these stars are significantly longer than the time-steps of our simulations, and so the instantaneous recycling approximation is

relaxed; we assume that recycling from intermediate mass stars occurs after a fixed time delay. Weighting by the IMF slope, over the range $1 \leq m/\mathrm{M}_\odot \leq 8$, the typical mass is $\sim 2\,\mathrm{M}_\odot$ (for both the wdIMF and sIMF); we therefore adopt a delay of 1 Gyr, corresponding to the main sequence lifetime of a $2\,\mathrm{M}_\odot$ star (Schaller et al. 1992).

For the current study, we ignore the effects of Type Ia supernovae. As noted by GM97, these supernovae do not produce significant amounts of carbon, nitrogen, or oxygen (relative to SNeII), elements that form the basis of the analysis which follows.

The mass, energy and heavy elements are smoothed over the neighbouring gas particles using the SPH smoothing algorithm. For example, in the timestep in which mass is released from a star particle due to a Type II supernova explosion, the increment of the mass of the j-th neighbour particle is

$$\Delta M_{SN,j} = \frac{m_j}{\rho_{g,i}} M_{SN,i} W(r_{ij}, h_{ij}) \tag{3.4}$$

where

$$\rho_{g,i} = \langle \rho_g(x_i) \rangle = \sum_{j \neq i} m_j W(r_{ij}, h_{ij}) \tag{3.5}$$

and $W(r_{ij}, h_{ij})$ is an SPH kernal.

Tables 3.1 (SNeII) and 3.2 (low- and intermediate-mass stars) list the IMF-weighted stellar yields (in solar masses ejected per solar mass of stars formed) adopted in our analysis; in both tables, the first block represents the sIMF yields and the second block, the wdIMF. Four (three) different metallicities are highlighted for massive (intermediate mass) stars.

The overproduction of carbon and nitrogen with respect to oxygen for IMFs dominated by white dwarf precursors, can be best appreciated by referring to figure 3.2. Shown here are the adopted stellar yields' [C,N/O][2] as a function of initial mass; both [C/O] and [N/O] are significantly in excess of solar for $m \leq 8\,\mathrm{M}_\odot$. In comparison, the oldest stars of the Galactic halo show [C/O]$\simeq$[N/O]$\simeq -0.5$ (Timmes, Woosley & Weaver 1995). We can anticipate that an IMF in which a large number of these intermediate mass stars are present will result in an overabundance of carbon and nitrogen compared to solar abundances.

The uncertainty in the stellar yields of zero metallicity stars was one of the few caveats that accompanied the earlier semi-analytical models of GM97 and Fields

[2] $[\mathrm{C/O}] \equiv \log(\mathrm{C/O}) - \log(\mathrm{C/O})_\odot$

Table 3.1: IMF-weighted stellar yields adopted for massive ($m \geq 10\,M_\odot$) stars.

		Salpeter (1955) - sIMF		
Metallicity	$0.0 \leq Z/Z_\odot < 10^{-4}$	$10^{-4} \leq Z/Z_\odot < 10^{-1}$	$10^{-1} \leq Z/Z_\odot < 1.0$	$1.0 \leq Z/Z_\odot$
Element				
C	6.12×10^{-4}	8.46×10^{-4}	8.39×10^{-4}	8.53×10^{-4}
O	2.74×10^{-3}	5.99×10^{-3}	6.55×10^{-3}	7.26×10^{-3}
N	3.25×10^{-5}	3.20×10^{-5}	6.09×10^{-5}	3.05×10^{-4}
Ne	2.08×10^{-4}	7.32×10^{-4}	5.47×10^{-4}	6.92×10^{-4}
Mg	1.42×10^{-4}	2.83×10^{-4}	3.17×10^{-4}	4.14×10^{-4}
Si	1.80×10^{-4}	5.88×10^{-4}	6.06×10^{-4}	7.60×10^{-4}
Fe	4.78×10^{-4}	4.76×10^{-4}	7.86×10^{-4}	7.05×10^{-4}
[C/O]	-0.16	-0.35	-0.40	-0.44
[N/O]	-0.98	-1.33	-1.09	-0.44
		Chabrier et al. (1996) - wdIMF		
C	3.62×10^{-6}	5.49×10^{-6}	6.06×10^{-6}	5.77×10^{-6}
O	7.71×10^{-6}	1.47×10^{-5}	1.76×10^{-5}	2.12×10^{-5}
N	1.20×10^{-6}	1.21×10^{-6}	1.47×10^{-6}	3.31×10^{-6}
Ne	8.66×10^{-7}	6.14×10^{-6}	1.61×10^{-6}	3.07×10^{-5}
Mg	5.63×10^{-7}	7.32×10^{-7}	8.30×10^{-7}	1.36×10^{-6}
Si	1.72×10^{-6}	3.62×10^{-6}	2.92×10^{-6}	4.04×10^{-6}
Fe	6.00×10^{-6}	3.94×10^{-6}	1.02×10^{-5}	6.41×10^{-6}
[C/O]	0.167	0.067	0.032	-0.070
[N/O]	0.14	-0.14	-0.13	0.13

Table 3.2: IMF-weighted stellar yields adopted for low- and intermediate-mass ($m \leq 8\,M_\odot$) stars.

		Salpeter (1955) - sIMF	
Metallicity	$5 \times 10^{-3} \leq Z/Z_\odot < 10^{-1}$	$10^{-1} \leq Z/Z_\odot < 1.0$	$1.0 \leq Z/Z_\odot$
Element			
C	6.82×10^{-4}	7.26×10^{-4}	1.20×10^{-3}
O	1.27×10^{-5}	1.18×10^{-4}	1.11×10^{-3}
N	1.32×10^{-3}	1.37×10^{-3}	1.21×10^{-3}
Ne	1.06×10^{-5}	1.56×10^{-5}	2.36×10^{-5}
Mg	5.95×10^{-7}	1.19×10^{-5}	1.26×10^{-4}
Si	6.46×10^{-7}	1.29×10^{-5}	1.36×10^{-4}
Fe	1.07×10^{-6}	2.14×10^{-5}	2.26×10^{-4}
[C/O]	2.22	1.28	0.529
[N/O]	2.95	2.00	0.97
		Chabrier et al. (1996) - wdIMF	
C	3.96×10^{-3}	3.10×10^{-3}	3.96×10^{-3}
O	7.67×10^{-5}	4.54×10^{-4}	4.31×10^{-3}
N	2.42×10^{-3}	1.43×10^{-3}	1.74×10^{-3}
Ne	3.32×10^{-5}	5.70×10^{-5}	8.60×10^{-5}
Mg	9.81×10^{-7}	4.47×10^{-5}	4.70×10^{-4}
Si	1.07×10^{-6}	4.85×10^{-5}	5.11×10^{-4}
Fe	1.76×10^{-6}	8.05×10^{-5}	8.48×10^{-4}
[C/O]	2.21	1.32	0.46
[N/O]	2.44	1.43	0.54

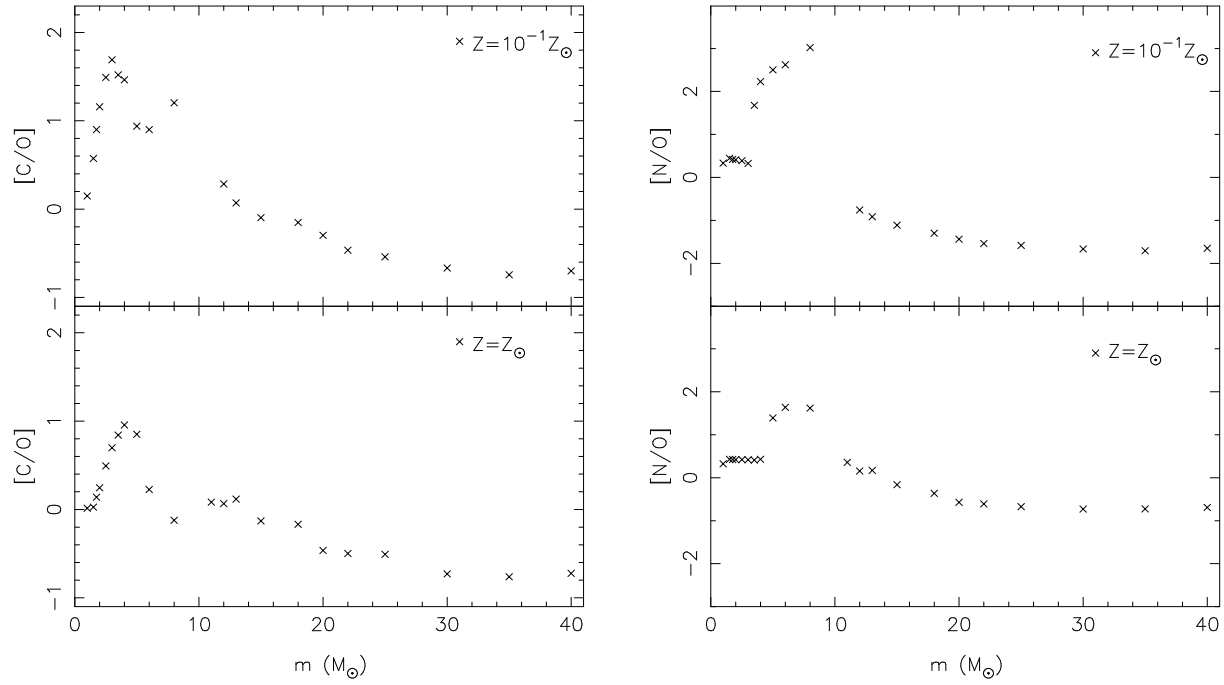

Figure 3.2: Ratio of carbon (left panels) and nitrogen (right panels) to oxygen for the adopted stellar yields - Woosley & Weaver (1995) yields were adopted for Type II supernova progenitors ($m \geq 10\,M_\odot$), while the low- and intermediate-mass yields of van den Hoek & Groenewegen (1997) were used for $m \leq 8\,M_\odot$.

et al. (2000). As noted by Marigo et al. (2001) "the distinct evolutionary behaviour of these (zero metallicity) stars may also imply a very distinct nucleosynthesis and chemical pollution of the interstellar medium"; at issue here is the production of carbon and nitrogen in Population III stars. *If* it could be shown that neither element was synthesised or ejected into the ISM in the early Universe, a "loophole" could then exist that would allow a white dwarf-dominated Galactic halo without violating the elemental abundance patterns in the halo today. The new stellar evolution models described by Abia et al. (2001) suggest that large quantitative differences do not exist between extant low-metallicity models (which undergo thermal pulses and eject significant carbon and nitrogen) and Population III (at least for masses $4 \leq m/\mathrm{M}_{\odot} \leq 7$; for masses $m \leq 4\,\mathrm{M}_{\odot}$, the Population III yields remain uncertain). Our models are qualitatively robust against the specific choice of yield compilation.

3.2.2 The Model

We calculate semi-cosmological models, following the technique described by Kawata (1999, 2001). Our seed galaxy is an isolated sphere upon which small-scale density fluctuations corresponding to a cold dark matter (CDM) power spectrum are superimposed. These initial density fluctuations are generated using COSMICS (Bertschinger 1995). The effects of longer wavelength fluctuations are incorporated by enhanced density of the sphere and the application of a spin parameter λ responsible for initiating rigid rotation of the overdense sphere. This spin parameter is defined

$$\lambda \equiv \frac{J|E|^{1/2}}{GM_{tot}^{5/2}}, \tag{3.6}$$

where E is the total energy of the system, J the total angular momentum, M_{tot} the total mass of the sphere (dark matter + gas). Mass fluctuations (rms) in a sphere of radius $8h^{-1}\,\mathrm{Mpc}$ are denoted $\sigma_{8,in}$, and normalise the amplitude of the CDM power spectrum. According to Katz & Gunn (1992) and Steinmetz & Muller (1995), a large value of $\sigma_{8,in}$ leads a large transfer of angular momentum from the gas particles to the dark matter particles, and a bulge larger than observed in the Milky Way; in order to avoid this, we consider the Galaxy to be formed in an environment where the small scale density perturbation is smoother than the mean value suggested in standard CDM cosmology. We set $\sigma_{8,in} = 0.1$. The expected collapse redshift is given by z_c. The amplitude of the top-hat density perturbation δ_i is approximately

Table 3.3: The three models adopted in the current analysis; the initial mass function (IMF) is the only variable.

	IMF	
Model	$Z < 0.05\ Z_\odot$	$Z > 0.05\ Z_\odot$
model 1	Salpeter	Salpeter
model 2	Chabrier	Chabrier
model 3	Chabrier	Salpeter

related to initial and collapse redshift by $z_c = 0.36\delta_i(1 + z_i) - 1$ (Padmanabham 1993). Thus δ_i is determined for a given z_c at z_i. We set $z_c = 2.0$. The simulated galaxies described here have total mass $M_{tot} = 5 \times 10^{11}\,\mathrm{M}_\odot$, approximating the total mass of the Milky Way within 50 kpc (Wilkinson & Evans 1999). For our models, the initial conditions are uniquely determined by the choice of λ, M_{tot}, $\sigma_{8,in}$, and z_c.

Using a comparable semi-cosmological model, Katz & Gunn (1991) found that a seed galaxy with a large spin parameter evolves into a disk system. Our best Milky Way models require $\lambda = 0.07$, in order to remain consistent with the Galaxy's present-day disk properties. We assume a flat ($\Omega_o = 1$) universe with baryon fraction $\Omega_b = 0.1$ and Hubble constant $\mathrm{H}_o = 50\,km\,s^{-1}\,Mpc^{-1}$; evolution within isolated galaxy simulations using top hat overdensities are not greatly influenced by choice of cosmology. Evolution is traced from an initial redshift $z_i = 40$ to the present.

The initial conditions used are somewhat artificial, and do not exactly reflect hierarchical formation of the Milky Way as expected in CDM cosmologies. However, this approach still traces hierarchical build up of a galaxy, self-consistently treating its chemical and dynamical history, and is sufficient for the purposes of documenting the effects between different IMFs.

Our study relies on the chemical enrichment processes of SPH, as described in section 3.2.1. In order to ensure that such processes are not determined by the resolution adopted, we perform the study at three different resolution regimes. The resolution regimes employ 6142, 18342, and 40958 particles (initially split evenly between gas and dark matter). The results presented in this paper are from the highest resolution models; the results of different resolution regimes varied only marginally quantitatively, and the analysis and conclusions presented hold in all three; we therefore only present the highest resolution models. Our highest resolution models have dark matter (baryonic) particles of mass $2.2 \times 10^6\,\mathrm{M}_\odot$ ($2.4 \times 10^5\,\mathrm{M}_\odot$), which

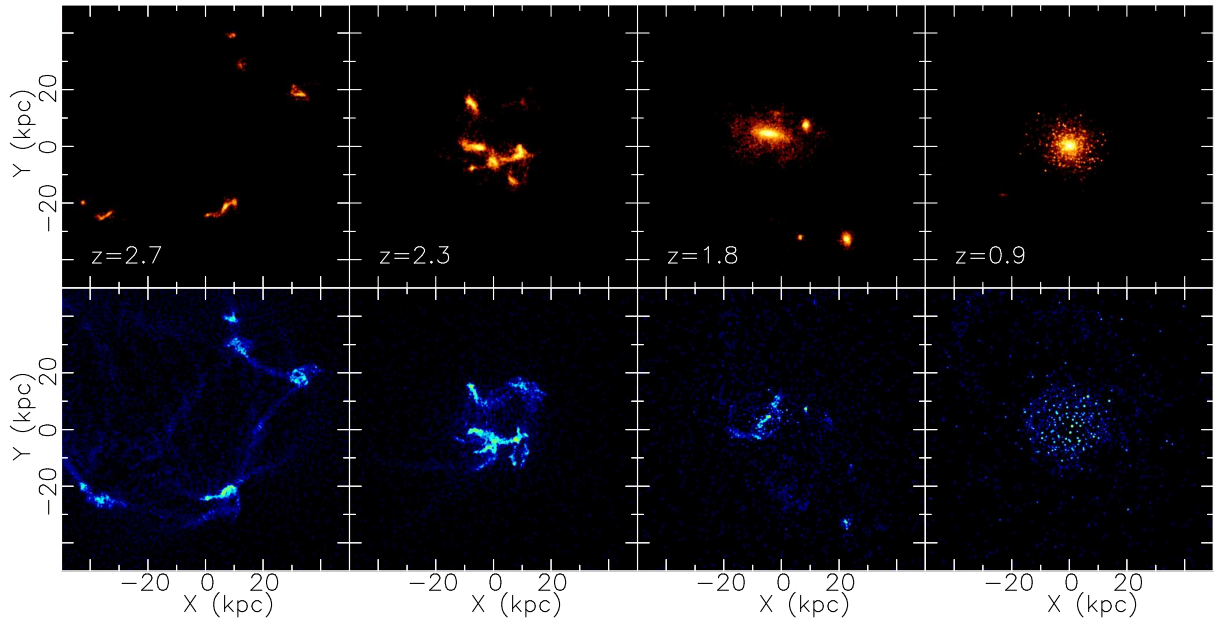

Figure 3.3: Density plot of the projection onto the X-Y plane of the evolution of stars (upper row) and gas (bottom row) during the major star forming epoch of model 3.

is comparable in resolution with other recent simulations of disk galaxy formation (e.g. Abadi et. al 2003)[3]. The gravitational softening length is 0.79 kpc (1.6 kpc) for baryonic (dark matter) particles.

As noted earlier, the primary "variable" in our simulations is the initial mass function (IMF). Three different scenarios have been considered here - models 1 and 2 assume the Salpeter (1955) and Chabrier et al. (1996) IMFs, respectively, regardless of metallicity; model 3 assumes the Chabrier et al. IMF (wdIM) for metallicities below 5% solar, and the Salpeter IMF (sIMF) elsewhere, as summarised in table 3.3.

3.3 Results

Figures 3.3 and 3.4 show the X-Y and X-Z projections of the morphological evolution for model 3, over the redshift range $z = 2.7$ to $z = 0.9$; models 1 and 2 are qualitatively similar. The Z-axis corresponds to the initial rotation axis. Sub-clumps associated with early star formation can be traced to initial small-scale density fluctuations, and are clearly seen by redshift $z \approx 2.5$. These sub-clumps

[3]In galaxy formation simulations including cooling, the physical resolution determines the computational costs rather than the total number of particles.

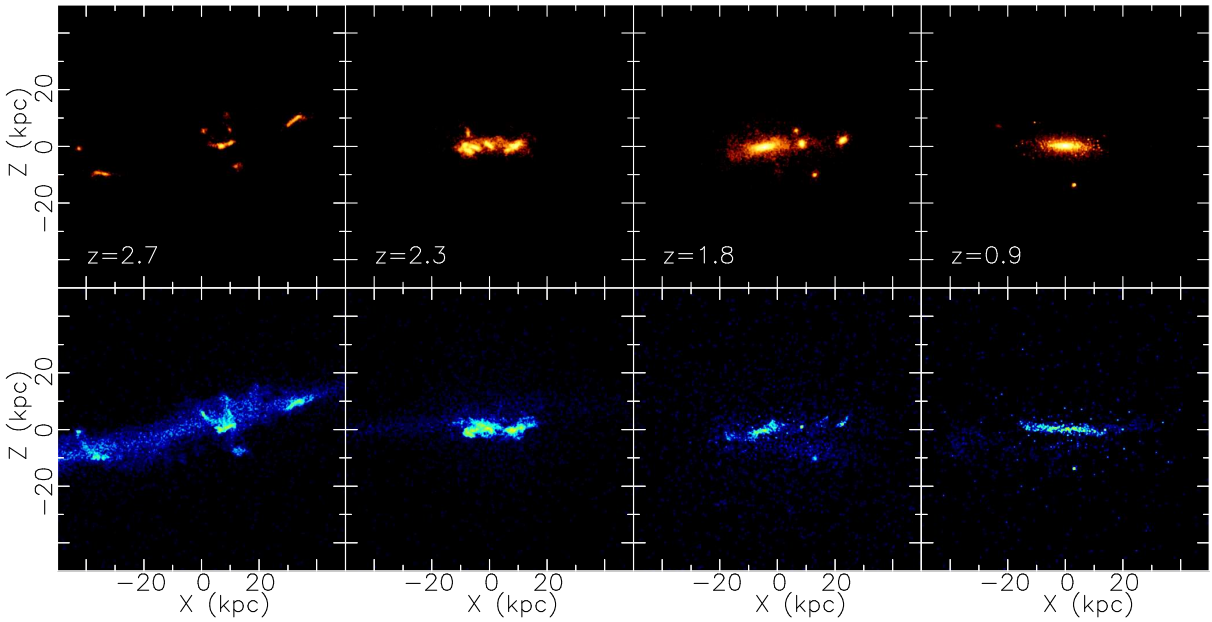

Figure 3.4: Density plot of the projection onto the X-Z plane of the evolution of stars (upper row) and gas (bottom row) during the major star forming epoch of model 3.

merge hierarchically until redshift $z \approx 1.7$; by redshift $z \approx 1.6$, large sub-clumps merging in the centre of the Galaxy (where the disk is forming) is responsible for the bulk of star formation. An epoch of accretion ($1.2 \lesssim z \lesssim 0.9$) witnesses the formation of the majority of the high-metallicity ($Z > 0.05\,Z_{\odot}$) stars, and the disk-like structure of the Galaxy becomes evident. The star formation histories of the three models are shown in figure 3.5. The system barely evolves morphologically after redshift $z \approx 0.8$. While not shown, we confirm that the radial scale lengths for our simulated disk at $z = 0$ (both gas and stellar) match those of the Milky Way.

Density maps of the final distributions ($z = 0$) of star and gas particles for model 3 are shown in figure 3.6. The X-Y (upper row) and X-Z (bottom row) planes are shown. Note that the low-metallicity ($Z < 0.05\,Z_{\odot}$) stars of the Galaxy preferentially populate the halo and thick disk, while the metal-rich ($Z > 0.05\,Z_{\odot}$) component populates the bulge and thin disk.

3.3.1 White Dwarf-dominated Halo

In this section we investigate whether our models 2 and 3 produced a halo that contains a significant amount of mass tied up in white dwarf stars. We make a comparison of the resulting halo and disk white dwarf densities of our three models,

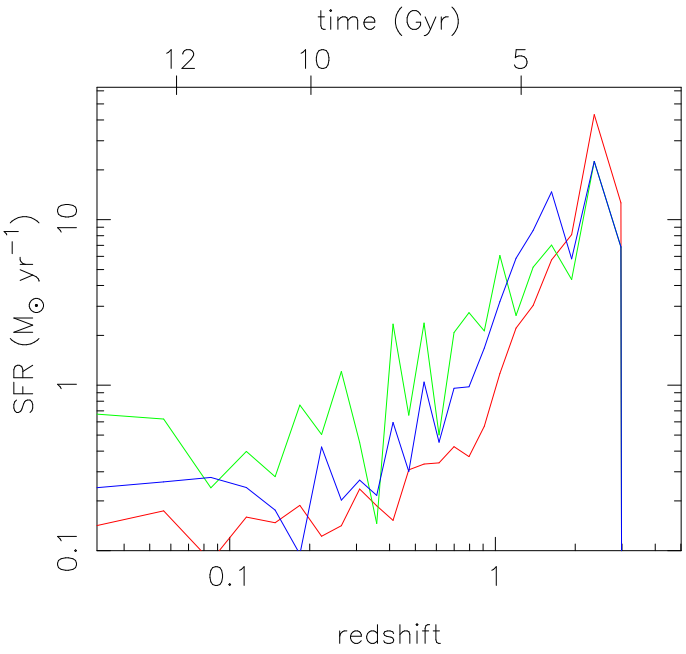

Figure 3.5: Evolution of the global star formation rate (SFR) of model 1 (red line), model 2 (green) and model 3 (blue).

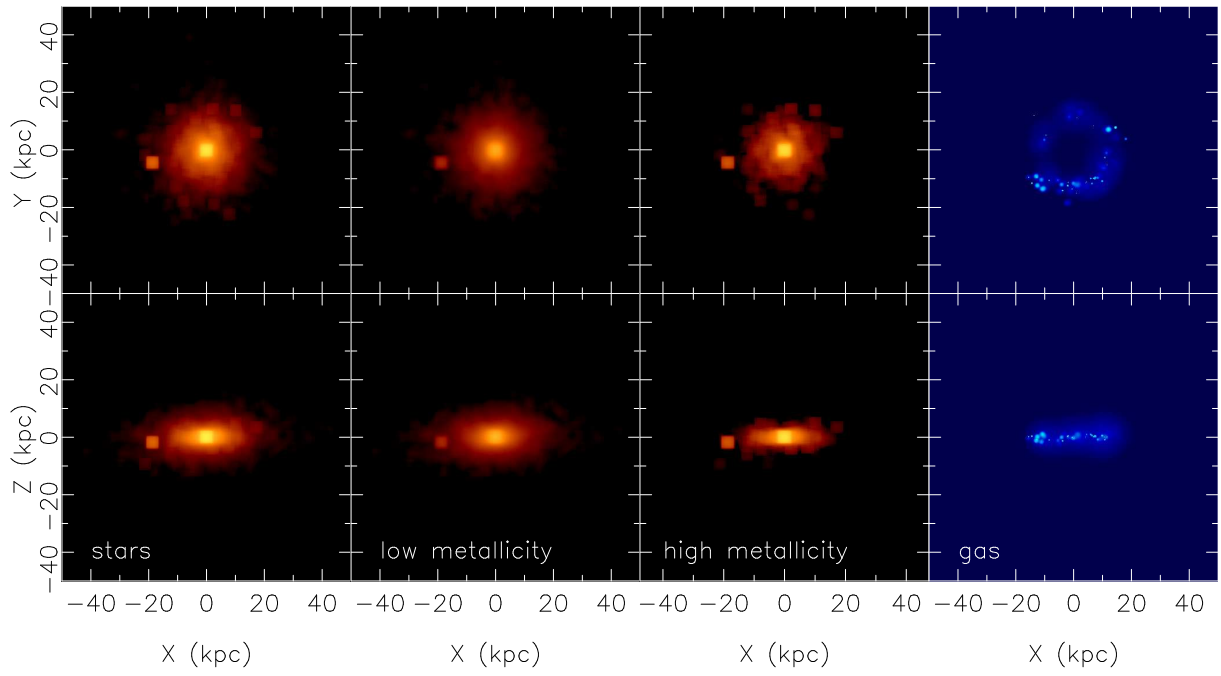

Figure 3.6: Density map of the final ($z = 0$) distribution of star particles (left panel), low-metallicity ($Z < 0.05\,Z_\odot$) stars, high-metallicity ($Z > 0.05\,Z_\odot$) stars, and gas particles, for model 3, in the X-Y (upper row) and X-Z (bottom row) planes.

derived using the different assumed IMFs. The halo stars are defined as star particles in the region $4 < R_{\rm XYZ} < 20$ kpc and $|{\rm Z}| > 4$ kpc. The *mean* halo white dwarf number densities n for each of the IMF models discussed in section 2.1 are shown in table 3.4, where n is defined as

$$n = \frac{1}{V} \sum_i m_{s,i} \int_{1\,{\rm M}_\odot}^{8\,{\rm M}_\odot} \Phi(m)\,{\rm d}m \tag{3.7}$$

The summation is over star particles older than 1 Gyr (the lifetime of a $2\,{\rm M}_\odot$ stars, and also the time delay adopted in our chemical evolution modeling of white dwarf progenitors- recall section 3.2.1) and located in the designated halo region. It is important to note that the absolute values of the densities is sensitive to the definition of the region selected; the densities are shown to provide details of how the number densities of white dwarfs altered between the three models.

As expected, model 2 (Chabrier IMF at all metallicities) results in significantly more white dwarfs in the halo (by a factor of 3.8), in comparison to model 1 (Salpeter IMF at all metallicities). The variable IMF of model 3 (Chabrier at low-metallicities and Salpeter elsewhere) results in a factor of 3.5 increase in the halo white dwarf population with respect to model 1. In other words, model 3 increases the number of halo white dwarfs to almost the same degree as model 2, compared with the canonical Galactic models which use a Salpeter IMF alone (i.e., model 1). The ability of model 3 to increase the number of halo white dwarfs by a similar amount to model 2, makes it an important component of chemo-dynamical models that aim to maximise the number of halo white dwarfs, while allowing higher metallicity stars to be distributed according to the Salpeter IMF.

We are further able to examine the ratio of white dwarf stars to main sequence stars in the halos of the three models. Using appropriate IMFs, we calculate $\sum_i^{halo} n_{{\rm WD},i}/n_{ms,i}$ giving a number ratio of white dwarf to main sequence stars in the halo region of 0.19 for model 1, 1.2 for model 2 and 1.0 for model 3. Here the number of white dwarfs is $n_{{\rm WD},i} = \int_{1M_\odot}^{8M_\odot} \Phi(m){\rm d}m$ if $t_{age,i} > 1$ Gyr and the number of main sequence stars is $n_{ms,i} = \int_{0.3M_\odot}^{1M_\odot} \Phi(m){\rm d}m$. We see that model 3 significantly increases the number of white dwarf halo stars, as required by our white dwarf halo scenario. This demonstrates that models 2 and 3 have resulted in creating a stellar halo that has a significant mass in the form of white dwarf stars. We found that this result was robust over a range of "regions" which could be used to define the halo. Unlike the values of densities quoted in table 3.3.1, *this allows a comparison*

Table 3.4: Total stellar and white dwarf number densities (in units of pc^{-3}) for the three models described here.

	model 1	model 2	model 3
Halo total stellar density	1.4×10^{-4}	1.5×10^{-4}	1.5×10^{-4}
Halo white dwarf density	1.7×10^{-5}	6.0×10^{-5}	6.5×10^{-5}

which is not directly sensitive to the region chosen as defining the halo.

The differences in evolution and final morphology of models 1 and 2 from model 3 are not significant enough to show as separate diagrams in section 3.3, yet they do have some impact on the total stellar densities of our simulated halo region. Factors which will influence these differences are; the different ejected mass due to different IMFs result in different masses, and hence dynamics, of the remnant stellar particles; different ejecta also results in different gas enrichment and mass and different star formation rates (figure 3.5); different cooling rates due to differences in metallicity of enriched gas particles; different energy feedback due to different supernova rates (although our implementation of such feedback is known to be highly inefficient in Tree-SPH codes). These are "secondary" effects of a different IMF on the white dwarf densities quoted in this section. As it is difficult to disentangle these effects, table 3.4 shows the total halo stellar densities of the three models in order to indicate the magnitude of their combined effects. Here, total stellar density means the value of the summation of the mass of star particles in the halo region, divided by the volume of the halo region. There is little difference between the models in such total stellar densities and thus these secondary effects are not what drives the differences in white dwarf densities between the models. The difference in the number densities of white dwarfs between models can therefore be attributed to the variation of the adopted IMFs.

3.3.2 Chemical Constraints

In this section, we examine the constraints set by observartions of chemical abundance - in particular carbon, nitrogen and oxygen - on the feasibility of our three models. We are especially interested in whether the variable IMF of model 3 alleviates the problem of carbon and nitrogen overproduction relative to oxygen, as originally noted by GM97. Figure 3.7 shows the [C/O] and [N/O] abundance ratios

as a function of global metallicity[4] $[Z]$ for the stellar particles in the solar neighbourhood for all models, to compare with observations of solar neighbourhood stars. We define the solar nighbourhood as the region bounded by $4< R_{\rm XY} <10$ kpc and $|{\rm Z}| <1.5$ kpc. Carbon and nitrogen are highlighted due to the fact that their dominant nucleosynthesis sites are the intermediate mass white dwarf precursors under discussion here.

We constrain our models with the observed abundance distribution pattern of carbon, nitrogen, and oxygen seen in the metal poor Population II stars, which are dominated by halo stars (hashed regions in each panel of figure 3.7). We remind the reader that Type Ia supernovae have not been included in the present anaylysis. As such, we take the total metallicity $[Z]$ to act as a proxy for [Fe/H], without violating the validity of the simulations (since Type Ia supernovae are not critical contributors to the Galaxy's CNO abundances). The points in figure 3.7 correspond to those simulated star particles that reside, at the present epoch, in the solar neighbourhood defined above. No kinematical (i.e., disk versus halo kinematics) cut has been applied since the observational data appertains to solar neighbourhood stars without kinematic selection.

The solid lines in each panel of figure 3.7 correspond to the mass-weighted mean stellar metallicity of the simulation. For model 1, we can see that there is essentially no variation in [C,N/O] for halo metallicities (i.e., $[Z] \lesssim -1$), with the simulated halo particles occupying the same parameter space as the data (hashed regions). As the chemical enrichment from low- and intermediate- mass stars becomes important, [C,N/O] approaches the solar ratio and the dispersion increases, both remaining in keeping with the observations of the solar neighbourhood distributions (Timmes et al. 1995). Not surprisingly, this is consistent with the conventional picture in which the sIMF (model 1) scenario is assumed to hold.

Model 2 (middle panels of figure 3.7) shows the clear signature of carbon and nitrogen overproduction. As the intermediate mass stars that are responsible for the nucleosynthesis of the bulk of these elements pass through the asymptotic giant branch, the resulting [C/O] and [N/O] quickly exceeds the halo observational constraints by more than two orders of magnitude: an invariant wdIMF model cannot be made consistent with the data. This is consistent with the analytical chemical evolution analysis of GM97.

[4] $[Z]=\log_{10}(Z/Z_{\odot})$

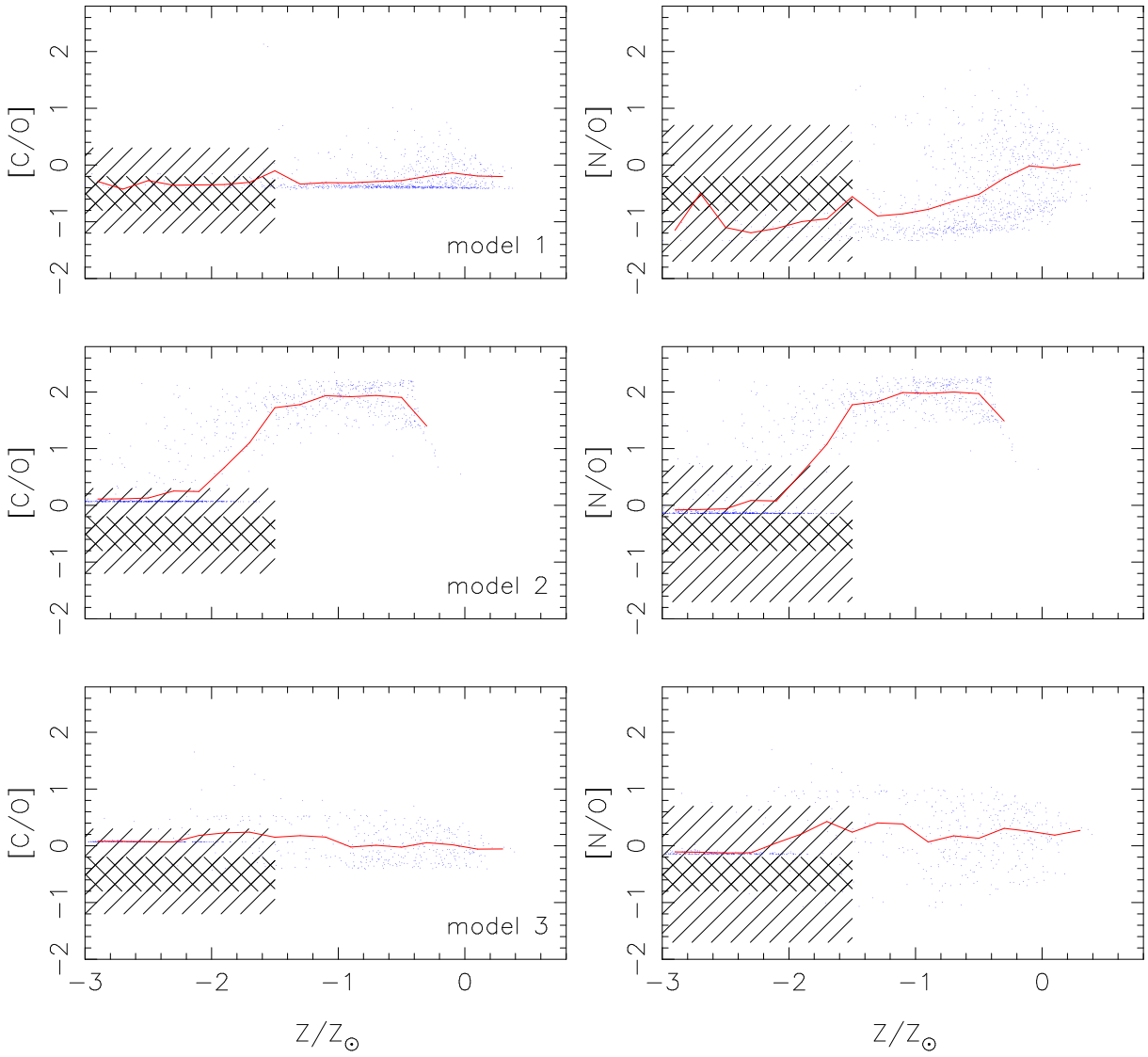

Figure 3.7: The values of [C,N/O] for simulated star particles in the solar neighbourhood plotted against their metallicity [Z]=$Z/Z_\odot$ at redshift z=0. The results of model 1 are in the upper panels, below which are the results for models 2 and 3 respectively. The red trend lines show the mass-weighted mean values of the simulations. The hatched regions correspond to the observational constraints listed by Timmes et al. (1995). All of the ∼150 halo stars shown in figures 13 and 14 of Timmes et al. lie within the bounds of the outer hatched regions, while ∼80% of the sample lies within the inner regions.

The lower panels of figure 3.7 demonstrate that model 3 (the variable IMF) does somewhat mitigate the overproduction of carbon and nitrogen at low metallicities. Below $[Z]\approx-1$, model 3 traces model 2; above $[Z]\approx-1$, the Salpeter (1955) component of the variable IMF begins to dominate star formation (and its associated element production), suppressing the extreme overproduction of the invariant wdIMF model 2. Ultimately, [C/O] and [N/O] approach that of the model 1 (sIMF), reaching the scaled-solar ratio at $[Z]\sim0$. While a definite improvement (in the sense that the factor of $\gtrsim 100$ overproduction in carbon and nitrogen seen in model 2 no longer exists), model 3 still leads to a factor of ∼5-10 carbon and nitrogen excess (with respect to oxygen) at metallicities in the range $-2.5 \lesssim [Z] \lesssim -1$.

Two features of the plots figure 3.7 in are worth further comment here. In models 2 and 3 we notice a number of stars in a horizontal line with values of [C,N/O]∼ 0. These stars were formed from gas polluted by massive stars, prior to intermediate star's yields being ejected. Reference table 3.1 which shows that the wdIMF massive star's ($>10\,M_\odot$) integrated yields have [C,N/O]∼ solar. Also note the limit of [C,N/O] of ∼ 2.2 in all models in figure 3.7 which comes from the low metalicity intermediate mass stellar yields, as seen in table 3.2.

3.4 Discussion

Ascribing the detection of the 13-17 microlensing events seen toward the LMC to an intervening halo white dwarf population implies that perhaps 20%−30% of Galaxy's dark matter is tied up in these stellar remnants (Alcock et al. 2000). This would correspond to a local white dwarf halo number density of $\sim2\times10^{-3}\,\mathrm{pc}^{-3}$. In contrast, Gould et al. (1998) used subdwarf star counts and an assumed Salpeter (1955) IMF, to conclude that the local spheroid white dwarf number density was $2.2\times10^{-5}\,\mathrm{pc}^{-3}$ (i.e., two orders of magnitude smaller). More recently, the high proper motion survey for cool white dwarfs conducted by Oppenheimer et al. (2001) claimed a local halo white dwarf number density of $2.2\times10^{-4}\,\mathrm{pc}^{-3}$.[5] Whether the Oppenheimer et al. white dwarfs are actually members of the halo, as opposed to the thick disk, is still a matter of debate (e.g. Gyuk & Gates 1999; Reid & Sahu 2001). Hansen (2001) argues that if the halo is dominated by white dwarfs, ∼80% of these remnants lie beyond the detection limit of Oppenheimer et al. - that is, the white dwarf-

[5]The re-analysis conducted by Gibson & Flynn (2001) suggests that the Oppenheimer et al. (2001) number density should be revised downward by 40% to $1.3\times10^{-4}\,\mathrm{pc}^{-3}$.

dominated halo issue has not yet been resolved and future (deeper) surveys must be undertaken before the final word on the subject can be pronounced.

Regardless of the current observational constraints, it is recognised that populating the Galactic halo with a dynamically-dominant white dwarf component demands a significant modification to the underlying stellar IMF (e.g. GM97). A Chabrier IMF (1996), peaked in the white dwarf progenitor range, is one such possibility, although this IMF cannot apply at all times since we observe today a fairly conventional Salpeter (1955) or Scalo (1986)-like distribution. Metallicity may be the controlling factor in "switching" from the Chabrier-like to Salpeter-like IMF; a physical motivation for such a switch can be found in the studies of Yoshii & Saio (1987), Nakamura & Umemura (2001), Bromm et al. (2001) and Abel, Bryan & Norman (1999, 2001) . Making our IMF dependent upon metallicity in our variable model is further motivated by the different MDF's of the Galactic disk and halo regions; if one wishes to populate only the halo with large numbers of white dwarf stars, then it is the low metalicity stars which should have an IMF biased toward white dwarf progenitor stars. This appears necessary if we are to explain MACHO observations by invoking white dwarf stars.

Our chemodynamical simulations employing a hybrid IMF (white dwarf-dominated at metallicities $[Z]<-1.3$, and "conventional" at metallicities $[Z]>-1.3$) are successful in increasing the Galactic halo white dwarf fraction (in comparison with models employing a Salpeter 1955 IMF alone) without violating present-day observable local carbon and nitrogen Pop II abundance constraints. These results are caused by low metallicity stars preferentially being found in the halo region as seen in figure 3.6. Low metallicity stars are formed before and during the major star formation epoch caused by the collapse of the whole system. These stars are scattered by violent relaxation. Later, gas polluted by past star formation accretes smoothly and the metal rich disk component developes. This picture is consistent with previous chemo-dynamical studies of a Milky Way like galaxy (Steinmetz & Muller 1995; White et al. 2000; Bekki & Chiba 2001; Abadi et al. 2003). This metallicity segregation is what allows our simple variable IMF to populate the low metallicity stars of the halo with a large number of white dwarf stars. The discrepency between observed metallicity distributions of Galactic halo and disk stars mean that our scheme of varying the IMF according to metallicity would seem appropriate, indeed necessary, if we are to explain MACHO events by white dwarfs.

That said, our best models were only capable of increasing the number of halo

white dwarfs by a factor of 3-4 (table 3.4) before violating the constraints of an overproduction of carbon and nitrogen compared to oxygen. This factor is between our simulated models, and unlike the absolute densities is not significantly affected by the region selected as defining the halo. How does this factor relate to observed white dwarf densities? The Gould et al. value of 2.2×10^{-5} pc^{-3} assumes a Salpeter IMF; increasing this by a factor of 3-4 corresponds to halo white dwarf mass fractions of ∼1-2% - halo white dwarf mass fractions beyond this limit are not supported by our simulations.

Attempts to increase the halo white dwarf fraction further necessitate significant revision to our fairly conventional star formation formalism. We attempted to force the halo white dwarf issue by substantially increasing the efficiency of star formation (c_* in equation 3.1) in low-metallicity star-forming regions. We also tried decreasing the density threshold for star formation ρ_{crit} in these same regions.[6]. Both *ad hoc* revisions introduced moderate increases in the halo white dwarf fraction. For example, increasing c_* by a factor of ten and decreasing ρ_{crit} by the same factor of ten, led to a halo white dwarf density of $1.3\times10^{-4}\,\mathrm{pc}^{-3}$ (c.f. model 3 entries of table 4). While such a density would be consistent a factor of ~ 8 incease of halo white dwarf densities over the Salpeter IMF model, this "extreme" model suffers from the same carbon and nitrogen overproduction which plagued model 2 (section 3.3), mitigating its usefulness.

The hybrid IMF preferred here varies in a very simple manner in that the $0.05\,Z_\odot$ transition metallicity for changing from the wdIMF to sIMF regime was a somewhat arbitrary choice. We found that adopting a lower metallicity for the transition (e.g. $0.01\,Z_\odot$) does diminish the carbon and nitrogen overproduction, but at the expense of reducing the halo white dwarf mass fraction. Thus, it becomes clear that a trade-off exists between increased white dwarf halo densities and the overproduction of carbon and nitrogen compared to oxygen; any significant increases in white dwarf numbers are accompanied by worsening of the overproduction of carbon and nitrogen, as well as contamination of the disk with an unacceptable number of white dwarf stars. Our simulations suggest that attempts at increasing the number of halo white dwarf beyond that obtained in model 2 (∼1-2% of the halo, by mass) will violate these constraints.

Our best hybrid IMF model, while an improvement over purely white dwarf-

[6]both these simulations were done using $\mathrm{n}_{tot} = 18342$

dominated IMF models, still overproduces stars with supersolar [C/O] and [N/O] ratios in the metallicity range $-2.5 \lesssim [Z] \lesssim -1$. Modifications to the star formation efficiency and threshold were incapable of eliminating this overproduction. As such, more extreme scenarios may need to be invoked in order to suppress the formation of these stars. An early Galactic wind, fine-tuned such that the carbon and nitrogen ejecta from the wdIMF component of our hybrid IMF is removed from the system before being incorporated into the stars which ultimately form the Population II halo of the Milky Way, is one such potential modification (e.g. Fields et al. 1997; GM97). Although we do take into account the energy feedback of SNe (section 3.2.1), our preferred model 3 does not develop a Galactic wind. The precise efficiency of SNe feedback remains therefore uncertain; in a future work, we will explore more extreme feedback scenarios in an attempt to suppress excess carbon and nitrogen overproduction at early times. This study will also include the effects of Type Ia SNe, although we remind the reader that this inclusion should have little impact upon the results presented here (as SNe Ia are negligible contributors to the carbon, nitrogen, and oxygen yields - see section 3.2.1).

3.5 Summary

We have undertaken galactic chemodynamical simulations of the formation and evolution of the Milky Way, exploring a region of parameter space designed to test the hypothesis that the Galaxy's halo has a significant dynamical white dwarf component (perhaps as high as 30% by mass). This is the first numerical examination of the white dwarf-dominated hypothesis, and a natural extension to the earlier semi-analytical investigation of Gibson & Mould (1997). Consistent with Gibson & Mould, we have found that carbon and nitrogen overproduction (by factors in excess of 100) are endemic to purely white dwarf-dominated IMF models. For the first time, we have shown that a hybrid white dwarf-dominated/Salpeter style IMF with a transition metallicity between the two of $Z = 0.05\,Z_{\odot}$ can lead to a Milky Way model that is marginally consistent with virtually all available present-day constraints. A mild overproduction of carbon and nitrogen remains (although this overproduction is reduced by more than an order of magnitude); an early Galactic wind may alleviate this overproduction, an hypothesis we will explore in a future study. Our best model can lead to a halo white dwarf mass fraction a factor of ~ 4

greater than expected with a more conventional IMF (corresponding to $\sim 1-2\%$ of the mass of the halo), but values in excess of this cannot be accommodated within our chemo-dynamical framework.

Chapter 4

Halo Stars in Phase Space

4.1 Introduction

Proposed scenarios for galaxy formation are dominated by two canonical models: the rapid "monolithic collapse" of a proto-galactic cloud and the hierarchical build-up from low mass fragments, commonly referred to as "satellite accretion" (Searle & Zinn 1978). The former model was best articulated by Eggen, Lynden-Bell & Sandage (1962, hereafter ELS); key supporting evidence for the ELS picture was the apparent correlation between eccentricity (ε) and metallicity of halo stars (figure 4.1). Using a large and reliable dataset of halo objects selected without kinematic bias however, Chiba & Beers (2000, CB00 hereafter) found no strong correlation between ε and metallicity (figure 4.2). Bekki & Chiba (2000) argued that this lack of correlation is naturally explained by hierarchical clustering scenarios of galaxy formation. CB00 did, however, identify a concentration of stars of $\varepsilon \sim 0.9$ and [Fe/H] ~ -1.7. They suggested that this population of stars formed from infalling gas during an early stage of Galaxy formation, in a manner similar to an ELS collapse.

Current cosmological theories of structure formation have more in common with accretion scenarios, such as that proposed by Searle & Zinn (1978). Evidence in support of satellite accretion during our Galaxy's formation can be found in the observations of considerable substructure in the halo (e.g. Ibata, Gilmore & Irwin 1994; Majewski, Munn & Hawley 1996; Helmi et al. 1999; CB00; Ibata et al. 2003). Helmi & White (1999) noted that satellites disrupted several billions years ago will not retain the spatial correlations required to allow identification. On the other hand, these authors demonstrated that the trail of stars left by a disrupted dwarf

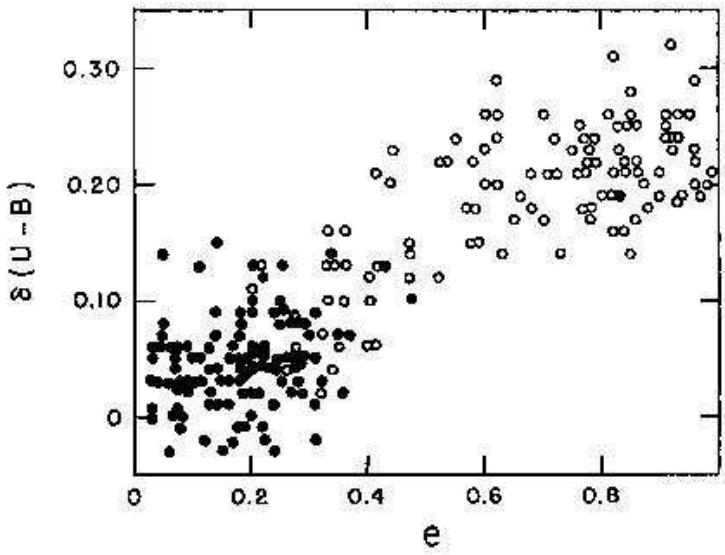

Figure 4.1: Plot of halo stars in the plane of $\delta(U-B)$ vs. eccentricity, taken from Eggen, Lynden-Bell & Sandage 1962 (ELS). $\delta(U-B)$ is a measure of the stars' metallicity, and the correlation apparent in the sample was cited as evidence for the galaxy having undergone a rapid collapse.

satellite *will* retain strong correlations in velocity space. Furthermore, the integrals of motion (E,L,L_z) are conserved quantities, and should evolve only slightly within the relatively stable potential of a galaxy after the halo is virialized. This space of adiabatic invariants is a natural space to search for signatures of an accretion event (e.g. Helmi & de Zeeuw 2000).

We were motivated to run a grid of chemodynamical simulations in order to contrast the effects of the two collapse scenarios on the evolution of the Milky Way. The two models described here vary primarily in their degree of clustering, and we examine the properties of the resulting simulated galaxies, in order to uncover present-day "signatures" of the models' initial conditions and evolution.

Details of our code and the models used in this study are provided in section 4.2. Section 4.3 presents the evolution and clustering histories of the simulated galaxies. We focus on the eccentricity distribution of our simulated galaxies' halo stars, and on comparison with observations. Tracing the evolution of stars originating in recently accreted satellite galaxies provides a clue to the source of high-eccentricity halo stars. In section 4.4 we show that such stars occupy restricted regions of phase space, a signature of common ancestry. Similar analysis of the CB00 dataset shows that the identified "clump" of high-eccentricity, low-metallicity, halo stars occupies a similar

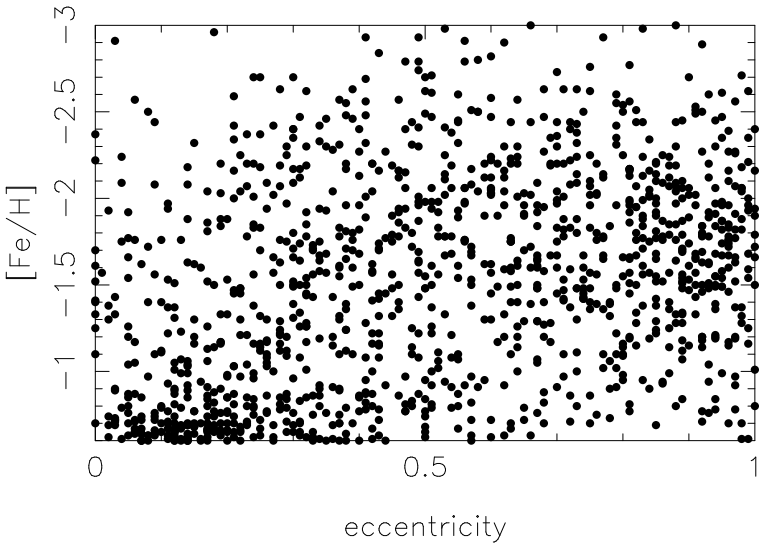

Figure 4.2: Plot of halo stars from the catalogue in Chiba & Beers (2000), in the plane of metallicity versus eccentricity. The correlation seen in the ELS data is not present. However, a clump of high eccentricity ($\varepsilon \sim 0.9$) stars with metallicities, [Fe/H] ~ -1.7, is apparent.

restricted region of phase space. The implications for theories of galaxy formation and their observational signatures are discussed in section 4.5.

4.2 The Code and Model

Our Galactic Chemodynamical code (GCD+) models self-consistently the effects of gravity, gas dynamics, radiative cooling and star formation. Type Ia and Type II supernova feedback is included. We relax the instantaneous recycling approximation when monitoring the chemical enrichment history of our simulated galaxies.

The semi-cosmological version of GCD+ used here is based upon the galaxy formation model of Katz & Gunn (1991). The initial condition is an isolated sphere of dark matter and gas, onto which small scale density fluctuations are superimposed, parameterised by σ_8. These perturbations are the seeds for local collapse and subsequent star formation. Solid-body rotation corresponding to a spin parameter λ is imparted to the initial sphere. For the flat CDM model described here, the relevant parameters include $\Omega_0 = 1$, $H_0 = 50$km s^{-1} Mpc^{-1}, total mass ($5 \times 10^{11}\,\mathrm{M}_\odot$), baryon fraction ($\Omega_b = 0.1$), and spin parameter ($\lambda = 0.0675$). We employed 38911 dark matter and 38911 gas/star particles, making the resolution of this study comparable to other recent studies of disk galaxy formation (e.g. Abadi et al. 2003).

The two models described here differ only in the value of σ_8. In model 1, $\sigma_8 = 0.5$, as favoured in standard CDM ($\Omega_0 = 1$) cosmology. In model 2, we explore the use of a smaller value for σ_8 of 0.04, a value that results in a more rapid, dissipative, collapse.

4.3 Simulation Results

Figure 4.3 illustrates the evolutionary histories of model 1, and figure 4.4 the evolution of model 2, as density plots of star particles (panels with black backgrounds) and gas particles (blue panels), with the redshift of each snapshot shown in its respective star panel. Model 1 demonstrates classical hierarchical clustering - gas collapses into the local dense regions seeded by the initial small-scale perturbation, with star formation occurring subsequently in these over-dense regions. Stars continue to form in sub-clumps, as well as in the central region as a disk galaxy is built up. We see less clumping in model 2, with gas streaming homogeneously toward the centre of the galactic potential, resulting in most of the star formation occurring in the central regions.

We analysed the bulk properties of our simulation at $z = 0$ and confirmed that they were consistent with the simulations of Katz (1992), Steinmetz & Muller (1995), Berczik (1999), and Bekki & Chiba (2001). The predicted surface density profiles, metallicity gradients, specific angular momenta of gas and stars, and rotation curves for our models did not differ significantly from previous studies, or between our own two models. We suffer from the same classical overcooling problem encountered in earlier studies (White & Frenk 1991). This results in excessive rates of star production at early epochs, overly rapid metal enrichment, and a halo metallicity distribution function peaked approximately one dex higher than that observed (Ryan & Norris 1991). The field of metallicity distribution functions is the subject of a future, lengthier, analysis, but we do note that this offset in the halo MDF peak does not impact on our analysis here (as we can still adopt a differential metallicity cut to delineate between the halo and thin disk in our simulation). We did find a difference in the orbital eccentricity distribution of the simulated solar neighbourhood halo stars of the two models. After Bekki & Chiba (2000), individual stellar eccentricities were calculated by allowing the orbits of star particles to evolve for 1.8 Gyrs under the gravitational potential of the simulated disk galaxy achieved at

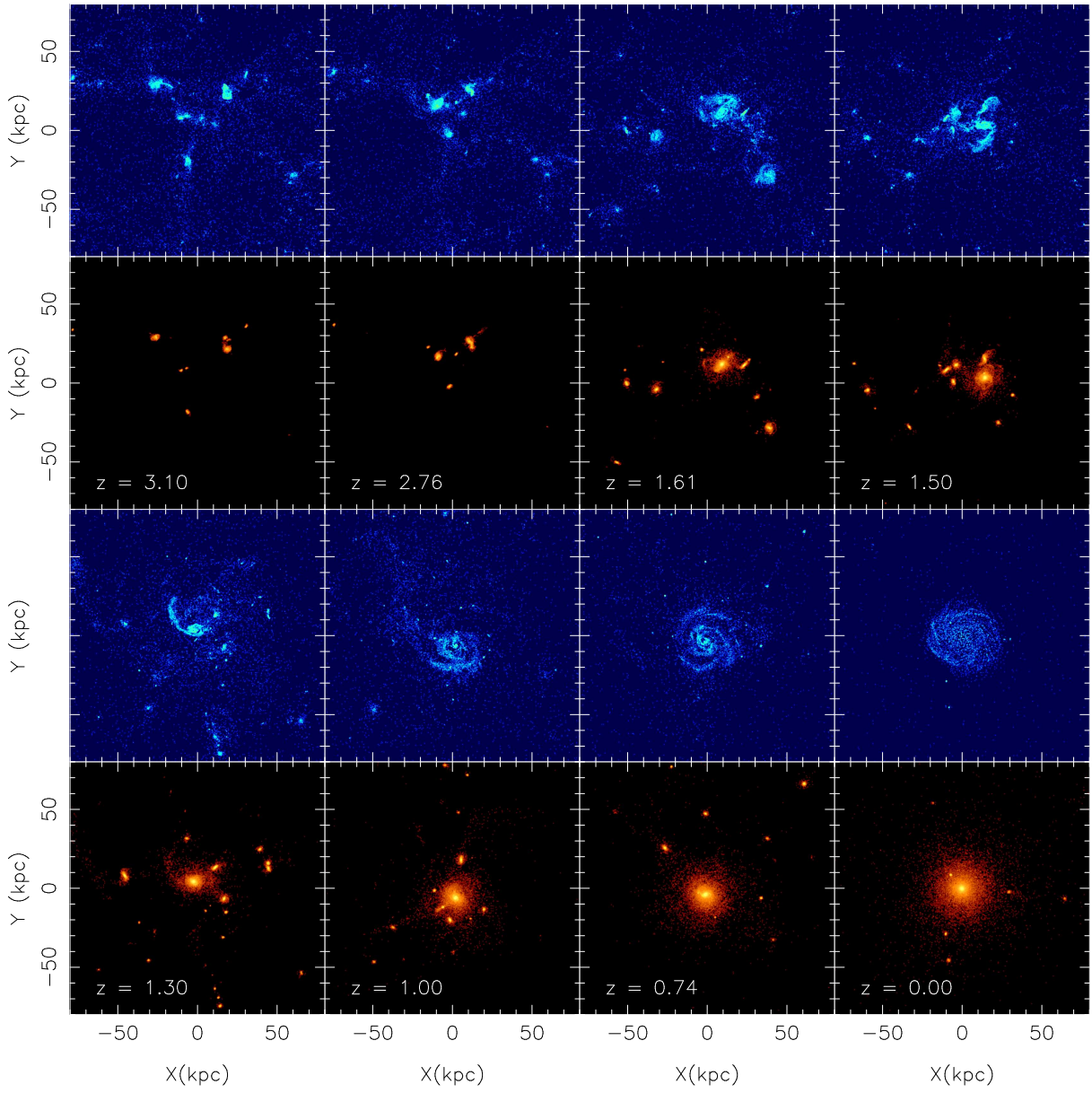

Figure 4.3: X-Y stellar (black backgound) and gas (blue background) density plots of the evolution of model 1. The Z axis is defined to be the initial axis of rotation. Star panels are labelled with redshifts, and appear below their corresponding gas panels. Hierarchical clustering is evident in model 1. Gas collapses into local dense regions, and this is where star formation takes place.

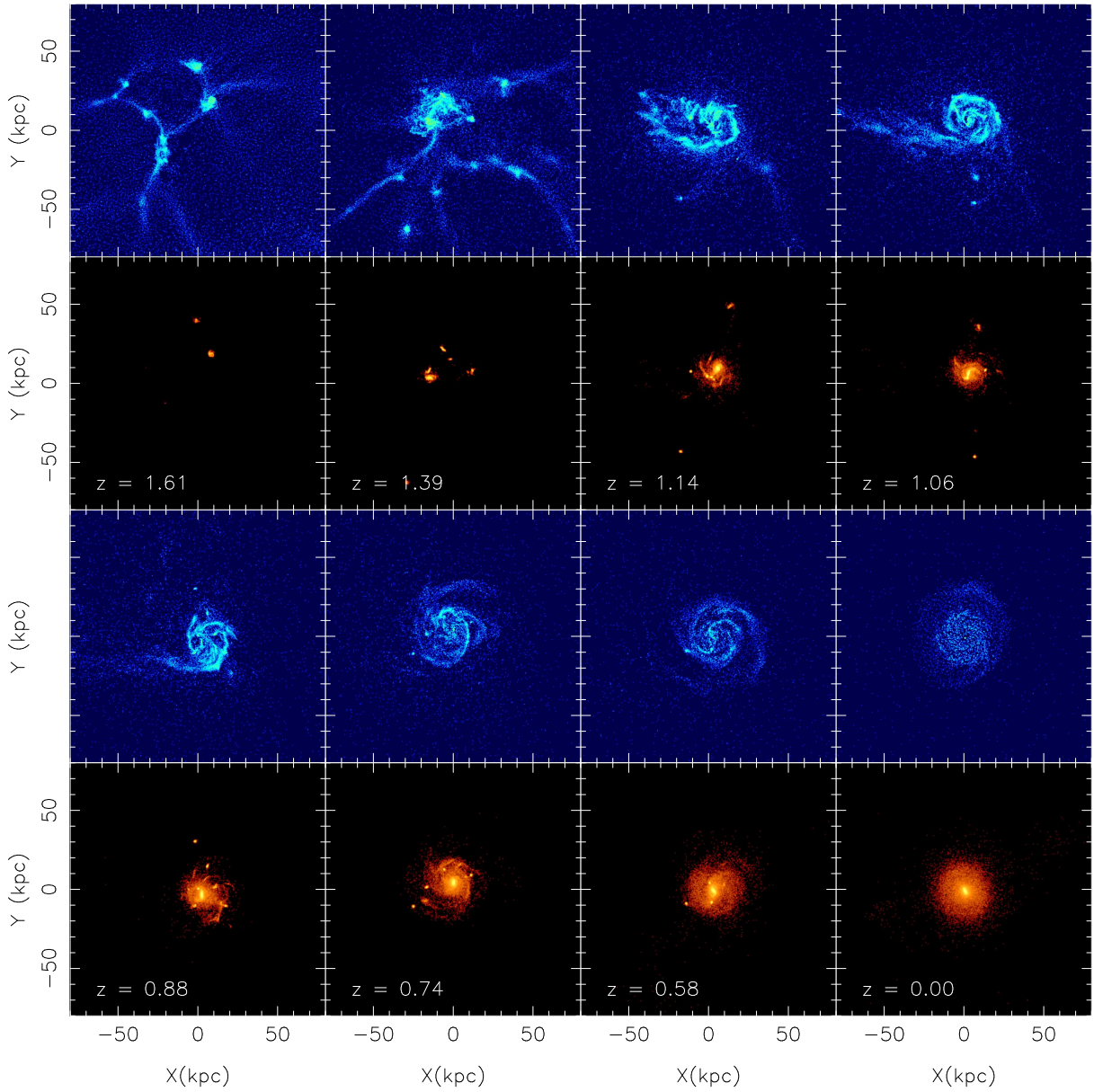

Figure 4.4: X-Y as for figure 4.3 for model 2. Epochs are chosen (with redshifts labelled) so that roughly the same stellar mass is present in corresponding the panels of figure 4.3. It is apparent that gas collapse and star formation are more centralised in model 2.

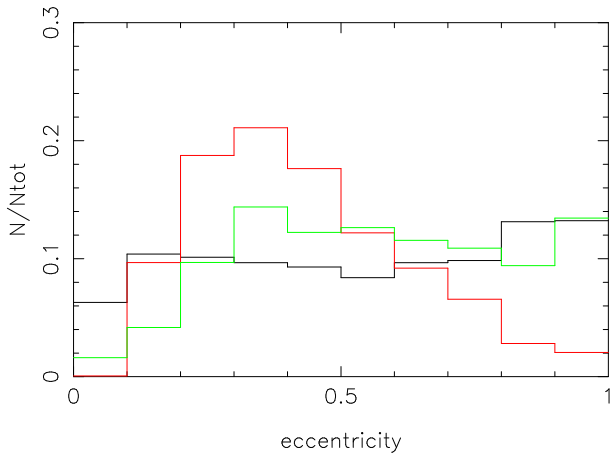

Figure 4.5: Present-day eccentricity distribution of halo stars at the solar circle for our two models - the green line represents model 1, while the red line represents model 2. The black line corresponds to the observational dataset of Chiba & Beers (2000). Model 1 leads to a greater number of high-eccentricity halo stars in the solar circle.

$z = 0$. Eccentricities ε were then derived using $\varepsilon = (R_{apo} - R_{peri})/(R_{apo} + R_{peri})$, where R_{apo} (R_{peri}) is the apogalactic (perigalactic) distance from the centre of the simulated galaxy. Halo stars are defined to be simulated star particles with [Fe/H] < -0.6. Due to the higher-than-expected absolute value for the halo MDF (alluded to earlier), this metallicity cut may lead to an underestimate of the halo population, but the final halo "sample" is representative.

The green line of the histogram in figure 4.5 shows the eccentricity distribution of halo star particles in the solar circle of model 1, with the red line representing model 2. The solar circle is defined as an annulus of the galactic disk[1], bounded by $5 < \mathrm{R_{XY}} < 12$ kpc and $|\mathrm{Z}| < 2$ kpc, where Z corresponds to the rotation axis and $\mathrm{R_{XY}} = \sqrt{(\mathrm{X}^2 + \mathrm{Y}^2)}$. Each bin shows the fraction of such star particles lying in a given eccentricity range. Also shown (solid line) is the observational constraint from CB00. Model 1 produced a greater number of high-eccentricity ($\varepsilon > 0.8$) solar circle halo stars, and is in better agreement with observation.

Considering the analysis of ELS, whose rapid collapse model resulted in highly eccentric halo stars, it was not unreasonable to expect that the more dissipative,

[1]The volume encompassed by our so-called "solar neighbourhood" annulus is roughly an order-of-magnitude larger than the analog employed in the observational dataset by CB00. We have ensured that this apparent volume "mismatch" does not impact upon our results by testing for sensitivity to azimuthal variations within the annulus through randomly subdividing the simulated dataset into random octiles. The effects described here in phase-space are robust to this azimuthal subdivision.

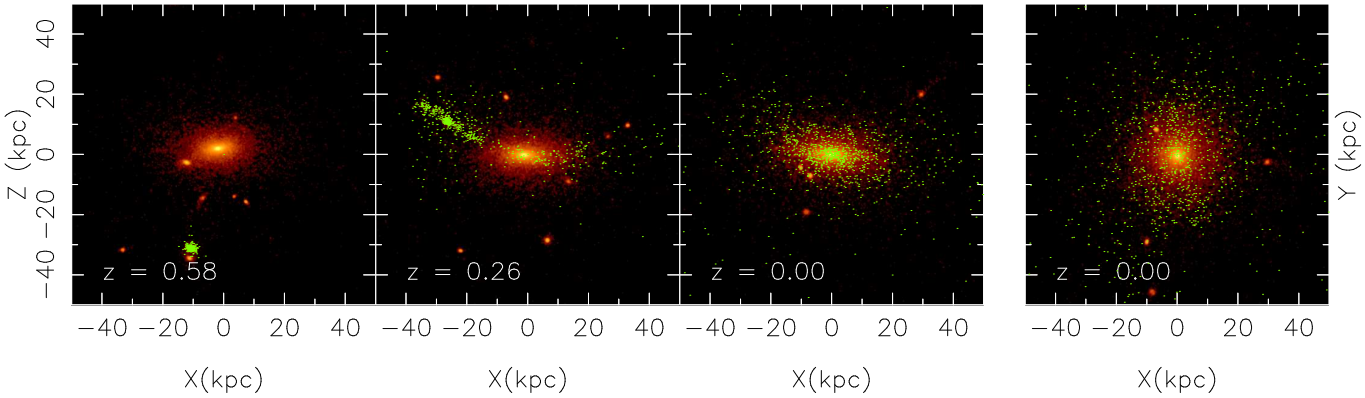

Figure 4.6: X-Z plots of the accretion of the largest satellite, S1, are shown as green dots. The plots start at $z = 0.58$, with disruption of the satellite underway by $z = 0.26$ and by $z = 0$ the stars from the satellite have been accreted into the halo of the final galaxy. A density plot of the star particles of the evoloving galaxy is shown in the background. The X-Y plane of the accreted satellite at $z = 0$ is also shown, in the last panel.

"monolithic" nature of the collapse of model 2 would result in a higher number of high eccentricity halo stars. This prompted a more detailed examination of the collapse time of model 2. Using analysis of the evolution of top hat overdensities with the collapse redshift $z_c = 1.75$, which we adopt (Padmanabhan 1993), the collapse timescale t_{coll} of model 2 is estimated to be $\sim$1.4 Gyrs, thus not satisfying the conditions originally proposed by ELS, $t_{coll} << t_{sf}$ (where t_{sf} is the star formation timescale). While embracing the spirit of ELS within the current cosmological paradigm, model 2 should not be considered a perfect analogue to the ELS rapid collapse scenario.

As the difference between model 1 and model 2 is in the clustering history, our result suggests that the Milky Way may have experienced significant clustering processes during its formation. To clarify this hypothesis, we examine the specific accretion history of each model, tracing the eccentricity distribution functions for the stars associated with each disrupted satellite. In model 1, we identify two satellites at $z = 0.46$ that have merged into the halo of the host galaxy by $z = 0$. These are the final significant merger events in the simulated galaxy's formation. The largest such dwarf galaxy (hereafter S1), with stellar mass $\sim 10^9\,\mathrm{M}_\odot$, was on on a precessing polar orbit[2]. We trace the evolution of S1 in green dots in figure 4.6, beginning at

[2]The stellar mass of the satellite appears too large considering the inferred mass of the Galaxy's stellar halo (e.g. Morrison 1993). We emphasise however that the *fractional* contribution of S1 to the simulated halo ($\sim$10 %) is reasonable, even if the *absolute* mass is overestimated. This latter overestimation is an artifact of the overcooling problem alluded to earlier, and does not impact

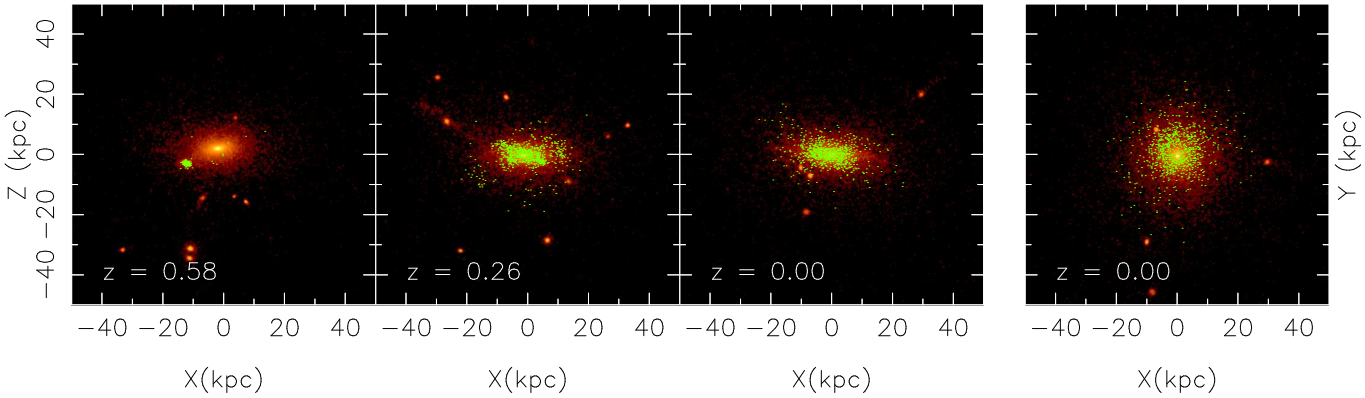

Figure 4.7: As for figure 4.6, for a second satellite, S2, which is also accreted into the halo of the galaxy, Disruption for this satellite begins after $z = 0.46$, is well advanced by $z = 0.26$, and the satellite is accreted to the halo by $z = 0$. The stars from S2 end up in a slightly more flattened distribution than the stars of S1.

$z = 0.58$, prior to disruption. By $z = 0.26$, tidal forces have begun stripping stars from S1, and by $z = 0$, its stars are spread effectively throughout the halo. Accretion of a second satellite, identifed as S2, is shown in figure 4.7. Again, it is evident that stars from the satellite accrete predominantly to the halo of the galaxy.

The histogram of figure 4.8 shows the eccentricity distribution of solar circle halo stars that originated in the satellites identified at $z = 0.46$, plotted with a red line. The y-axis is normalised by the total number of solar circle halo stars in each eccentricity bin. The green line is those stars from S1. We notice that the majority of these halo stars are of high-eccentricity, and that S1 in particular contributes $\sim$20 % of all high-eccentricity halo stars in the solar circle at $z = 0$.

4.4 Phase Space Analysis

In figure 4.9, we plot the phase space distributions of solar circle stars of model 1. Figures 4.9 a-c show: velocity directed radially away from the galactic center V_{rad} versus rotational velocity in the plane of the disk V_ϕ; velocity out of the plane V_z versus V_ϕ; and V_{rad} versus V_z. Figure 4.9 d plots the integrals of motion, projected angular momentum L_z versus the absolute value of the energy (|E|). Stars originating in S1 are marked as open circles. We see that such stars occupy a restricted region of phase space. It is worth noting that these results are qualitatively similar

upon the phase-space conclusions described here. Overcooling is a serious problem plaguing all chemodynamical codes, and is addressed in a more detailed paper to follow.

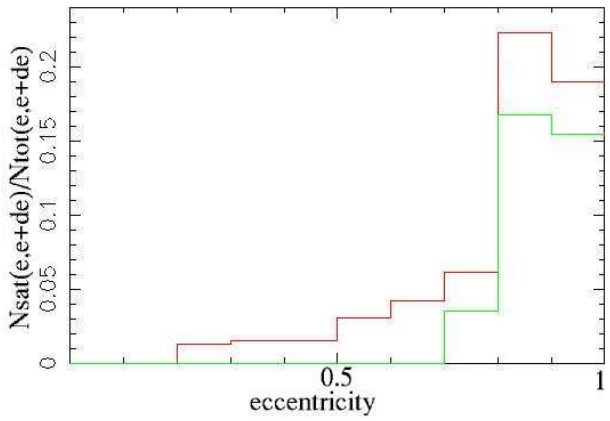

Figure 4.8: The red line shows the eccentricity distribution of solar circle halo stars that were located in satellites at redshift $z = 0.46$. The green line shows stars originating from a single such satellite (S1). The y-axis is normalised by the total number of star particles in each eccentricity bin (from figure 4.5).

to those of Helmi & White (1999) and Helmi & de Zeeuw (2000), both of which follow (at higher spatial resolution) the accretion of stars in a *static* potential, in which little disruption to the adiabatic invariants would be expected. Thus our study confirms that these results hold when the formation processes of the galaxy are self-consistently simulated, and hence the potential in which the satellite is disrupted is dynamic. In fact, our final velocity phase space distribution (figure 4.9 a-c) is reminiscent of figure 5 of Helmi & White, bearing in mind that most of our stellar orbits will be at intermediate points between their pericenter and apocenter. Further, the distribution of the disrupted stars in integrals of motion space (figure 4.9 d) is similarly in good qualitative agreement with those for satellites in figure 7 of Helmi & de Zeeuw.

Motivated by the high-eccentricity seen in the accreted satellite stars (as highlighted in figure 4.8), we then examined the phase space distribution of the clump of high-eccentricity metal-deficient halo stars identified by CB00. Figure 4.10 shows the sample of CB00 stars within 2.5 kpc of the Sun with [Fe/H] ≤ -1, plotted in the same phase space projections as the simulated data in figure 4.9. Highlighted by open circles are stars with $\varepsilon > 0.8$ and $-2.0 <$ [Fe/H] < -1.4. A wider range of energies is seen in the observed dataset, in comparison with the simulations shown in figure 4.9 d. The latter indicate that recently accreted satellite stars will be of higher energy (lower |E|) on average than halo field stars, as their stellar orbits will be less bound. We thus make an arbitrary cut in energy in order to separate the field

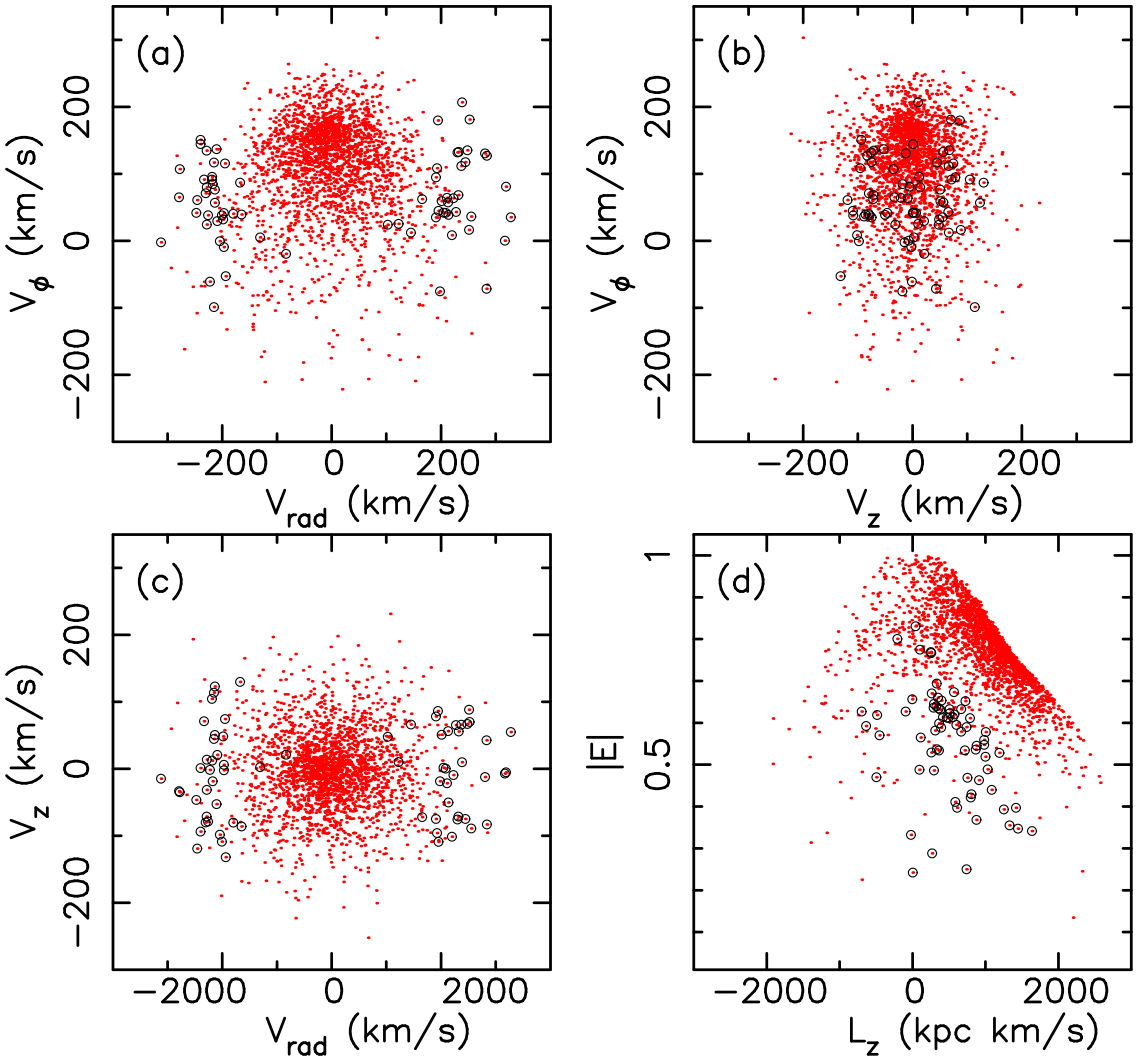

Figure 4.9: (a)-(c): Velocity space (V_ϕ, V_{rad}, V_z) projections of the present-day solar circle stars of model 1. Open circles denote the subset of stars originating in S1. (d): The distribution for the same stars in integrals of motion space - i.e., the absolute value of the total energy (|E|) versus projected angular momentum (L_z).

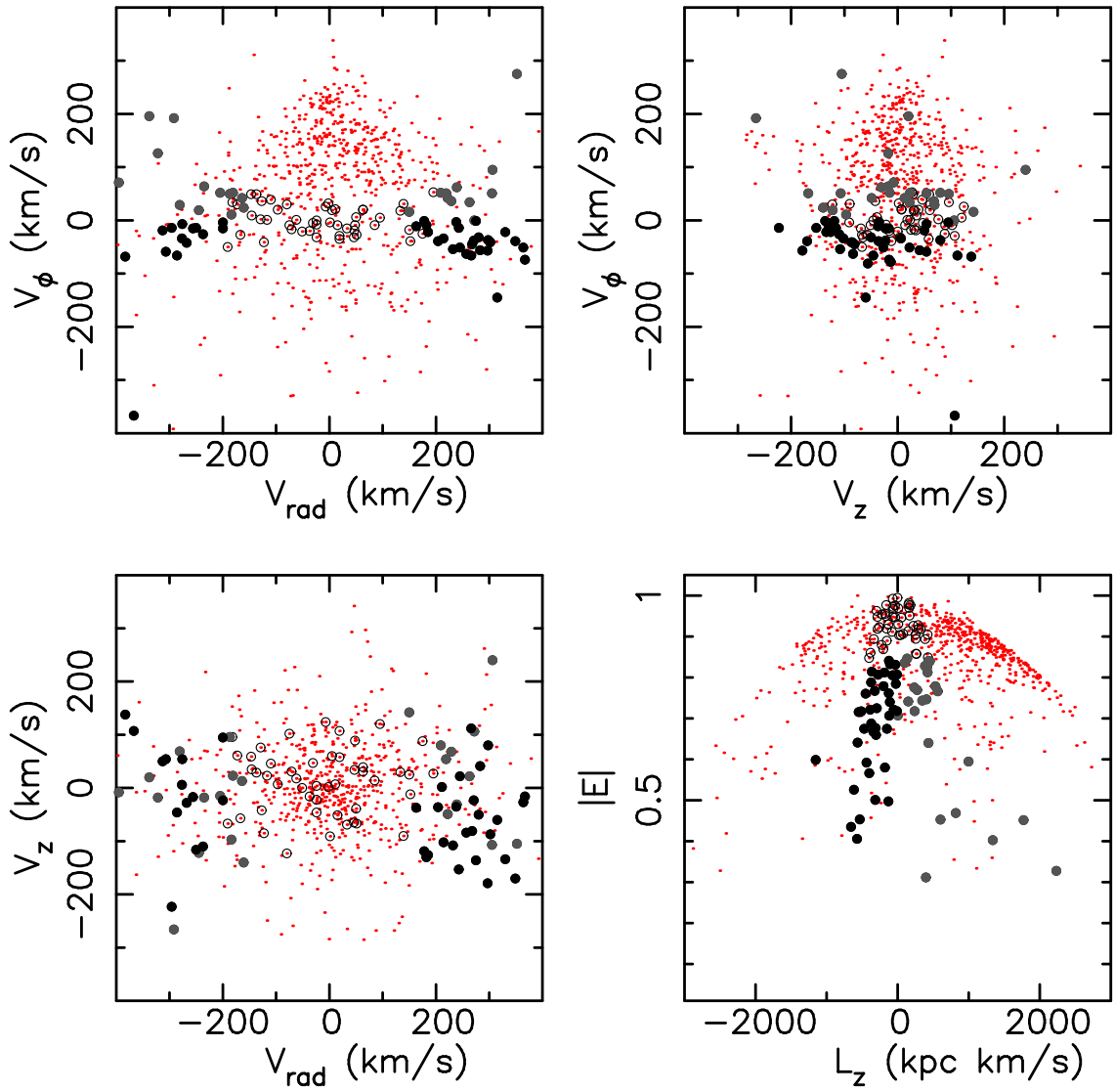

Figure 4.10: Velocity and integrals of motion phase space for the 729 Chiba & Beers (2000) stars within 2.5 kpc of the Sun with [Fe/H] < -1. (a)-(c): velocity space; (d): energy versus projected angular momentum. Stars with eccentricity $0.8 < \varepsilon < 1.0$ and metallicity $-2.0 <$ [Fe/H] < -1.4 are represented as open circles. Solid black circles denote stars of high energy, while solid grey circles correspond to high energy stars with $-800 < L_z < 0$ kpc km/s.

stars from those we suspect come from an accreted satellite, and the new subset of stars are marked by solid circles. We notice immediately that these stars are more tightly confined in phase space, and closely resemble the distribution of the accreted satellite in our simulation.

4.5 Discussion

We have simulated self-consistently two models representing the formation of a Milky Way-like galaxy using our N-body/SPH chemodynamical code `GCD+`. The models differ only in the amplitude of small scale density perturbations σ_8 incorporated into the initial conditions. This results in different merging histories, which we then use to search for distinctive present-day chemical and kinematical signatures of the simulated galaxies' early formation epochs. In model 1, stars form in local dense regions of gas, seeded by a value of σ_8 comparable to current CDM orthodoxy. The galaxy subsequently builds up via a series of mergers in the manner of standard hierarchical structure formation scenarios. A low value of σ_8 in model 2 results in a more dissipative collapse of the baryonic matter, with star formation occurring predominantly in the galaxy's central regions. Both models result in disk galaxies with remarkably similar qualities; model 1, however, produces a greater number of high-eccentricity halo stars, and in this regard is in better agreement with the observational dataset of CB00. By tracing the merging histories of satellites in model 1, it becomes apparent that a significant number of high-eccentricity halo stars originate in accreted dwarf galaxies. In fact, almost 20 % of high-eccentricity halo stars located in the solar circle originate in one satellite, of stellar mass $\sim 10^9\,\mathrm{M}_\odot$, which was on a precessing polar orbit and was accreted over the past $\sim$5 Gyrs.

Thus our simulation suggests that stars from an accreted satellite that was on a polar orbit can constitute part of the galaxy's halo, and that such stars have highly eccentric orbits. Originating in accreted polar satellites, these stars would not gain the angular momentum induced by the tidal torque of the external gravitational field that results in the rotation of the disk component of the galaxy. Such stars will fall toward the centre of the galactic potential and end up on highly eccentric orbits.

The existence of an apparent correlation between metallicity and eccentricity in halo stars was interpeted by ELS as a sign that rapid collapse drives the formation of

the Galaxy. Our study suggests that another way of creating such high-eccentricity halo stars is through the recent accretion of polar orbit satellites. Furthermore, dwarf galaxies of stellar mass $\sim 10^9\,M_\odot$ typically have appropriate average metallicities to be the source of this group of stars with [Fe/H] ~ -1.7 (e.g. Mateo 1998). Velocity phase space and the space of adiabatic invariants is where we would expect substructure within the halo due to past merging to be apparent. The distribution in such space of an accreted satellite of our simulated galaxy resembles that of previous studies that traced the disruption of dwarf galaxies in static potentials, in particular figure 5 of Helmi & White (1999). The greater dispersion in the distributions of our simulation can most likely be attributed to the dynamic nature of the potential in our full simulation of Galactic evolution, eroding the invariance of the integrals of motion. The identified concentration of high-eccentricity, low-metallicity, halo stars from CB00 occupy a very similar, restricted, region of phase space to the simulated accreted satellite.

The possibility that this concentration of stars in the eccentricity-metallicity plot is caused by satellite accretion was previously noted by Dinescu (2002). In the metallicity range $-2.0 <$ [Fe/H] < -1.5 of the CB00 data, Dinescu notes an excess of stars in retrograde orbits with rotational velocity (V_ϕ) ~ -30 km s^{-1}, from that expected from a "pure" halo. She identifies these stars as candidates for having been torn from the system that once contained ω Cen. ω Cen is believed to be the nucleus of a disrupted, accreted dwarf galaxy (e.g. Lee et al. 1999; Majewski et al. 2000), is in a retrograde orbit, and has an orbital eccentricity of $\sim$0.67. Using a simple disruption model, Dinescu showed that the tidal streams tend to have higher orbital eccentricity than the disrupted satellite. Along with the mean metallicity of ω Cen being [Fe/H] $= -1.6$, the inference is that the clump of high-eccentricity halo stars identified in CB00 contains a significant number of stars which have been tidally stripped from ω Cen. Our simulations provide a degree of support for this hypothesis. Taking only those stars with $L_z < 0$ in figure 4.10 d, we see a clump of stars with intermediate energies and $L_z \sim -400$ kpc km s^{-1}. These stars are identified in all phase space plots by black circles; we see that the distribution becomes more restricted in each velocity space dimension, and there is greater concordance with Helmi & White's (1999) idealized satellite accretion studies.

The key question we wish to address remains ... *what are the implications for the competing galaxy formation paradigms?* A brief response is as follows: CB00

observed no correlation between eccentricity and metallicity for halo stars near the Sun, obviating the need for a "rapid collapse" picture of the formation of the Galaxy (ELS). However, CB00 do interpret a clump of high-eccentricity low-metallicity ([Fe/H]~ -1.7) stars in their dataset in terms of ELS - i.e. as a relic of a rapid collapse phase. Our simulations suggest that an equally plausible origin for this population is the recent accretion of a polar orbit satellite in the Galactic halo.

Chapter 5

Stellar Halo Constraints on Simulated Late-Type Galaxies

5.1 Introduction

Formation scenarios for the Milky Way have been dominated by two canonical models: the rapid collapse of a proto-galactic cloud (Eggen, Lynden-Bell & Sandage 1962), and the hierarchical build up from low mass fragments (Searle & Zinn 1978). Burkert (2001) reviews evidence that the early dissociation of gas from dark matter in the first stages of the hierarchical build-up allows these two models to be combined into one consistent formation scenario. In this scenario, the Galactic spheroid is formed by hierarchical merging of substructures, while the disk components result from the smooth infall of diffuse gas. This picture is consistent with the predictions of classical cold dark matter (CDM) scenarios (White & Frenk 1991; Kauffmann et al. 1993)

Simulations now show that the observed large scale properties of galaxies can be reproduced within CDM cosmological models. For example, Steinmetz & Muller (1995) studied the chemo-dynamical evolution of disk galaxies, and succeeded in distinguishing the chemical properties between halo, disk and bulge stars. Raiteri, Villata, & Navarro (1996) and Berczik (1999), reproduced the correlation between [O/Fe] and [Fe/H] of solar neighbourhood stars by tracing the metal enrichment by Supernovae Type II (SNe II) and Type 1a (SNe Ia). Steinmetz & Navarro (1999), Navarro & Steinmetz (2000), and Koda, Sofue, & Wada (2000) discussed the zero point of the Tully-Fisher relationship by analysing the end products of

their chemical evolution and stellar population synthesis models. The observed eccentricity-metallicity relation of Milky Way halo stars has also been successfully reproduced (Bekki & Chiba 2000; Brook et al. 2003).

However, several problems continue to plague these simulations. Notoriously, the resulting structures are deficient in angular momentum (e.g. Navarro, Frenk & White 1995). The simulations also fail to create galaxies in which most baryonic matter resides in the thin disk, as observed in the Milky Way. Typically, these simulations result in a stellar halo which is as massive or more massive than the stellar disk. For example, in a recent high resolution study, Abadi et al. (2003) create a galaxy with a stellar halo which contains over 60% of the total stellar mass of the system, and a thin disk which constitutes only 17 % of the stellar mass, more akin to an S0 than a late type disk galaxy. Such massive stellar halos inevitably have a greater metallicity than observed in late type spirals. This leaves open the question of the formation processes which lead to late type disk galaxies such as the Milky Way, within the context of hierarchical structure formation scenarios.

It has long been postulated that energy feedback from SNe is necessary to solve many of the above problems. Unfortunately, energy feedback from SNe explosions remains one of the most difficult processes to model in galaxy formation simulations, largely because feedback occurs on sub-resolution scales. A number of different SNe feedback implementations have been employed in chemo-dynamical codes; for a survey of such methods, see Thacker & Couchman (2000, TC hereafter).

Katz (1992) smooths thermal energy into nearest neigbour gas particles using the smoothed particle hydrodynamic (SPH) kernel. This feedback scheme is known to be largely inefficient, as the characteristic timescale of radiative cooling in the high density regions, where star formation typically occurs, is shorter than the dynamical timescale. Navarro & White (1993) extend this technique to include both thermal and kinetic energy. A parameter, f, controls the fraction of energy input as kinetic as opposed to thermal energy. Although f and the total amount of energy both may vary, this feedback scheme is common to many galaxy formation simulations (e.g. Steinmetz & Navarro 2002; Kobayashi 2002; Nakasato & Nomoto 2003; Abadi et al. 2003). Representations of the multi-phase interstellar medium are made by Hultman and Pharasyn (1999) and by Springel & Hernquist (2003), but these studies are limited by the dynamical dependence of the two phases. In Gerritsen (1997), energy is returned by heating an individual SPH particle, a technique that is successful for simulating dwarf size systems. TC and Kay et al. (2002) examine a scheme in

which the feedback region is adiabatic. Such a feedback scheme was shown to be more effective in an isolated, dwarf type galaxy than in a MilkyWay-sized galaxy.

In this study, we examine the link between the energy feedback and the properties of the final galaxy; specifically the halo/disk stellar mass ratio and the halo metallicity distribution function (MDF). We demonstrate the importance of feedback in regulating star formation in the small systems that collapse at early epochs of galaxy evolution. In section 5.2, details of our chemo-dynamical code, `GCD+`, and our two models incorporating different feedback schemes are provided. We examine and compare the properties of the two simulated galaxies in section 5.3, concentrating on the halo/disk stellar mass ratio and the halo MDFs of the simulated disk galaxies. One feedback model results in a galaxy which is a better representation of a late type galaxy than the other. In section 5.4, we trace the baryons that form the disk of the galaxies, highlighting the processes that lead to the difference in the fraction of stars ending up in the disk rather than the halo. The discussion in section 5.5 summarises the contribution of this study to our understanding of how thin disks form from structures within CDM cosmologies.

5.2 The Code and Model

Our Galactic chemo-dynamical code, `GCD+`, self-consistently models the effects of gravity, gas dynamics, radiative cooling and star formation. We include SNe II and SNe Ia feedback, and avoid use of the instantaneous recycling approximation in modelling the chemical enrichment. Details of `GCD+` can be found in chapter 2. We describe here only the details concerning the inclusion of SNe energy feedback.

We assume that 10^{51}ergs is fed back as thermal energy from each SNe. In our *thermal feedback model*, denoted "TFM" hereafter, energy from SNe II and SN Ia is smoothed over surrounding gas particles according to the SPH kernel, in the form of thermal energy (following Katz 1992).

Our second model incorporates a different feedback mechanism for SNe II. These SNe trace starburst regions, and are therefore more susceptible to the inefficiency of the feedback algorithms used in the TFM. In our *adiabatic feedback model*, "AFM" hereafter, gas within the SPH smoothing kernel of SNe II explosions is prevented from cooling. This adiabatic phase is assumed to last for the lifetime of the lowest mass star which ends as a SNe II, i.e. the lifetime of an $8\,M_\odot$ star ($\sim$100 Myr). In

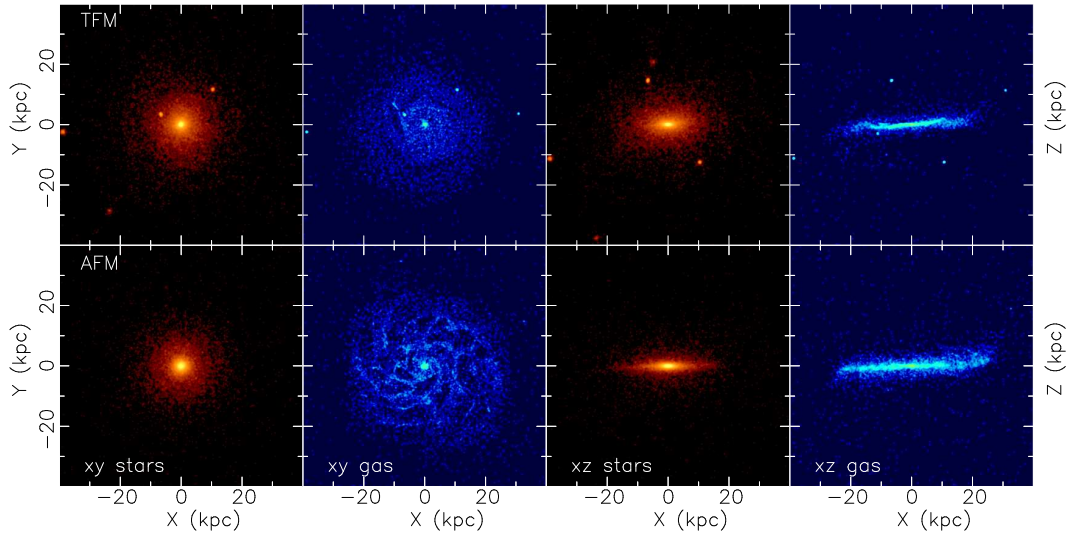

Figure 5.1: Density plots for TFM (top) and AFM at z=0. Stars and gas are shown face-on (X-Y plane) and edge-on (X-Z). In the TFM, a thin disk is evident in the gas distribution, but the galaxy's stellar mass is dominated by halo stars, and resembles an S0 galaxy. In the AFM, the galaxy is dominated by a thin stellar disk. A large gaseous thin disk, still undergoing star formation, has also formed.

the AFM, the energy released by SNe Ia, which do not trace starburst regions, is fed back as thermal energy. The AFM is similar to a model presented in TC.

We use semi-cosmological simulations that are based upon the galaxy formation model of Katz & Gunn (1991). The initial condition is an isolated sphere of dark matter and gas, onto which small scale density fluctuations are superimposed, parameterised by σ_8. These perturbations are the seeds for local collapse and subsequent star formation. Solid-body rotation corresponding to a spin parameter, $\lambda \equiv J|E|^{1/2}/GM_{tot}^{5/2}$, is imparted to the initial sphere, where J, E and M_{tot} are the total angular momentum, energy, and mass of the system respectively. Relevant parameters include the total mass ($5\times10^{11}\,\mathrm{M}_\odot$), baryon fraction ($\Omega_b$=0.1), spin parameter ($\lambda$=0.0675) and σ_8=0.5. We employed 38911 dark matter and 38911 gas/star particles, making the resolution of this study comparable to other recent studies of disk galaxy formation (e.g. Abadi et al. 2003).

We again emphasise that the two models analysed here are identical, except in the way in which the energy from SNe II affects the surrounding gas.

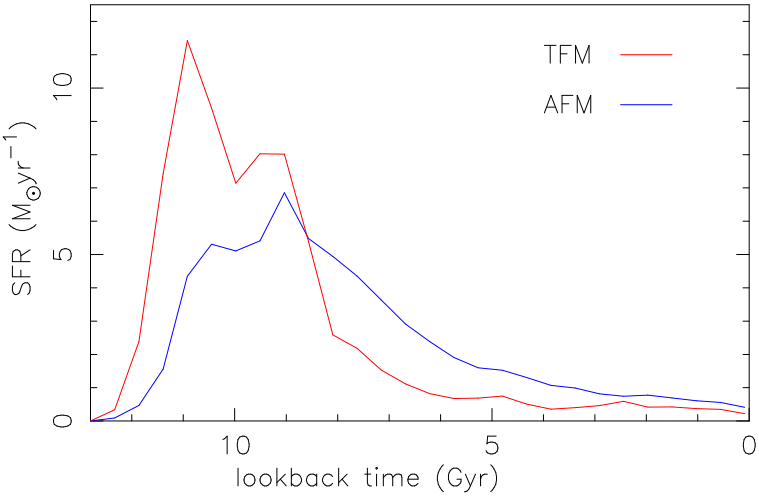

Figure 5.2: Global star formation rate (SFR) as a function of lookback time for the two supernova energy feedback models applied to the same CDM overdensity. Inefficient feedback of the TFM results in high SFR at early times compared to the AFM.

5.3 Results

Figure 5.1 shows a density plot of the final stellar and gaseous components of the two models. Both simulations result in flattened stellar structures and thin gaseous disks. In the TFM, the stellar mass is dominated by halo stars, and a thin disk is evident in the gas distribution. The final galaxy more closely resembles an S0 galaxy than a late type spiral. Star formation is rapid during early epochs (figure 5.2), as a result of the inefficiency of the feedback. The peaks in the star formation rates are related to early major merger episodes. Star formation continues at a steady rate, primarily in the disk, over the last ∼7 Grys, a relatively quiescent period with only a few minor merger events.

It is clear from the edge on view of the stellar populations in figure 5.1 that the AFM has created a more dominant stellar disk. Star formation in the AFM is suppressed at early epochs (figure 5.2) compared to the TFM. The signatures of the early mergers of the TFM are also evident in the AFM star formation peaks, a result of the identical initial conditions. The greater availability of gas means the AFM creates more stars at later times than the TFM: $\sim 1.9\times10^{10} M_\odot$ compred with $\sim 8.2\times10^{9} M_\odot$ in the last 8 Gyrs. The result is the creation of a more dominant stellar disk. A large gaseous thin disk, still undergoing star formation, has also formed. The mass of cold gas ($T<4\times10^5$K) associated with the disk is larger for the AFM, $\sim 9\times10^{9} M_\odot$ than for the TFM, $\sim 5\times10^{9} M_\odot$.

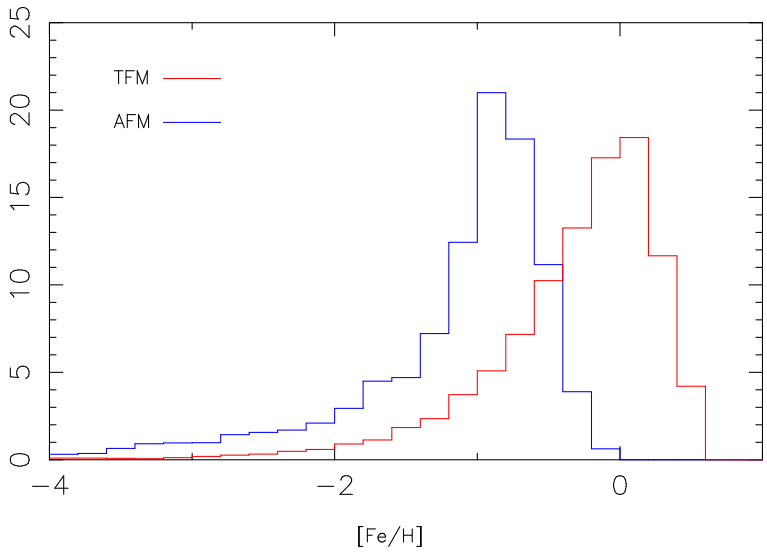

Figure 5.3: Halo metallicity distributions for the TFM (red line) and AFM (blue line), giving the relative fraction of halo stars within a given metallicity bin. Halo stars are defined by weighting star particles by mass within the regions 4<R<50 kpc and |Z|>4 kpc.

In this study, we focus on the mass and metallicities of the stellar halos of our simulated galaxies. Halo stars are defined spatially using two hemispheres defined by 4<R<50 kpc and |Z|>4 kpc. The density gradient in shells of these hemispheres is integrated over the sphere out to 50 kpc to find the mass of the stellar halo. Disk stars are defined by the distribution of specific angular momentum (Lz_s) as a function of specific binding energy(E_s). It is clear from figure 5.1 that the gas particles are predominantly in a disk, resulting in their confinement to a small region in Lz_s vs. E_s space. This same region is used to define simulation disk stars; cuts in the Z components of velocity ($|V_Z|$<65 km/s) and position (|Z|<1 kpc) have also been imposed.

The stellar population of the TFM is dominated by halo stars; indeed, the stellar halo is a factor of 1.2 times more massive than its stellar disk population. The AFM has a halo/disk mass fraction ∼6 times smaller, more closely resembling a late type galaxy. Nevertheless, this fraction is still almost an order of magnitude larger than the halo/disk ratio of the Milky Way. The large mass of the stellar halo in the TFM is intimately linked to its high metallicity, as seen in figure 5.3. The peak of the halo MDF has shifted from [Fe/H]∼0 for the TFM (red line), to [Fe/H]∼−1.0 for the AFM (blue line), a full factor of ten in metallicity. The peak of the halo MDF in the AFM is somewhat higher than that of the Milky Way halo MDF, which

peaks at [Fe/H]~-1.5 (Ryan & Norris 1991), but is lower than the peak for M31, [Fe/H]~-0.7 (Durrell et al. 1994). These results suggest that strong feedback from SNe is important for the formation of the stellar halos of disk galaxies.

Recently, significant progress has been made on the theoretical and observational signatures of satellite accretion in present day stellar populations, e.g. Helmi & White 2000; Bekki & Chiba 2001; Brook et al. 2003. Moreover, the model used in TC that incorporated adiabatic feedback was shown to have a greater effect on smaller systems. Thus, the subclumps of the simulation were a natural place to search for the formation processes responsible for the different galaxy properties produced by the different models.

In figures 5.4-5.11, we show the disruption process for two typical satellites from each of the TFM and the AFM. Red particles are stars present in the satellite prior to any disruption. Gas particles are green. Star particles formed after the disruption process begins are blue. A grey scale density plot of the simulation stars is in the background. There are $\sim$1000 baryon particles in each satellite, corresponding to $\sim10^9\,M_\odot$. Six time-steps are shown, both face-on and edge-on, for these typical merging events.

The disruption of one satellite in the TFM, TS1, is shown in the panels of figures 5.4-5.5. The satellite begins as a dense, stellar dominated system. This is a result of rapid early star formtion, between 11 and 8 Gyrs ago (figure 5.12 red line). By 4.7 Gyrs ago, the satellite is disrupted and star formation has ceased within the dwarf. By 3.6 Gyrs ago, accretion is well underway. Due to their collisionless nature, the accreted stars spread throughout the halo by z=0. Gas from the satellite falls to the disk region of the host galaxy, where new stars (blue) are born. The amount of gas falling into the disk region, and forming stars, is small as most gas has been exhausted before the satellite merged. The disruption of a second satellite in the TFM, TS2, is also shown in the panels of figures 5.6-5.7. TS2 is accreted at an ealier time than TS1, with disruption well under way by 6.7 Gyrs ago. Again, the star formation rate is high at early epochs (figure 5.13 red line), and stars accrete predominantly to the halo of the galaxy.

In satellite AS1 from the AFM, star formation in the subclumps is regulated (figure 5.12, blue line) prior to disruption. Gas remains less densely concentrated than stars and is preferentially stripped. This pre-enriched gas dissociates from the dark matter, and accretes smoothly on to the disk region. On the other hand, stars from the satellite are accreted into the halo of the galaxy by z=0. Therefore, the

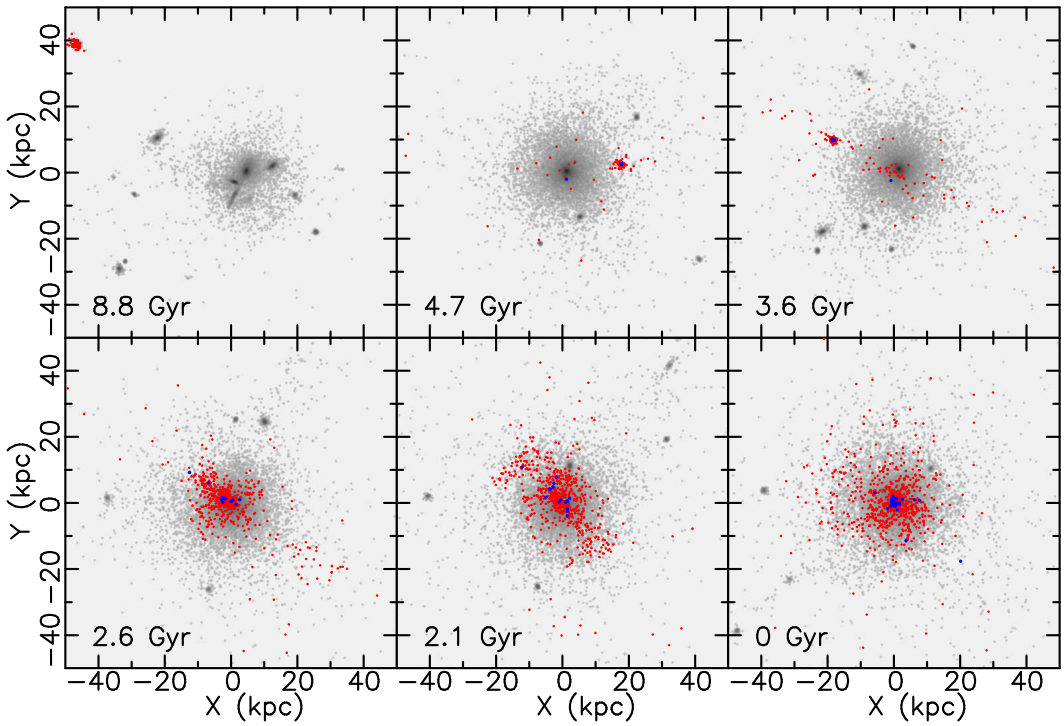

Figure 5.4: The disruption process for a typical satellite from the TFM, TS1, shown in the X-Y plane. Red particles are stars present in the satellite prior to any disruption. Gas particles are green. Star particles formed after the disruption process begins are blue. Six snapshots of the model are shown for this typical merging event. The box sides are 50 kpc. In the TFM, gas falls to the centre of sub-clumps, rapidly forming stars. Thus, prior to disruption, the satellite has little gas content. The stars are accreted onto the halo of the galaxy.

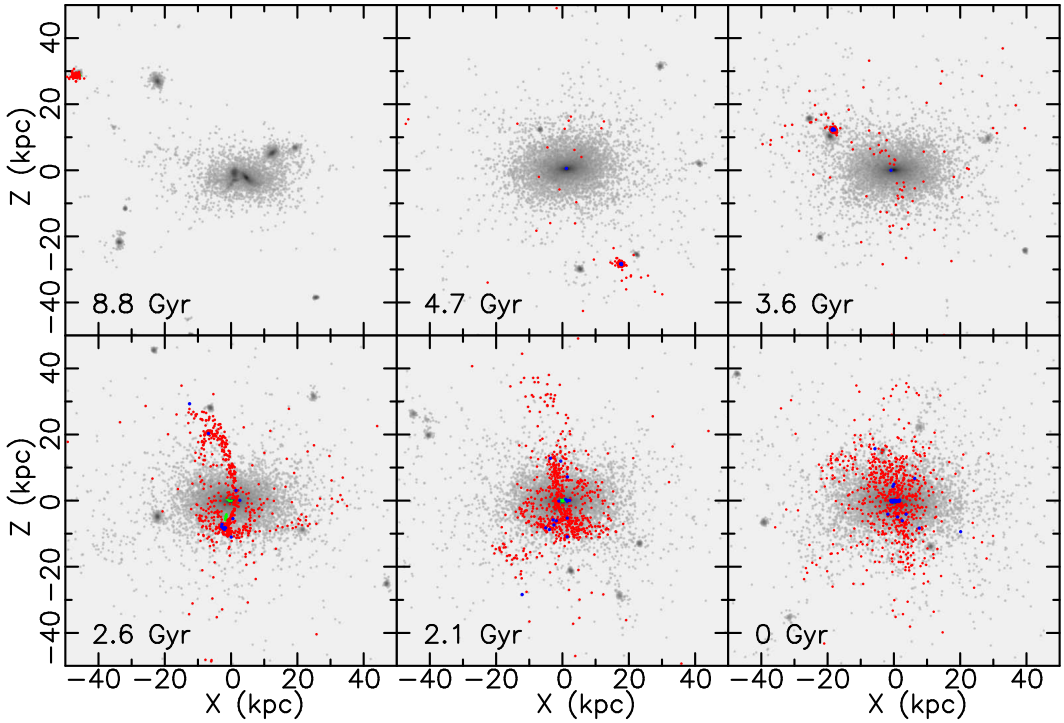

Figure 5.5: The disruption of TS1 shown in the X-Z plane. All other details as in figure 5.4. From side-on, it is apparent that old stars accrete to the stellar halo of the simulated galaxy.

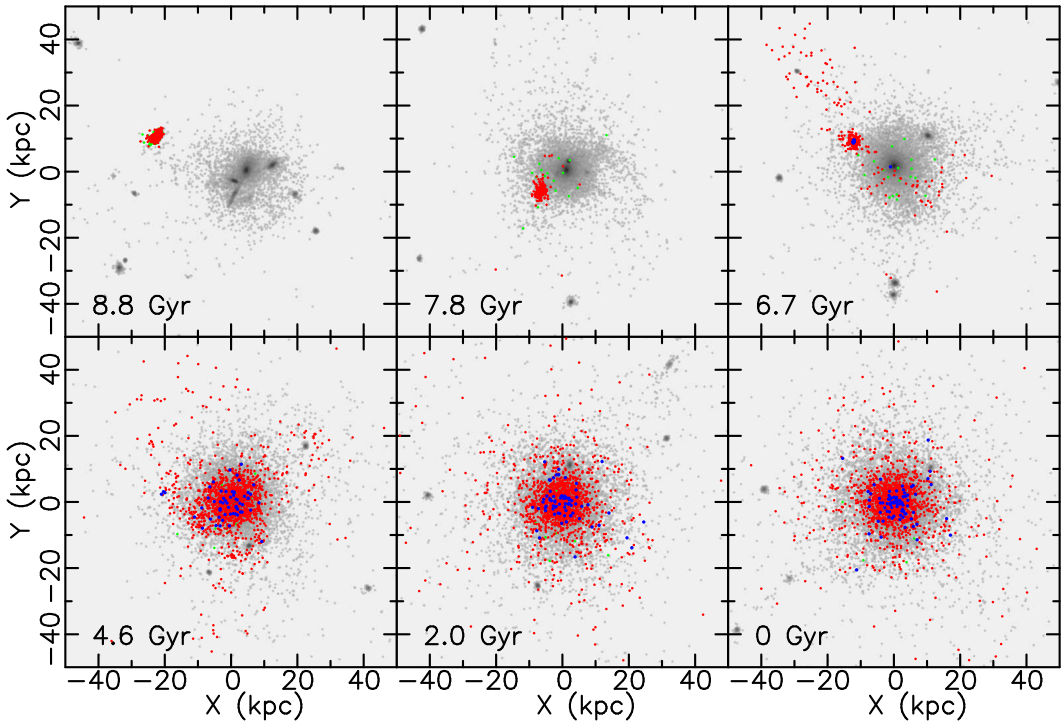

Figure 5.6: Same as figure 5.4, for the accretion of a second satellite, TS2, in the TFM. Again we see a satellite with little gas, whose stars are accreted predominantly into the galactic halo. Stars born after the disruption of the satellite begins (blue) are more centralised than old stars (red).

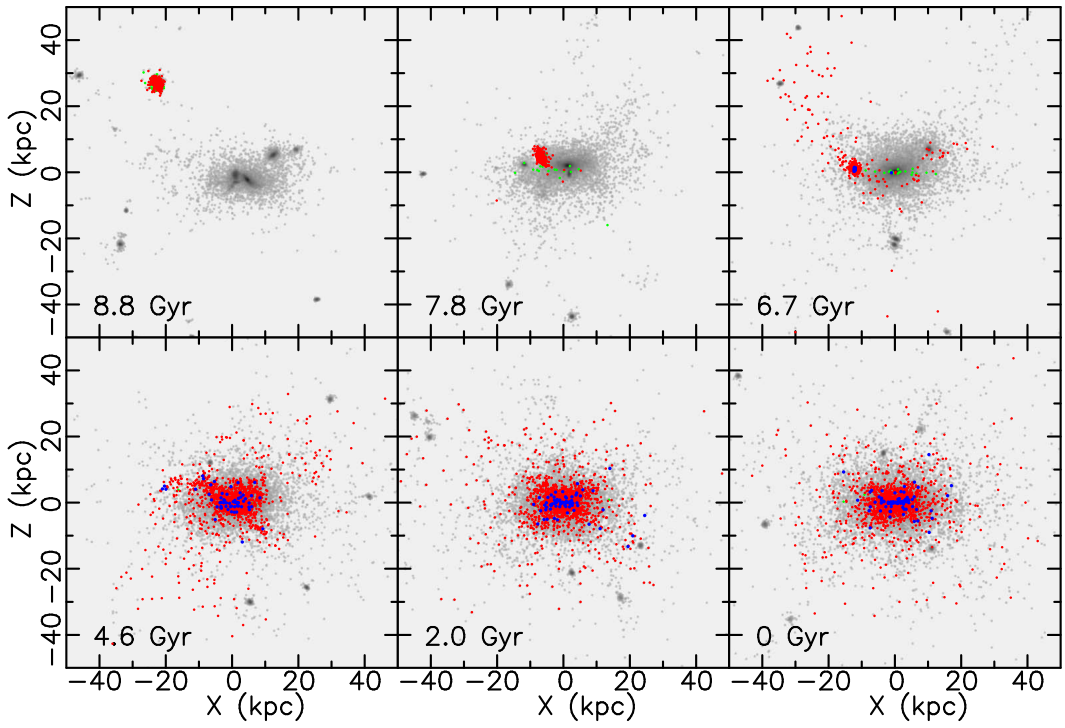

Figure 5.7: As for figure 5.6, in the X-Z plane. The number of new (blue stars) associated with the accretion is low. Most baryonic material accreted from TS2 is accreted as stars, and finishes in the halo of the galaxy.

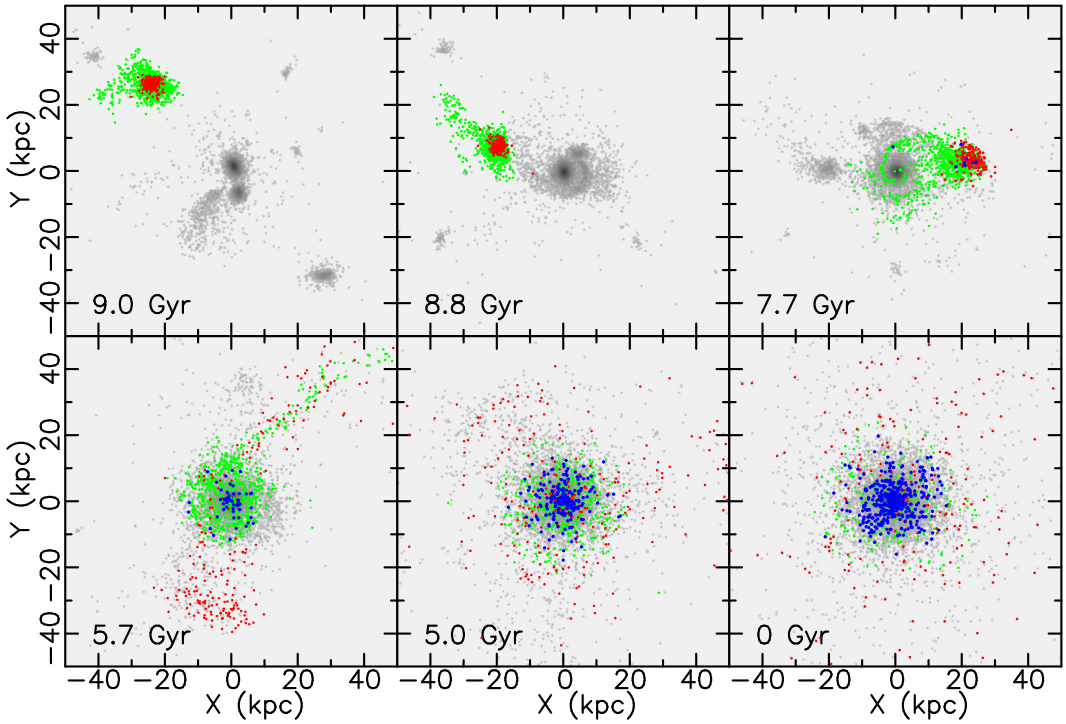

Figure 5.8: The disruption process for a typical satellite, AS1, from the AFM. Red particles are stars present in the satellite prior to any disruption. Gas particles are green. Star particles formed after the disruption process begins are blue. Four edge-on snapshots of the model are shown for this typical merging event. In the AFM, gas remains less densely concentrated than stars and is preferentially stripped, decoupling from the dark matter. The stripped gas accretes smoothly to the disk region. Stars from the satellite are accreted into the halo of the galaxy by z=0. Pre-enriched gas stripped from the satellites feeds the thin disk, where new stars (blue) are born over the past ∼8 Gyrs.

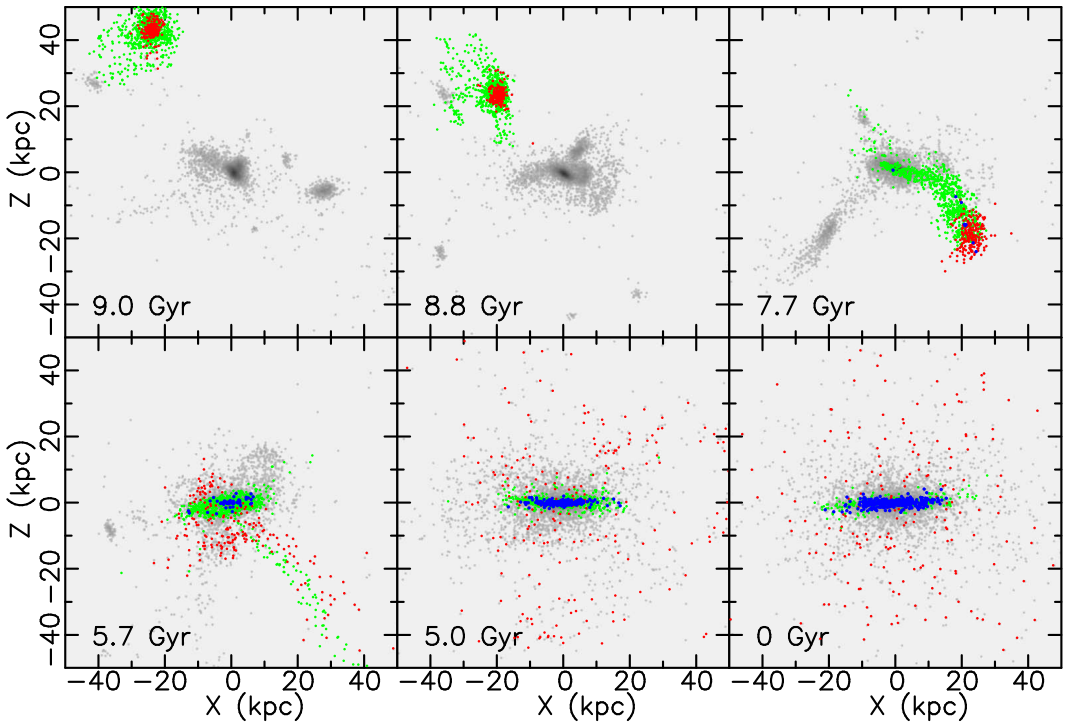

Figure 5.9: As for figure 5.8, in the X-Z plane. It is clear in this plane that gas (green particles) accreted from AS1 falls to the disk, where new stars (blue) are born, whereas stars accreted from the satellite end up in the galactic halo.

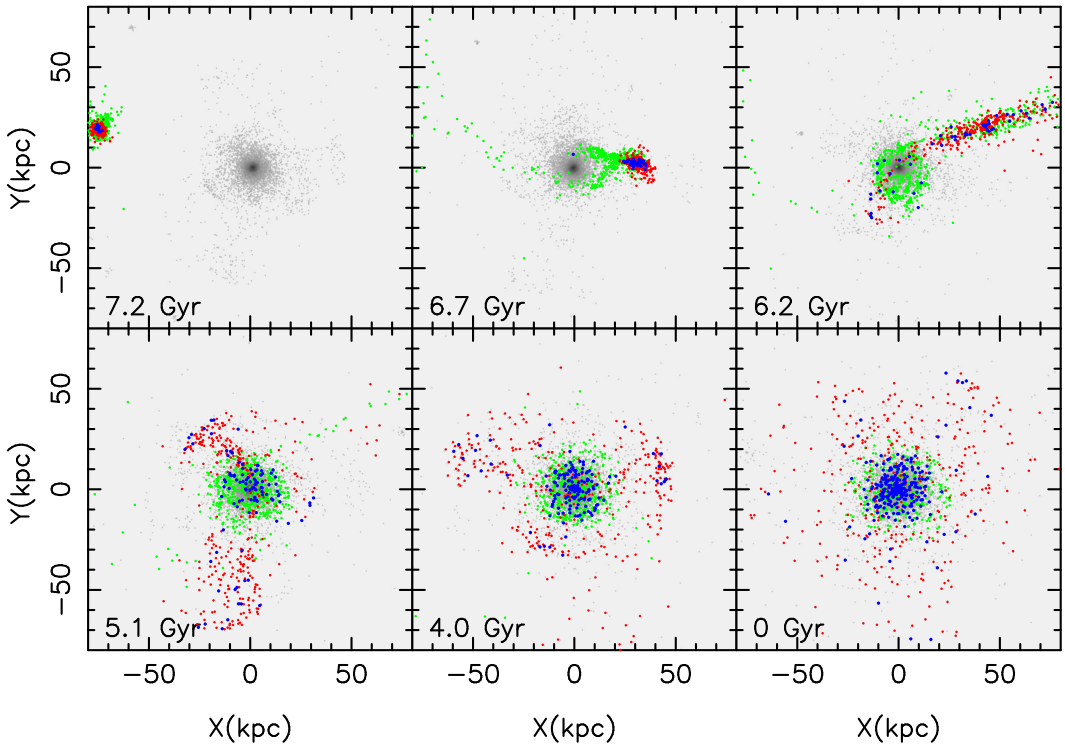

Figure 5.10: As for figure 5.8, for a second satellite, AS2, from the AFM. Again the effect of gas remaining less densely concentrated than stars is apparent, and stripped gas accretes smoothly to the disk region. Stars from the satellite are accreted into the halo of the galaxy by z=0. New stars (blue) are born in the disk over the past ∼8 Gyrs.

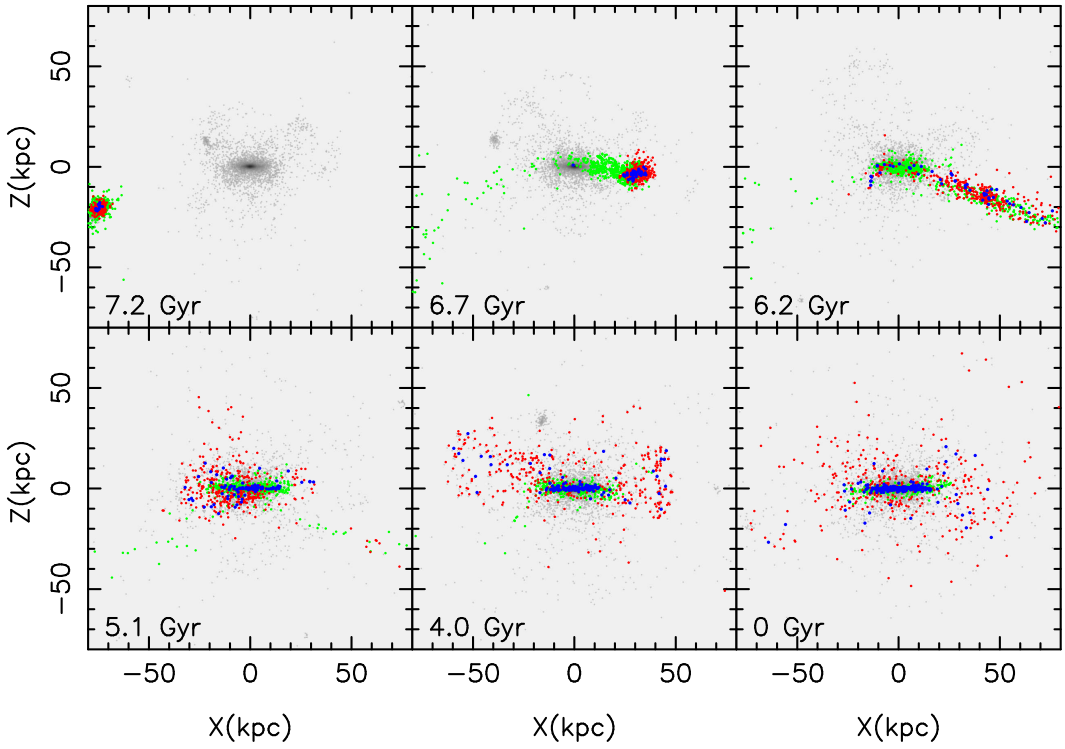

Figure 5.11: The satellite in figure 5.10, shown in the X-Z plane. Again it is evident that stars present as accretion begins (red particles) end up in the halo of the galaxy. The edge-on view makes it clear that gas (green particles) accretes to the disk where new stars (blue) are born.

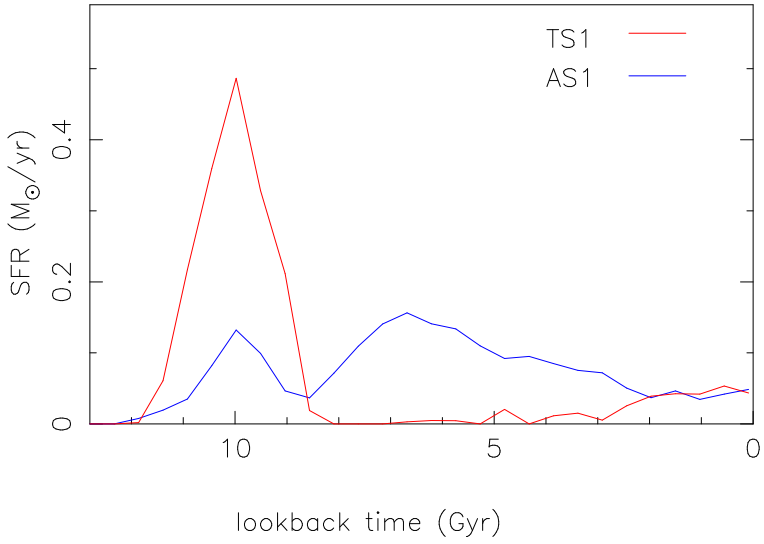

Figure 5.12: Total star formation rates (SFR) within the satellite systems TS1 of the TFM (red line), seen in figures 5.4-5.5, and AS1 from the AFM (blue line), seen in figures 5.8-5.9. As in the host galaxy, star formation is early and rapid in the satellite TS1 of the TFM, compared to the star formation in satellite AS1 of the AFM.

stars that end up in the halo are the oldest stars formed in the subclumps, as well as the most metal poor, as chemical enrichment has been suppressed in these small systems by the strong feedback in the AFM. Disruption of a second, more massive satellite ($\sim 2{\times}10^9\,M_\odot$), AS2 from the AFM is also shown, with regulated early star formation (figure 5.13, blue line), and gas accreting to the disk region where new stars are born.

The accretion events shown in this section occur at intermediate age in the galaxy formation process. They do not demonstrate that late accreting satellites are the source of all disk and halo material. Rather, they evince the effectiveness of SNe feedback on satellites. AFM also leads to regulated star formation in the smaller systems that have collapsed at high redshift, as is clear from figure 5.2. In a CDM cosmology, the stellar halo is likely to be built up by the accretion of a significant number of such small systems, including tidally-stripped stars during multiple mergers of building blocks at high redshift (Bekki & Chiba 2001). Our results demonstrate that the AFM produces enough SNe energy to suppress star formation and chemical enrichment in the building blocks of galaxy formation, and that this leads to a less massive, more metal poor, stellar halo that is in better agreement with observation.

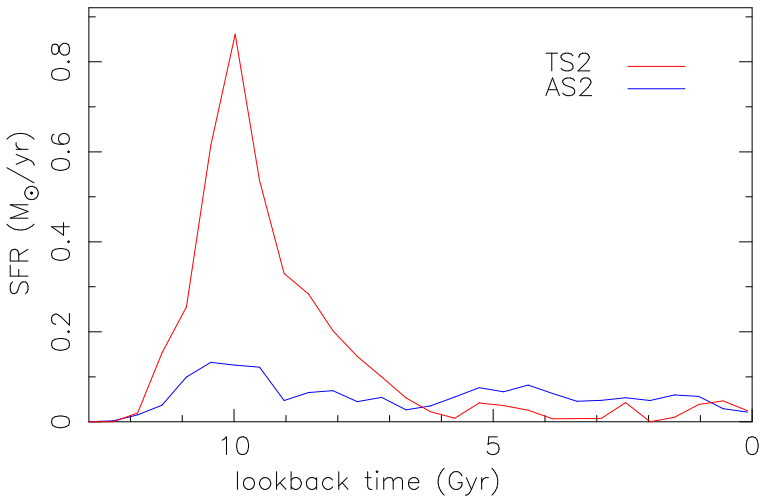

Figure 5.13: Total star formation rates (SFR) within the satellite systems TS2 of the TFM (red line), seen in figures 5.6-5.7, and AS2 from the AFM (blue line), seen in figures 5.10-5.11. Again, star formation is early and rapid in the satellite TS2 of the TFM compared to AS2 of the AFM.

5.4 Discussion

Energy feedback has emerged as a possible solution to several of the problems that plague models of the formation of late type disk galaxies in CDM scenarios. Despite this recognition, the manner in which feedback is incorporated into SPH codes remains problematic. In this study we have been concerned primarily with the effects of feedback on the mass and metallicity distribution of the stellar halos of simulated galaxies, and its capacity to regulate star formation in high-redshift galactic building blocks.

We implement two different feedback schemes into a seed galaxy with the same initial perturbation. Incorporating thermal feedback similar to that of Katz (1992) results in a flattened, disk-like galaxy that resembles those of previous studies (e.g. Steinmetz & Mullar 1995; Berzcik 1999; Abadi et al. 2003). The fundamental problem is that the ratio of the mass of the halo and disk components is much too high and the metallicity of the halo component is also too high in comparison to the observations of the Millky Way; in both cases by about a factor of 10. There is less conflict with observations of M31. In the TFM, the gas cools to the centre of building blocks, rapidly forming stars (figure 5.2). The rapid star formation cycles also result in metallicities that quickly approach solar levels and more stars with high metallicity. Due to the collisionless nature of the stellar component, these stars

end up in the halo of the host galaxy after tidal disruption. The halo thus becomes very massive and very metal rich.

With the AFM, gas is delayed from cooling in star burst regions. Star formation is regulated in small systems, such as building blocks, and lower fractions of the initial baryonic content of these building blocks are converted to stars. These building blocks thus have lower metallicity stars and a hotter, more diffuse gas content, allowing gas to be dissociated from the collapsing dark matter that drives structure formation. During the tidal disruption of these building blocks, the gas is preferentially stripped and, due to its dissipative nature, accretes smoothly onto the thin disk; this pre-enrichment helps in alleviating the G-dwarf problem (Fenner & Gibson 2003). The stars that are formed in these building blocks are accreted preferentially into the halo of the galaxy. As a smaller fraction of baryons are turned into star particles in the building blocks in the AFM, the halo of the resulting host galaxy is less massive and more metal poor. Also, even if they are accreted into the galaxy at a later epoch than the gas, the stars stripped from these building blocks are older than the stars that subsequently form in situ in the thin disk: halo stars are old and metal poor, disk stars are new and metal rich. The result is a disk galaxy that is a far better realisation of the Milky Way and M31, compared to the canonical TFM.

Besides observations of the Milky Way's stellar halo mass and MDF, which have been the main focus of this paper, additional Local Group observations provide a measure of support for the processes outlined here. The Magellanic Stream is consistent with the suggestion that gas is preferentially stripped from accreting satellite galaxies (Putman et al. 1998). The Sagittarius Dwarf and Sagittarius stream are totally stellar (Koribalski et al. 1994; Burton & Lockman 1999), suggesting that this accreted satellite had previously lost its gas. The fact that Local Group dwarf spheroidals are gas poor, and preferentially closer to the centre of the Milky Way than gas rich dwarf irregulars provides further evidence, albeit circumstantial, that gas from satellites is stripped prior to stellar accretion (van den Bergh 1999).

At this point, we note that we tested several other techniques in an attempt to reproduce a halo mass and MDF closer to those observed in the Milky Way. These included varying the star formation efficiency, adjusting the amount of feedback incorporated as kinetic energy, and implementing "re-ionisation epochs" during which radiative cooling was essentially "squelched"(Somerville 2002). None of these adjustments were successful in lowering the mass and metallicity of the simulated stellar halo. To date, only the AFM has succeeded in lowering the metallicity and mass

of the simulated galaxies' stellar halos significantly. We believe that the observed properties of the stellar halo provide strong constraints on disk galaxy formation models, and suggest that many previous studies have inevitably failed to reproduce these properties. The success of the AFM lies in two features: its ability to regulate star formation at early epochs (figure 5.2), and the fact that its effect is more pronounced in smaller systems (the early collapsing subclumps and later-forming dwarf galaxies) than in a Milky Way-sized system.

Our simulations emphasise that it is critical for disk galaxy formation in a CDM context that building blocks and later-accreting satellites be gas dominant. We regard our simulations as a successful realistion of the scenario sketched by Burkert (2001), which emphasised the need for an early phase of gas heating and dissociation from dark matter in forming the Milky Way within hierarchical cosmologies.

Chapter 6

The Emergence of the Thick Disk in a CDM Universe

6.1 Introduction

Since its existence was detected through star counts by Gilmore & Reid (1983), the thick disk has become established as a component of the Milky Way that is distinct from the thin disk. It is hoped that the old age of the stars associated with the thick disk of the Milky Way will allow it to serve as a fossil record of the formation processes of the early parts of Galactic evolution.

Several large surveys have been undertaken to constrain the properties of the Milky Way's thick disk. The local density of thick disk stars is about 6-13% of that of the thin disk (e.g. Chen et al. 2001); the thick disk has a scale height of 0.6-1 kpc (e.g. Phelps et al. 1999, Ojha 2000, Chen et al. 2001), about three times larger than the thin disk; its stars are old, almost exclusively older than 12 Gyrs (e.g. Gilmore & Wyse 1985; Edvardsson et al. 1993; Fuhrmann 1998). Thick disk stars have a wide range of metallicity, $-2.2 \leq$[Fe/H]≤ -0.5, (Chiba & Beers 2000, hereafter CB), although the metal weak ([Fe/H]< -1.0) tail of the distribution contributes only $\sim$1 % of the thick disk (Martin & Morrison 1998), and may be a different population to the canonical thick disk (Beers et al. 2002). We also note that Feltzing, Bensby & Lundström (2003, hereafter FBL) find that the thick disk metallicity distribution extends to metallicities higher than [Fe/H]$= -0.5$. The metallicity distribution peaks at [Fe/H]~ -0.6 (Gilmore & Wyse 1985; Wyse & Gilmore 1995; CB). Thick disk stars are also characterised by their warm

kinematics and a rotation that lags behind the thin disk, e.g. Strömgren (1987) finds (σ_U,σ_V,σ_W)=(65,54,38)km/s, V_{lag} ∼40 km/s.

There is mounting evidence that the chemical trends in the thick and thin disk stars are different (Fuhrmann 1998; Prochaska et al. 2000; Tautvaisiene et al. 2001; Schröder & Pagel 2003; Mashokina et al. 2003, hereafter MGTB; Reddy et al. 2003; FBL; also see Chen et al. 2000 for an alternative view). An important diagnostic derived from this divergence the α-element to iron abundance ratio, which indicates different formation timescales for the thin and thick disk. The enhanced α-element abundances (compared to iron) that are observed in thick disk stars indicate a short formation timescale in which enrichment is dominated by Type II supernovae (SNe II). Although FBL found evidence of Type Ia supernovae (SNe Ia) enrichment in the most metal rich of the thick disk stars, their values for [α/Fe] are systematically higher than thin disk stars with the same [Fe/H]. Fuhrmann (1998), Gratton et al. (2000), and Mashonkina & Gehren (2001) conclude that star formation in the thick disk lasted less than 1 Gyr, while correlations of various chemical elements in thick disk stars lead MGTB to estimate this time scale to be ∼0.5 Gyrs. MGTB also conclude that the homogeneity of abundances of thick disk stars indicates that it formed from well-mixed gas, a conclusion that is consistent with the results of Nissen & Schuster (1997), Fuhrmann (1998), and Gratton et al. (2000).

Over the past decade, N-body cosmological simulations have been successful in reproducing many properties of disk galaxies. Employing a new implementation of SNe feedback, Brook et al. (2003, BKGF hereafter) recently simulated a realistic disk galaxy with a stellar mass dominated by a young stellar disk component, surrounded by a less massive, old, metal poor, stellar halo. In this chapter, we examine this simulated disk galaxy for evidence of a thick disk component, searching for clues as to the origins of the thick disk within the hierarchical galaxy formation of a CDM context.

In section 6.2, we outline details of our N-body chemo-dynamical evolution code, `GCD+`, and the semi-cosmological galaxy formation model that we invoke. Initial conditions are chosen that lead to the formation of a late type galaxy, whose properties are presented in section 6.3. Further study of our simulated galaxy provides evidence for the existence of a distinct thick disk population, similar to that of the Milky Way. This allows us, in section 6.4, to trace the major thick disk formation epoch and propose a thick disk formation scenario. In section 6.5 we compare our scenario to other theories of thick disk formation, and discuss how current observational data

may discriminate between these theories.

6.2 The Code and Model

This chapter analyses data from the simulated late type galaxy of the *Adiabatic Feedback Model* from BKGF. We briefly review some features of the code and model. Our galactic chemo-dynamical evolution code, `GCD+`, self-consistently models the effects of gravity, gas dynamics, radiative cooling, and star formation. We include SNe Ia and SNe II feedback, tracing the lifetimes of individual stars, which enables us to monitor the chemical enrichment history of our simulated galaxies. Details of `GCD+` can be found in Kawata & Gibson (2003).

We assume that 10^{51} ergs is fed back as thermal energy from each SNe. The energy released by SNe is fed back as thermal energy, and smoothed over the nearest neighbour gas particles according to the SPH kernel. This feedback scheme is known to be inefficient (Katz 1992). To address this problem, gas within the SPH smoothing kernel of SNe II explosions is prevented from cooling, creating an adiabatic phase for gas heated by such SNe. This is similar to a model presented in Thacker & Couchman (2000).

The semi-cosmological version of `GCD+` used in this study is based upon the galaxy formation model of Katz & Gunn (1991). The initial condition is an isolated sphere of dark matter and gas. The top-hat overdensity has an amplitude, δ_i, at initial redshift, z_i, which is approximately related to the collapse redshift, z_c, by $z_c = 0.36\delta_i(1 + z_i) - 1$ (e.g. Padmanabhan 1993). We set $z_c = 1.8$, which determines δ_i at $z_i = 40$. Small scale density fluctuations are superimposed on the sphere, parameterised by σ_8. These perturbations are the seeds for local collapse and subsequent star formation. Solid-body rotation corresponding to a spin parameter, λ, is imparted to the initial sphere to incorporate the effects of longer wavelength fluctuations. A large value of λ is chosen along with initial conditions in which no major merger occurs in late epochs (z <1), in order to ensure a disk galaxy is formed. For the model described here, the relevant parameters include the total mass, 5×10^{11} $M_\odot$, baryon fraction, $\Omega_b = 0.1$, star formation efficiency, $c_* = 0.05$, spin parameter, $\lambda = 0.0675$ and $\sigma_8 = 0.5$. We employed 38911 dark matter and 38911 gas/star particles, making the resolution of this study comparable to other recent studies of disk galaxy formation (e.g. Abadi et al. 2003).

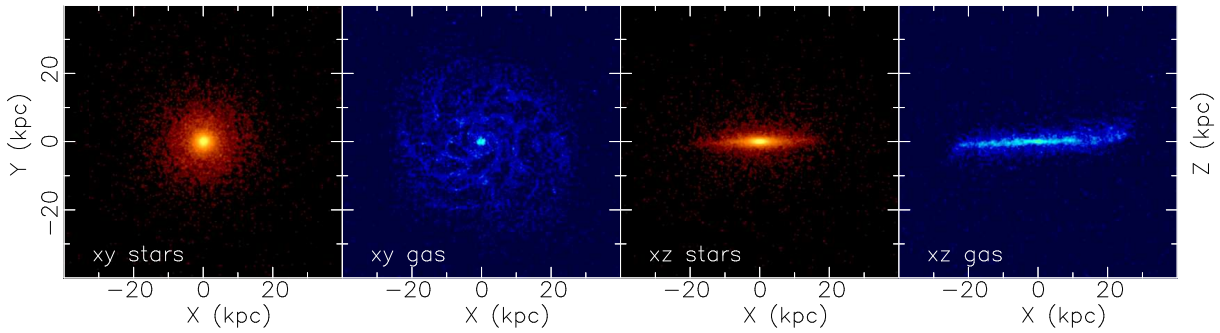

Figure 6.1: z=0 density plots for stars and gas in both the X-Y (face on) and X-Z (edge on) planes. The galaxy is dominated by a stellar disk. A large gaseous thin disk, still undergoing star formation, has also formed.

6.3 Properties of Final Galaxies

Figure 6.1 shows a density plot of the final stellar and gas populations of the simulated galaxy, viewed face-on and edge-on. The stellar mass is dominated by a young disk component. A large gaseous thin disk, still undergoing star formation, has also formed. The stellar population of the low mass stellar halo component is old and metal poor. The star formation history is shown in figure 6.2, which plots look-back time against the star formation rate (SFR). The SFR peaks ∼9 Gyrs ago. The SFR then declines over the next 4-5 Gyrs, but is reasonably steady over the last ∼5 Gyrs.

For this study, we are interested in the thick disk component. In observations of the Milky Way, the peculiar velocity of stars is a useful diagnostic to distinguish thick disk stars from thin disk stars. For observed solar neighbourhood stars, it is well established that there is a relationship between velocity dispersion and age. Figure 6.3 shows the observed relation as grey symbols, with error bars, as read from figure 3 of Quillen & Garnett (2001), who use the data of Edvardsson et al. (1993). The velocity dispersion data plateau between the ages of ∼10 and 2 Gyrs; these stars belong to the old thin disk. A slight decrease in dispersion is apparent for star particles less than ∼2 Gyrs old. Notably, the velocity dispersions increase abruptly, approximately doubling, ∼10 Gyrs ago. These older stars belong to the thick disk[1]. In figure 6.3 we use "+" symbols to plot the relation between the three components of the velocity dispersion, and the stellar age, for solar neighbourhood star particles in our simulation. The solar neighbourhood is defined as the annulus

[1]We note that a more recent study by Nordstrom et al. (2004) revisits this relation, and finds that the thin disk stars do show a slight increase of velocity dispersion with age, but stars older than ∼10 Gyrs were excluded from their study.

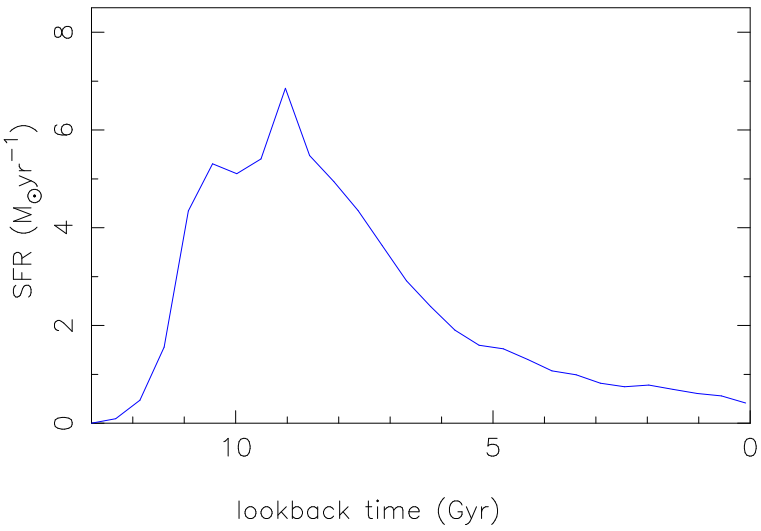

Figure 6.2: Global star formation rate (SFR) as a function of look-back time for our simulation. A peak of star formation is evident ∼9 Gyrs ago.

4< R_{XY} <12 kpc and |Z| <1 kpc. The three features relating to the young thin disk, the old thin disk, and the thick disk, are reproduced in our simulated galaxy.

Interestingly, the advent of an abrupt increase in velocity dispersion in our simulations corresponds to the end of the peak of the SFR (figure 6.2). This motivated us to explore the main processes that were taking place during the epoch of the peak star formation rate, when stars of age >8 Gyrs were forming rapidly. This epoch appears to be associated with thick disk formation. Figure 6.4 displays the evolution of the stellar (upper panels) and gaseous (lower panels) density distribution of the simulated galaxy during this epoch, between 9.5 and 8.3 Gyrs ago. The epoch is characterised by a series of merger events, and is by far the most chaotic period during the galaxy's evolution. At the beginning of this epoch, ∼10 Gyrs ago, at least four proto-galaxies of significant mass exist. These building blocks are gas rich, with combined gas mass of $\sim 2.4\times10^{10}\,M_\odot$, compared with stellar mass of $\sim 7.0\times10^{9}\,M_\odot$. By ∼8 Gyrs ago, a single central galaxy has emerged. The flattened nature of this central galaxy is apparent in the last panel of figure 6.4, yet the disk has significant thickness. The thin disk forms in the quiescent period of the remaining 8 Gyrs.

There is an offset in the timescales of thick disk formation between the simulation and observation, with the abrupt increase in velocity dispersion occurring around 10 (8) Gyrs ago for observations of the Milky Way (simulated galaxy). To further investigate this offset, we examine a simulation that evolves to a disk galaxy for which the collapse redshift, $z_c = 2.2$, occurs earlier than the model examined so

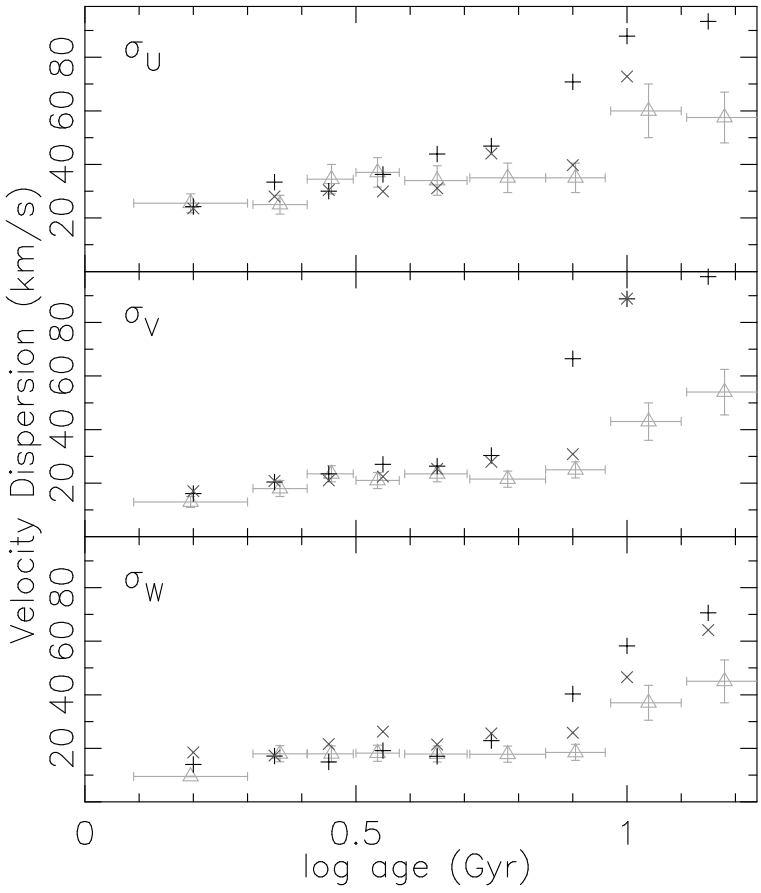

Figure 6.3: Age-velocity dispersion relation in the U, V and W direction for solar neighbourhood simulation star particles. An abrupt increase in the velocity dipersion is apparent at look-back time of ∼8 Gyr.

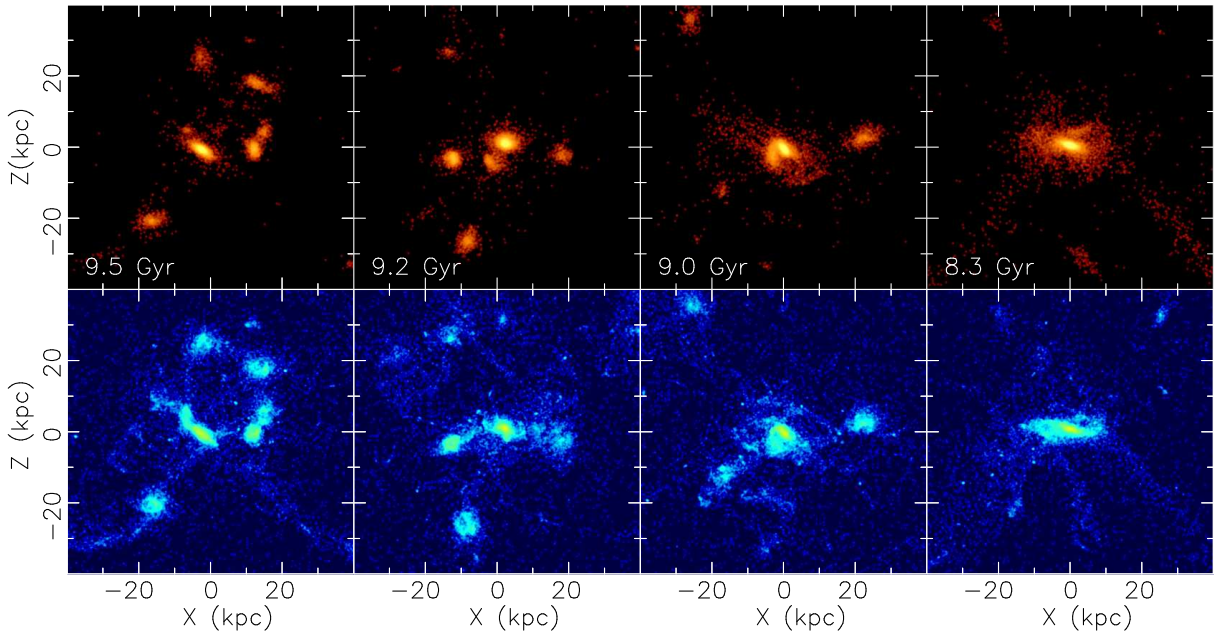

Figure 6.4: The evolution of the galaxy during the era that coincides with the discontinuity in the velocity dispersion plot indicates that thick disk stars are formed. This epoch is charaterised by multiple mergers of gas rich building blocks, resulting in the formation of a central galaxy.

far in this paper. This galaxy resembles the Milky Way less well insofar as it has a large bulge component, yet it also has a prominent disk. The major merging epoch of this galaxy is earlier than for our previous model, and this is reflected in the relation between velocity dispersion and age represeted by "×" in figure 6.3, where the abrupt increase in velocity dispersion has been pushed back to ∼10 Gyrs. The implication is that the offset is a result of the specific merging histories of the different galaxies.

6.4 Discussion

Our results indicate that the thick disk is created in an epoch of multiple mergers of gas-rich building blocks, during which a central galaxy is formed. The stars that form during this merging period, when a high SFR is triggered (figure 6.2), are the dominant source of thick disk stars. A significant fraction of the gas accreted to the central galaxy during this epoch carries the angular momentum of the proto-galactic cloud, imparted by the large scale structure of the Universe. This angular momentum results in the rotation and flattening of the final central galaxy. Yet this epoch is characterised by violent interactions, and the forming gas disk can be

described as dynamically hot, resulting in the high velocity dispersion of the stars forming in the disk. The result is the formation of a thick disk. Infalling gas after this multiple merger epoch settles smoothly to a thin disk.

Several formation scenarios for the thick disk were presented by Gilmore et al. (1989): 1) a slow, pressure-supported collapse that follows the formation of halo Population II stars (Larson 1976); 2) violent dynamical heating of the early thin disk by satellite accretion (Quinn et al. 1993) or violent relaxation of the Galactic potential (Jones & Wyse 1983); 3) accretion of thick disk material directly (Statler 1988; Bekki & Chiba 2000; Abadi et al. 2003); 4) enhanced kinematic diffusion of the thin disk stellar orbits (Norris 1987); and 5) a rapid dissipational collapse triggered by high metallicity (Wyse & Gilmore 1988). To determine which of these processes was the major driver of thick disk formation, observational evidence for the metallicity, ages, and chemical abundances of thick disk stars may be compared to the various predictions of each scenario.

Lack of a vertical metallicity gradient in the thick disk (Gilmore et al. 1995), as well as a lack of large intermediate age thick disk population would seem to rule out the slow collapse of scenario 1). The lack of overlapping age distributions between thick and thin disk stars, as well as the discontinuity in their chemical abundances, argues against the enhanced kinematic diffusion scenario 4). Further evidence against such a scenario is the size of the discontinuity in velocity dispersion, which appears to be too great to be explained by the known heating mechanisms, i.e. local gravitational perturbations in the thin disk such as giant Molecular Clouds (Spitzer & Schartzschild 1953) or transient spiral structure (Barbanis & Woltjer 1967; Carlberg & Sellwood 1985). Freeman (1991) suggested that these disk heating mechanisms saturate or become inefficient at $\sigma \sim$30 km/s. Lack of correlation between the scale length of the thick and thin disk components of disk galaxies observed by Dalcanton & Burnstein (2002, DB hereafter) also contradicts scenario 4) for thick disk formation in other galaxies. If the thick disk were composed primarily of material accreted slowly over time from many smaller satellites on suitable orbits, as in scenario 3), then the metallicity of the stars would be too low to explain the observed peak metallicity of the thick disk. The well known metallicity-mass relation of galaxies would require accretion of massive satellites ($>10^{10}\,M_{\odot}$), destroying the thin disk, in order to obtain metallicities of [Fe/H]~-0.6, unless the accreted satellites are gas rich and the accretion process induces a significant self-enrichment (Bekki & Chiba 2002). In addition, recent high resolution spectroscopic observa-

tions of individual stars in dwarf spheroidals (dSphs), find solar α-element to iron abundance ratios (e.g. Shetrone et al. 2001, 2003) that differ significantly from observed [α/Fe] and [Fe/H] in the thick disk. This indicates that the accretion of systems similar to dSphs is not the dominant source of thick disk stars.

The heating of the disk early in its violent evolution, as in scenario 2), is well supported by Galactic observations (Quillen & Garret 2001; Wyse 2000; Gilmore et al. 2002; Freeman & Bland-Hawthorn 2002; FBL). This scenario is consistent with the observed abrupt increase in velocity dispersions, the distinct chemical properties of the two disk components, and the homogeneity of thick disk abundances. We contend that our scenario of thick disk formation during the epoch of multiple mergers of gas-rich building blocks is consistent with scenario 2), and hence with these observations of the Milky Ways thick disk. We note that the scenario 2) suggests two possible heating mechanisms. In the first possible mechanism, a thin disk forms and is heated by an accretion event. Our simulations more closely resemble the mechanism of Jones & Wyse (1983), in which a thick disk forms during a violent relaxation of the galactic potential, prior to the formation of the thin disk. Evidence that the thick disk has had a more intense star formation history than the thin disk (e.g. Bensby et al. 2003; MGTB) would seem to favour the mechanism we propose over the "puffed up" thin disk, although neither mechanism proposed in scenario 2) is inconsistent with a rapid thick disk formation timescale (e.g. FBL). We note also that the in situ formation of the thick disk in our scenario leads to efficient self-enrichment. The increased cooling due to metals, as mentioned in scenario 5), ensures a rapid star formation rate in the thick disk.

The formation of the thick disk in the manner we have outlined is a natural consequence of the early, violent merging epoch of the CDM universe, indicating that thick disks should be a common component of disk galaxies. Recent, deep observations of a sample of 47 nearby edge-on galaxies by DB indicate that thick disks are widespread around disk galaxies. A lack of correlation between thick and thin disk scale lengths, as found by DB, is also explained by our formation scenario. Confirmation of these findings would strengthen the case for our thick disk formation scenario.

Chapter 7

Conclusions and Future Directions

The notion that stellar populations can be traced to their birthplace in the protogalactic cloud through a study of their chemical and kinematic properties was recently reviewed by Freeman & Bland-Hawthorn (2002), who nicknamed the pursuit "Galactic Archaeology". However ambitious it may seem, Galactic Archaeology is an instructive blueprint: it reminds us that processes and events at high redshift are responsible for many current observations of the Milky Way. By interpreting local observations within the context of the Cold Dark Matter paradigm, a connection is made with the distant Universe. Embracing an historical perspective, we endeavour to unravel a detailed physical understanding of the sequence of events which led to the formation of the Milky Way.

Prior to surveying present and future work, we present a brief summary of the key results of this thesis:

- *White dwarf stellar halo*: As chemical signatures of white dwarf progenitor stars, carbon and nitrogen abundances in the halo of a simulated galaxy were compared with observations for the Galactic halo. This has enabled us to place upper limits on the halo white dwarf population. Our results are inconsistent with a white dwarf component in the halo $\gtrsim 5\,\%$ (by mass), however mass fractions of $\sim$1-2 % cannot be ruled out.

- *Milky Way substructure*: The dynamical signatures of the formation of the stellar halo were examined. A group of simulated high-eccentricity stars were traced to disrupted satellites that had been accreted by the host galaxy. The phase space distribution of the accreted stars were compared with observed

high-eccentricity stars in the solar neighbourhood, providing evidence for a "stellar stream" in our own Galaxy.

- *Constraints set by the stellar halo*: The observed low metallicity and low mass of the Galactic stellar halo are typically invoked to constrain disk galaxy formation models. We demonstrate the importance of strong feedback - the mechanism that regulates star formation in Galactic building blocks - to models that successfully conform to observational constraints.

- *Thick disk formation*: An abrupt increase in the velocity dispersion versus stellar age relation provides evidence that a thick disk forms in our simulated disk galaxy. The thick disk in our simulation forms in a chaotic merging period at early epochs of galaxy formation. This formation scenario for the thick disk component of the Milky Way is shown to be consistent with observations.

Some of the following investigations have arisen directly from the issues raised by this thesis.

- *Heating of disk stars*: Heating of the thin disk stars by local gravitational disturbance or transient spiral structure was ruled out as the origin of the thick disk in chapter 6. However, recent results of Nordström et al. (2004) indicate that the kinematic diffusion of the thin disk has been enhanced over the past 8-10 Gyrs, presumably by mechanisms similar to those mentioned above. Preliminary analysis suggests that stars in our simulated thin disk do exhibit signs of heating. We intend to develop an explanatory framework for the observations by determining the influential parameters for the heating in our simulations.

- *Statistical thick disk study*: By examining a statistically significant number of simulated disk galaxies similar to the one examined in chapter 6, with varying masses, angular momentum and merging histories, we hope to predict the expected frequency of thick disks and to characterise thick disk properties such as age, metallicity and colour of the stellar populations.

- *Substructure*: Martin et al. (2004) have published evidence that a satellite has recently been accreted by the Milky Way, resulting in a population of stars with thick disk characteristics. Simulations by Abadi et al. (2004) suggest that

thick disk formation processes are dominated by accretion events. However, the scenario presented in chapter 6, in which the thick disk forms in an epoch of merging and high star formation early in the Galaxy's evolution, implies that only a minor proportion of thick disk stars are directly accreted. These studies are in addition to the now established role that accretion plays in building up the stellar halo (e.g. Ibata et al. 1994, Helmi et al. 2000, chapter 4 of this thesis). By combining new observations, such as those from the Sloan Digital Sky Survey, the Radial Velocity Experiment (RAVE) and GAIA (see below), we hope that the full extent to which accretion has contributed to both the stellar halo and thick disk will be revealed.

- σ_V *versus* R_{GAL}: Toomre (1964) demonstrated that the stability of a uniform cold disk requires the parameter, Q, to be greater than unity, where

$$Q = \frac{\sigma_R \kappa}{3.36 G \Sigma}, \tag{7.1}$$

σ_R is the radial component of velocity dispersion, κ is the local epicyclic frequency, Σ is the surface density, and G is the gravitational constant. Lewis & Freeman (1989) observe a relation between radial velocity dispersion and radius of the old Galactic disk, as would be implied from the Toomre parameter for a stable disk. Preliminary analysis of our simulations reveals a similar, if slightly weaker, negative trend of σ_R versus R_{GAL} to those observed. We intend to investigate the significance of this divergence from the observational data.

- *Self-consistent elliptical and disk simulations*: Models for simulating disk and elliptical galaxy formation have often required use of different values of various parameters, such the spin parameter. A further test of the feedback algorithm introduced in chapter 5 is to apply it to initial conditions that result in realistic elliptical galaxies as well as disk galaxies. Our preliminary studies of this are promising. We have run the *Adiabatic Feedback Model* (AFM, chapter 4) with the initial conditions of 2×10^{11} and 8×10^{11} solar masses from Kawata & Gibson (2003a). The resultant galaxies are morphologically elliptical. We have not yet completed a detailed analysis of these simulations, but we do find that star formation is ongoing at redshift zero. A further line of inquiry in this project will be to examine whether applying the AFM to SNe Ia affects the

ongoing star formation in ellipticals, and determining the effect of feedback from SNe Ia on disk galaxies.

- *Cosmological simulations with* GCD+: In this thesis, a semi-cosmological version of GCD+ was employed. As was prefaced in chapter 1, advantages exist in using a full cosmological code. Full cosmological simulations permit galaxy simulations with realistic halo masses, merging histories and tidal forces, i.e. the properties that ultimately provide angular momentum and determine the collapse redshift. A cosmological version of GCD+ employs the multi- resolution technique to simulate galaxy formation (Kawata & Gibson 2003b). A galaxy that resembles the Milky Way has been identified within GCD+ cosmological simulations (Gibson et al. 2003). We plan to employ the AFM to make mock observations of the simulated galaxy, and then to compare the "observed" values of angular momentum with the values derived directly from the simulated end products. A study such as this is not possible with a semi-cosmological model since a solid body spin parameter is included in the initial conditions.

- *Comparing galaxy formation models*: As noted in chapter 1, several different methods are used to model the formation of the Milky Way. Semi-analytic chemical galaxy evolution models of the Milky Way are able to reproduce the solar neighbourhood metallicity distribution function (MDF), e.g. Fenner & Gibson (2003), as well as broad chemical trends. Our simulations, using both the semi- and full- cosmological versions of GCD+, have also reproduced the local MDF and similar chemical trends. In all codes, these results are influenced by outflows and inflows of gas of varying chemical composition. It would be interesting to compare these models, to evaluate dynamical effects on the chemical evolution, and assess the different gas mixing assumptions of the two types of codes.

- *Disk-dark matter alignment*: Knebe et al. (2003) recently showed that the orbits of simulated galaxy cluster sub-halos are biased to lie along the major axis of the cluster, due to infall along filaments. They postulated that this bias may explain the Holmberg effect, if galaxy disks are perpendicular to the major axis of their dark matter halos. Using results from cosmological GCD+ disk galaxy simulations, we hope to establish how disks align with the tri-axial halos in which they reside.

Galactic astronomy will remain an exciting field for theorists and observers over the next decade and beyond. Planned surveys will provide an extraordinary abundance of information about the Milky Way's components. Moore's law coupled with sophisticated galaxy formation algorithms promise increasingly detailed modeling at higher and higher resolution. We embarked on the "journey" of this thesis by describing the sequence of discoveries that established our current understanding of our Galaxy and its constituents. Arriving at our present (albeit temporary) destination, it is perhaps fitting that we should preview the next historic phase of Milky Way exploration.

New Views of the Milky Way

For studies of the Milky Way, an exciting new observational era approaches. To understand the evolution of the Galaxy in a quantitative sense, it will be imperative to know the full multivariate distribution of stars over parameters such as age, metallicity, the three components of velocity, and the components of position. In particular, two new surveys, RAVE and GAIA promise to transform our knowledge of the stars that populate the Milky Way.

RAVE will conduct an all-sky survey to measure radial velocities, metallicities, and abundance ratios for 50 million stars. Phase I of RAVE is under way, using the UK Schmidt Telescope to survey 100,000 stars over 10,000 square degrees to I=12. Phase II will cover the sky to I=15, include 50 million stars, and run from 2006 to 2010. RAVE will provide a truly representative inventory of stellar radial velocities for all major components of the Galaxy; 26 million thin disk main sequence stars, 9 million thick disk stars, 2 million bulge stars, 1 million halo stars, and 12 million giant stars. The ability to combine the radial velocities with proper motions and parallaxes from other sources (USNO, Tycho-2, Hipparcos, GAIA) should accomplish an extraordinary advance in our understanding of our Galaxy.

The GAIA satellite is due for launch in 2010. The goal is to make the largest, most precise map of our Galaxy by surveying more than one billion stars, about one per cent of our Galaxy's population. GAIA will detect the motion of each star in its orbit around the Galactic Centre. GAIA will compile a complete sample of G sub-giants, which provide the most accurate ages for individual older stars, along with accurate kinematics and distances. The GAIA sample comprises a very significant radial zone in the Galactic disk: about 2 to 4 scale lengths from the Centre.

Ground-based metallicity data will complement chemical abundance estimates.

To interpret such unprecedented data sets, and disentangle the formation history of the Milky Way, theoretical models which can directly compare with observation are required. This will ensure that chemo-dynamical models for Milky Way formation continue to play an important role in Galactic Archaeology.

Bibliography

Aarseth S. 1963, MNRAS, 126, 223

Aaronson M. 1987 in *Nearly normal galaxies: From the Planck time to the present*; Proceedings of the Eighth Santa Cruz Summer Workshop in Astronomy and Astrophysics. New York, Springer-Verlag, 57-66.

Abadi M. G., Navarro J. F. & Steinmetz M. 2003, ApJ, 597, 21

Abadi M. G., Navarro J. F., Steinmetz M. & Eke V. R. 2003, ApJ, 591 499

Abia C., Dominguez I., Straniero O., Limongi M., Chieffi A., Isern J. 2001, ApJ, 557, 126

Abel T., Bryan G. & Norman M. 1999, in *Space*, meeting held in Paris, France, September 28th - October 1st, eds.F. Combes, G. Pineau des Forets. Cambridge University Press, Astrophysic Series

Abel T., Bryan G., Norman M. 2002, Science, 295, 5552, 93

Adams F. C. & Laughlin G. 1996, ApJ, 468, 586

Alcock C. et al., 2000 ApJ, 542, 281

Balsara D. 1995 AAS, 187 5204

Barnes J.E. & Hut P. 1986, Nature, 324, 446

Beers T.C. et al. 2002, AJ, 124, 931

Beers T. C. & Sommer-Larsen J. 1995, ApJS, 96, 175

Bekki K. & Chiba M. 2001, ApJ, 558, 666

Bekki K. & Chiba M. 2000, ApJ, 534, 89

Bekki K. & Shioya Y. 1998, ApJ, 497, 108

Bekki K. & Shioya Y. 1999, ApJ, 531, 108

Bensby T., Feltzing S., & Lundström I. 2003, A&A, 410, 527

Berczik P. 1999, A&A, 348, 371

de Bernardis P. et al. 2000, Nature, 404, 955

Bertschinger E., 2001 ApJS 137 1

Bromm V., Ferrara A., Coppi P. S. & Larson, R. B. 2001, AAS, 198, 603

Brook C. B, Kawata D. & Gibson Brad K. 2003, ApJ, 585 125

Brook C. B, Kawata D., Gibson Brad K., & Flynn C. 2004, MNRAS, 349, 52

Bruzual G. & Charlot S. 2003 MNRAS 344, 1000

Burkert, A. 2001, in *Cosmic Evolution*, Institut d'Astrophysique de Paris, eds. Vangioni-Flam E., Ferlet R., & Lemoine M. New Jersey: World Scientific, p.245

Burton W. B. & Lockman F. J. 1999, A&A, 349, 7

Carlberg R. G. 1984a ApJ, 286, 403

Carlberg R. G. 1984b ApJ, 286, 416

Carlberg R. G., Lake G. & Norman C. A. 1986 ApJ, 300, L1

Carney B. W., Latham D. W. & Laird J. B. 1990 AJ, 99, 201

Carney B. W., Latham D. W., Laird J. B. & Aguilar L. A. 1994 AJ, 107, 2240

Chaboyer B., Demarque P., Kernan P. J., & Krauss L. M. 1998, ApJ, 494, 96

Chabrier G., Segretain L. & Mera D. 1996, ApJ, 486, L21

Chen Y. Q., Nissen P. E., Zhoa G., Zhang H. W. & Benoni T. 2000, A&AS, 141, 491

Chiba M. & Beers T. C., 2000, AJ, 119, 2843

Clemens D. P. 1985, ApJ, 295, 422

Cole S., Aragon-Salamanca A., Frenk C. S., Navarro J. F. & Zepf S. E. 1994, MNRAS 271, 781

Cole S., Lacey C. G., Baugh C. M. & Frenk C. S., 2000 MNRAS, 319, 168

Crézé M., Chereul E., Bienayme O. & Pichon C. 1998 A&A 329 920

Christlieb N. et al. 2002 Nature, 419, 904

Dalcanton J. J. & Bernstein R. A. 2002, AJ, 124, 1328

Dalcanton J. J., Spergel D. N. & Summers F. J. 1997 ApJ, 482, 659

Davies R. L., Frogel J. A. & Terndrup D. M., 1991 AJ 102 1729

Davidge T. J. & Courteau S. 2002 AJ 123 1438

Dominguez I., Straniero O., Limongi M. & Chieffi A., 1999, ApJ, 524, 226

Dinescu, D. I 2002 in *Omega Centauri: A Unique Window into Astrophysics*, eds. F. van Leeuwen, G. Piotto & J. Hughes (San Francisco: ASP)

Durrell P. R., Harris W. E. & Pritchet C. J. 1994, AJ, 108, 2114

Edvardsson B., Anderson J., Gustafsson B., Lambert D. L., Nissen P. E. & Tomkin J. 1993, A&A 275, 101

Eggen O. J., Lynden-Bell D. & Sandage A. R. 1962, ApJ, 136, 748

Eke V. R., Cole S. & Frenk C. S. 1996, MNRAS, 282, 263

Fall S. M. & Efstathiou G. 1980 MNRAS, 193, 189

Feltzing S., Bensby T. & Lundström I. 2003, A&A, 397, 1

Fenner Y. & Gibson B. K. 2003, PASA, 20, 189

Fich M., Blitz L. & Stark A. A. 1989, ApJ, 342, 272

Fields B. D., Freese K. & Graff D. S. 2000, ApJ, 534, 265

Flynn C., Gould A. & Bahcall J. 1996, ApJ, 466, L55

Flynn C., Holopainen J. & Holmberg J. 2003, MNRAS, 339, 817

Flynn C., Sommer-Larsen J., Fuchs B., Graff D.S. & Salim S. 2001, MNRAS, 322, 553

Freeman K. C, 1987 ARA&A, 25, 603

Freeman K. C. 1991, in *Dynamics of Disk Galaxies*, eds. B. Sundelius, (Göteborgs University and Chalmer University of Technology, Göteborg Sweden), 15

Freeman K. C & Bland-Hawthorn J. 2002 ARAA, 40, 487

Frei Z., Guhathakurta P., Gunn J. E. & Tyson J. A. 1996 AJ,111,174

Frogel J.A., 1990, in *ESO/CTIO Workshop on Bulges of Galaxies* ESO, Garching, A92-18101 05-90, 177

Fuhrmann K., 1998, A&A, 338, 161

Fry A. M., Morrison H. L., Harding P. & Boroson T. A. 1999 AJ 118 1209

Gerritsen J. P. E. 1997, Ph.D. thesis, Kapetyn Ast. Inst.

Gibson B.K. et al. 2000 ApJ 529 723

Gibson B.K. & Flynn C. 2001 Science, 292, 2211

Gibson B.K. & Mould J.R. 1997, ApJ, 482, 98 (GM97)

Gilmore, G., 2001, in *Starbursts: Near and Far*, eds. Tacconi, L.J., Lutz, D., Springer-Verlag, Heidelberg, 34

Gilmore, G. 2003, in *Galaxy Evolution: Theory and Observations* eds. V. Avila-Reese, C. Firmani, C. Frenk & C. Allen Rev Mex AA, CS, vol. 17, 149

Gilmore G., & Reid N. 1983, MNRAS, 202, 1025

Gilmore G., Wyse R. F. G. & Kuijken K. 1989, ARA&A, 27, 555

Gilmore G., Wyse R. F. G. & Jones J. B. 1995, AJ, 109, 3

Gilmore G., & Wyse R. F. G. 1985, AJ, 90, 2015

Gingold R. A., Monaghan J. J. 1977, MNRAS, 181, 375

Girardi L., Bressan A., Bertelli G. & Chiosi C. 2000, A&AS, 141, 371

Goldman B. et al. 2002, A&A, 389, 69

Gould A., Flynn C. & Bahcall J. 1998, ApJ, 503, 798

Gratton R. G., Carretta E., Matteucci F. & Sneden C. 2000, A&A, 358, 671

Gratton R. G., Bragaglia A., Carretta E., Clementini G., Desidera S., Grundahl F., Lucatello S. 2003 A&A, 408, 529

Gyuk G. & Gates E. 1999, MNRAS, 304, 281

Hansen B. M. S. 1998 Nature, 394, 798

Hansen B. M. S. 2001, ApJ, 558, L39

Harris H. C. et al. 2001, ApJ, 549, L109

Helmi A. 2004 MNRAS in press

Helmi A., White S. D. M., de Zeeuw P. T. & Zhao H. 1999, Nature 402 53

Helmi A. & White S. D. M. 1999, MNRAS, 307, 495

Helmi A. & de Zeeuw H. S. 2000, MNRAS, 319, 657

Hernquist L. & Katz N. 1989, ApJS, 70, 419

Hodgkin S. T. et al., Nature, 2000, 403, 57

Honma M. & Sofue Y. 1997, PASJ, 49, 539

Hodge P. W. 1983 PASP, 95, 721

Hultman J. & Pharasyn A. 1999, A&A, 347, 769

Huchra J. & Brodie J. 1987, AJ, 93, 779

Ibata R. & Gilmore G. 1995, MNRAS, 275, 605

Ibata R., Gilmore G. & Irwin M. J. 1994, Nature, 370, 194

Ibata R.A., Irwin M., Bienaymé, O., Scholz R. & Guibert J. 2000, ApJ, 532, L41

Ibata R. A., Irwin M. J., Lewis G. F., Ferguson A. M. N. & Tanvir N. 2003 MNRAS 340 21

Ibata R. A., Richer H. B., Gilliland R. L. & Scott D. 1999, ApJ, 524, 95

Ibata R., Lewis G. F., Irwin M., Totten E. & Quinn T. 2001 ApJ 551 294

Iwamoto K., Brachwitz F., Nomoto K., Kishimoto N., Umeda H., Hix W. R & Thielemann F-K. 1999, ApJS, 125, 439

Käellander D. & Hultman J. 1998, A&A, 333, 399

Katz N., 1992, ApJ, 391, 502

Katz N. & Gunn J.E. 1991, ApJ, 377, 365

Katz N. 1992 ApJ, 391, 502

Katz N., Weinberg D. H., Hernquist L. 1996, ApJS, 105, 19

Kauffmann G. 1996 MNRAS, 294, 705

Kauffmann G., White S. D. M. & Guiderdoni B. 1993 MNRAS, 264, 201

Kay S.T., Pearce F.R., Jenkins A. et al. 2000, MNRAS, 316, 374

Kay S. T., Pearce F. R., Frenk C. S. & Jenkins A. 2002, MNRAS, 330, 113

Kawata D. 1999, PASJ, 51, 931

Kawata D. 2001, ApJ, 548, 703

Kawata D. & Gibson B. K. 2003a, MNRAS, 340, 908

Kawata D. & Gibson B. K. 2003b, MNRAS, 346, 135

Klypin A., Kratsov A. V., Valenzuela O. & Prada F. 1999, ApJ, 522, 8

Knebe A., Gill S. P. D., Gibson B. K., Lewis G. F., Ibata R. A. & Dopita M. A. 2004, ApJ, 603, 7

Koda J., Sofue Y. & Wada K. 2000, ApJ, 531, 17

Kobayashi C. 2002, Ap&SS, 281, 301

Kobayashi C., Tsujimoto T. & Nomoto K. 2000 ApJ, 539 26

Kobayashi C. 2004 MNRAS 347 740

Kato M. 1998, ApJ, 503, 155

Kochanek C. S. 1996 ApJ, 457 228

Kotenova E., Flynn C., Chiappini C. & Matteucci F. 2002, MNRAS, 336, 879

Koribalski B., Johnston S. & Otrupcek R. 1994, MNRAS, 270, 43

Kroupa P. 2001, MNRAS, 322, 231

Kuijken K. 1996, in ASP Conf. Ser. 91, *Barred Galaxies*, eds. R. Buta, D. A. Crocker & B. G. Elmegreen (San Francisco: ASP), 504

Larson R. B. 1969 MNRAS, 145, 405

Larson R. B. 1974a MNRAS, 166, 585

Larson R. B. 1974b MNRAS, 169, 229

Larson R. B. 1969 MNRAS, 173, 671

Lasserre T. et al. 2000, A&A, 355, 39

Lee Y-W., Joo J.-M., Sohn Y.-J., Rey S.-C., Lee H.-C. & Walker A. R. 1999, Nature, 402, 55

Lewis J. R. & Freeman K. C. 1989 Astron. J, 97, 139

Leggett S. K., Ruiz M. T. & Bergeron P. 1998, ApJ, 497, 294

Lin C. C. & Shu F. H. 1964, ApJ, 140, 646

Limongi M. & Chieffi A. 2003 in *From Twilight to Highlight: The Physics of Supernovae*. Proceedings of the ESO/MPA/MPE Workshop, Garching, Germany, p. 367.

Lucy L. 1977, AJ, 82, 1013

Loewenstein M. & Mushotzky R. F. 2001 AAS, 199 2505

Majewski S. R., Munn J. E. & Hawley S. L. 1996, ApJ, 459, 73

Makino J. 1991 PASJ, 43 859

Marigo P., Bressan A. & Chiosi C., 1996, A&A, 313, 545

Marigo P., Girardi L., Chiosi C. & Wood P. R. 2001, A&A, 371, 152

Mashonkina L. & Gehren T. 2001, A&A, 376, 232

Mashonkina L., Gehren T., Travaglio C. & Borkova T. 2003 A&A, 397, 275

Mateo M. L. 1998 ARA&A, 36, 435

Matteucci F. & François P. 1989, MNRAS, 239, 885

Martin N. F., Ibata R. A., Bellazzini M., Irwin M. J., Lewis G. F. & Dehnen W. 2004, MNRAS, 348, 12

McGaugh S. S. & De Block W. J. G. 1998, ApJ, 499, 41

Mendez R. A. 2002, A&A, 395, 779

Mendez R. A. & Minniti D. 2000 ApJ, 529, 911

Mera D., Chabrier G. & Schaeffer R., 1998, A&A. 330, 953

Mighell K. J. & Rich R. M. 1995 AAS, 186, 3906

Mo H. J., Mao S. & White S. D. M. 1998 MNRAS, 295 319

Morrison H. L. 1993, Astron. J., 106, 578

Moore B., Ghigna S., Governato F., Lake G., Quinn T., Stadel J. & Tozzi P. 1999, ApJ, 524, 19

Mori M., Yoshii Y. & Nomoto K. 1999, ApJ, 511, 585

Mulchaey J. S., Davis D. S., Mushotzky R. F. & Burstein D. 1993 ApJ, 404, 9

Mushotzky R. F. & Loewenstein M., Awaki H., Makishima K., Matsushita K. & Matsumoto H. 1994, ApJ, 436, L79

Nakamura F. & Umemura M. 2001, ApJ, 548, 19

Nakasato N. & Nomoto K. 2003, ApJ 588 842

Navarro J. F., Frenk C. S. & White S. D. M. 1995 MNRAS, 275, 56

Navarro J. F., Frenk C. S. & White S. D. M. 1997, ApJ, 490, 493

Navarro J. F. & Steinmetz M. 1997, ApJ, 478, 13

Navarro J. F. & Steinmetz M. 2000, ApJ, 538, 477

Navarro J. F & White S. D. M. 1993, MNRAS, 265, 271

Nelson C. A., Cook K. H., Axelrod T. S., Mould J. R. & Alcock C. 2002, ApJ, 573, 644

Nissen P. E. & Schuster W. J. 1997, A&A, 326, 751

Nordström B. et al. 2004, A&A in press

Ojha D. K. 2001, MNRAS, 322, 426

Oppenheimer B. R. et al. 2001, Science, 292, 698

Ostriker J. P. & Peebles P. J. E. 1973 ApJ, 186, 467

Phelps S., Meisenheimer K., Fuchs B., Wolf C. & Jahreiss H. 1999, in *Galaxy Evolution: Connecting the Distant Universe with Local Fossil Record*, Obs de Meudon, 1998.

Padmanabham T. 1993 *Structure Formation in the Universe*, Cambridge Univ. Press, Cambridge

Pagel B. E. J. & Tautaišiene G. 1995, MNRAS, 276, 505

Peebles P. J. E. 1969, ApJ, 155, 393

Peebles P. J. E. 1971, A&A, 11, 377

Prochaska J. X., Naumov S. O., Carney B. W., McWilliam A. & Wolfe A. M. 2000, ApJ, 120, 2513

Quillen A. C. & Garnett D. 2001. in *Galaxy Disks and Disk Galaxies*, ASP Conf. Ser., eds. G. Jose, S. J. Funes, E. M. Corsini, 230:87-88. San Francisco: Publ. Astron. Soc. Pac.

Raiteri C. M., Villata M. & Navarro J. F. 1996, A& A, 315, 105

Reddy B. E., Tomkin J., Lambert D. L. & Allende Prieto C. 2003, MNRAS, 340, 304

Reid N., Sahu K. C. & Hawley S. 2001, ApJ, 559, 942

Renzini A. & Voli M. 1981, A&A, 94, 175

Reylé C., Robin A. C. & Crézé M. 2001, A&A, 378, L53

Rich R. M. 2001 in *Astrophysical Ages and Timescales*, eds. T. van Hippel, N. Mansuset & C. Simpson, ASP Conf. Ser. 245, 216

Richer H. B., 2001, in *The Dark Universe: Matter, Energy and Gravity*, ed. M. Livio, Cambridge Univ. Press, Cambridge

Ryan S. G. & Norris J. E. 1991, AJ, 101, 1865

Salpeter E. E. 1955 ApJ, 121, 161

Sauman D. & Jacobson S. B. 1999, ApJ, 511, L107

Scalo J. M. 1986, Fund. Cosm. Phys., 11, 1

Schröder K. P. & Pagel B. E. J. 2003, MNRAS, 343, 1231

Schmidt B. P. et al. 1998 ApJ 507, 46

Searle L. & Zinn R. 1978, ApJ, 255, 357

Schaller G., Schaerer D. & Meynet G. 1992, A&AS, 96, 269

Somerville R. S. 2002 ApJ, 572, 23

Somerville R. S. & Primack J. R. 1999 MNRAS, 310, 1087

Spergel et al. 2003 ApJS, 148, 175

Springel V. & Hernquist L. 2003, MNRAS, 339, 289

Steinmetz M. 1996, MNRAS 278, 1005

Steinmetz M. & Müller E. 1994, A&A, 281, L97

Steinmetz M. & Müller E. 1995, MNRAS, 276, 549

Steinmetz M. & Navarro J. F. 1999, ApJ, 513, 555

Steinmetz M. & Navarro J. F. 2002, NewA, 7, 155

Strauss M. A. & Willick J. A. 1995, Phys. Rep., 261, 271

Stompor R. et al. 2001, ApJL, 561, 7

Sutherland R. S. & Dopita M. A. 1993, ApJS, 88, 253

Tautaišienė G., Edvardsson B., Tuominen I. & Ilyin I. 2001, A&A, 380, 578

Talbot R. J. & Arnett D. W. 1971, ApJ, 170, 409

Talbot R. J. & Arnett D. W. 1975, ApJ, 197, 551

Thacker R. J. & Couchman H. M. P. 2000, ApJ, 545, 728

Theis C., Burkert A. & Hensler G. 1992, A&A, 265, 465

Timmes F. X., Woosley S. E. & Weaver T. A. 1995, ApJS, 98,617

Tinsley B. M. 1980, Fund. Cosm. Phys., 5, 287

Torres S., García-Berro E., Burkert A. & Isern J. 2001, MNRAS 328, 492

Tripicco M. J. & Bell R. A. 1995 AJ 110 3035

Tyson J. A., Wenk R. A. & Valdes F. 1990 ApJL, 349, L1

van den Bergh, S. 1999 A&AR 9, 273

van den Hoek L. B. & Groenewegen M. A. T. 1997, A&AS, 123, 305

von Hoerner S., 1963 Z. Astrophys. 57, 47.

van Loon J. Th., Gilmore G. F., Omont A., Blommaert J A. D. L., Glass I. S., Messineo M., Schuller F., Schultheis M., Yamamura I. & Zhao H. S. 2003 MNRAS 338 857

Vazdekis A., Casuro E., Peletier R. F. & Beckman J. E. 1996, ApJS, 106, 307

Walker T. P., Steigman G., Kang H., Schramm D. M. & Olive K. A. 1991 ApJ, 376, 51

White S. D. M., Navarro J. F., Evrard A. E. & Frenk C. S. 1993, Nature, 366, 429

White S. D. M. & Rees M. J. 1978 MNRAS 183 341

White S.D.M. & Springel V., 2000, in *The First Stars*,eds. A. Weiss, T.G. Abel, V. Hill, Spinger-Verlag, Heidelberg, 327

White S. D. M. & Frenk C. S. 1991, ApJ, 379, 52

Wilkinson M. I. & Evans, N. W. 1999, MNRAS, 310, 645

Woosley S. E., Weaver, T. A. 1995, ApJS, 101, 181

Worthey G. 1994, ApJS, 94, 687

Wu K., Lahav O. & Rees M. 1999, Nature, 397, 225

Wyse R. F. G. 1999, *Baltic Astronomy*, 8, 593

Wyse R. F. G. & Gilmore G. 1995, AJ 110, 2771

Yoshii Y. & Saio H. 1986, ApJ, 301, 587

Zibetti S., White S. D. M. & Brinkmann J. 2004, MNRAS, 347, 556

Zaritsky D. in *The Third Stromlo Symposium: The Galactic Halo ASP Conference Series*, eds. B.K. Gibson, T.S. Axelrod, M.E. Putman, Vol 165, 1999, p. 34

Zaroubi S., Zehavi I., Dekel A., Hoffman Y. & Kolatt T. 1997, ApJ, 486, 21

Zinn R. 1985, ApJ, 293, 424

Publications

List of Publications

Refereed Journals

---

[6] **C. B. Brook**, D. Kawata, B. K. Gibson, K. C. Freeman:
The Emergence of the Thick Disk in a CDM Universe
Astrophys. J. submitted

[5] H.-C. Lee, B. K. Gibson, Y. Fenner, **C. B. Brook**, D. Kawata, A. Renda, J. Holopainen, C. Flynn:
Photometric Properties of White Dwarf Dominated Halos
accepted for publication in PASA

[4] **C. B. Brook**, D. Kawata, B. K. Gibson, C. Flynn:
Stellar Halo Constraints on Simulated Late-type Galaxies
Mon. Not. R. Astron. Soc. **349**, 52 (2004)

[3] **C. B. Brook**, D. Kawata, B. K. Gibson:
Simulating a White Dwarf-dominated Galactic Halo
Mon. Not. R. Astron. Soc. **343**, 913 (2003)

[2] **C. B. Brook**, D. Kawata, B. K. Gibson, C. Flynn:
Galactic Halo Stars in Phase Space: A Hint of Satellite Accretion?
Astrophys. J. Letter **585**, 125 (2003)

[1] **C. B. Brook**, D. Kawata, B. K. Gibson, C. Flynn:
On the origin of high eccentricity halo stars
Astrophys. & Sp. Sci. **284**, 845 (2003)

Proceedings

[3] **C. B. Brook**, D. Kawata, B. K. Gibson:
Phase Space Plots of Streams in the Halo, and their Chemical Tags
in Satellites and Tidal Streams, ING-IAC Joint Conference
eds. D. Martnez-Delgado & F. Prada, in press

[2] **C. B. Brook**, D. Kawata, B. K. Gibson, C. Flynn:
Simulating a White Dwarf Dominated Halo
in Astrophysical Supercomputing using Particle Simulations,
eds. J. Makino & P. Hut, (ASP, San Franciso), 381-382

[1] B. K. Gibson and **C. B. Brook**
Type Ia Supernovae and the Value of the Hubble Constant
in New Cosmological Data and the Values of the Fundamental Parameters
(IAU Symposium #201)
eds. A. Lasenby & A. Wilkinson, ASP Conference Series

Oral Presentations

[3] *Phase Space Plots of Streams in the Halo, and their Chemical Tags*
at Satellites and Tidal Streams, ING-IAC Joint Conference
La Palma, Canary Islands, Spain, May 26-30, 2003

[2] *High eccentricity halo stars in phase spase*
at The Evolution of Galaxies III, Kiel, Germany, July 2002

[1] *The origin of high eccentricity halo stars*
at the Astronomical Society of Australia Annual Science Meeting,
Mollymook, Australia, June 2002